ANL-6194
Reactors - General
(TID-4500, 15th Ed.)
AEC Research and
Development Report

ARGONNE NATIONAL LABORATORY
9700 South Cass Avenue
Argonne, Illinois

FAST FUEL TEST REACTOR - FFTR CONCEPTUAL DESIGN STUDY

by

R. Brubaker
H. H. Hummel
A. McArthy
A. Smaardyk

Reactor Engineering Division

and

J. H. Kittel

Metallurgy Division

August 1960

Operated by The University of Chicago
under
Contract W-31-109-eng-38

DISCLAIMER

TABLE OF CONTENTS

TABLE OF CONTENTS

TABLE OF CONTENTS

LIST OF TABLES

FAST FUEL TEST REACTOR - FFTR CONCEPTUAL DESIGN STUDY

by

R. Brubaker, H. H. Hummel, J. H. Kittel, A. McArthy, and A. Smaardyk

I. INTRODUCTION

Experimental facilities for the irradiation of fast reactor fuels, including those based on plutonium, are urgently needed to insure the successful development of fast breeding. Although EBR-I has limited facilities, the plutonium burnup that can be achieved per month on small samples is of the order of only 0.1%. The fast power-breeder reactors under construction have flux levels of interest, but the fuel-handling systems are inadequate for an experimental program. These reactors are designed without provision for test leads and instrumentation for control of the specimen. Also, they are intended for continuous operation, which restricts the conduct of an uninterrupted test program. Thus, there is a need for a Fast Fuel Test Reactor (FFTR) similar in purpose to the thermal test reactors that are suitable for the test of thermal fuels. For this reason this study has been directed toward a conceptual reactor plant design that would meet the requirements of an adequate fast fuel test program.

The design concept was carried through in sufficient degree in the following areas of preliminary concern:

(1) number and size of irradiation facilities;

(2) sample power requirements;

(3) plant layout to evaluate site requirements;

(4) plant and nuclear design parameters to evaluate essential equipment requirements;

(5) plant capital cost estimate;

(6) annual operating cost estimate; and

(7) estimate of construction time schedule.

The idea of using a beryllium-moderated reactor with a hard intermediate spectrum for testing fast reactor fuel elements was developed in the course of previous test reactor studies at Argonne National Laboratory.[1]

II. SUMMARY

The FFTR concept is a nuclear facility for the purpose of irradiating samples of fuels and structural components for use in fast reactors. The reactor core consists of a plate-type element in a square configuration. Beryllium metal between the fuel elements is used to obtain a neutron energy spectrum in the hard intermediate region. Such a system suggests considerable flexibility for varying moderating parameters by substituting steel for part or all the beryllium. The intermediate reactor concept allows higher fuel irradiation rates than are provided by a fast reactor of the same size and power, at the expense of some radial power variation in samples, not believed to be excessive. Cooling of the core and test specimens is accomplished by means of sodium coolant entering the reactor core at 316°C (600°F) and leaving at an average temperature of 427°C (800°F). The normal reactor power is 200 Mw(t). However, design allowances were made so that 250 Mw(t) may be rejected to the secondary NaK system and, hence, to the atmosphere by a NaK-to-air heat exchanger.

The reactor, fueled with U^{235}, will produce maximum sample fission rates equivalent to those provided by a fast flux in the range of 1×10^{16} n/(cm^2)(sec). Operation of the reactor is planned on a cyclic basis. For the changing of fuel and experiments the reactor is shut down for a reasonable period of time. The remote handling of the fuel is accomplished by means of a fuel-transfer cell located directly over the reactor and manipulators. This process is made visible by means of binoculars or other viewing equipment and through shielding windows in the fuel transfer cell. The upper parts of the fuel elements are observed after lowering the sodium level.

Pertinent design data are summarized in Table I.

Table I

FFTR DESIGN DATA

Power		
Reactor power, Mw(t) (nominal)		200
Heat flux, Btu/(hr)(ft^2), (watts/cm^2)		
Average		564,000 (178)
Maximum		975,000 (308)
Maximum-to-average ratio,	total	1.73
	axial	1.21
	radial	1.43
Power density, Mw/l		
Average		0.67
Maximum		1.17
Sample specific power, kw/g Pu^{239}		0.2-1.5

Table I (Cont'd.)

Power (Cont'd.)	
Control element surface area, ft^2 (m^2)	10 (0.93)
Safety element surface area, ft^2(m^2)	10 (0.93)
Core	
Geometrical arrangement	right circular cylinder
Overall dimensions	
Diameter, in. (cm)	31 (79)
Height, in. (cm)	24 (61)
Total volume, l	298
Composition	
Total U^{235} inventory, kg	~150
Vol % UO_2 in core (ρ = 10.0 gm/cc),	7.75 max
Vol % UO_2 in type 304 stainless steel matrix	26.75 max
Vol % matrix in core	28.8
Total Vol % matrix and structural steel in core	37.4
Subassembly, including rods	121
Control rods	8
Safety rods	2
Fuel element assembly	
Element shape	plate
Overall dimensions, in. (cm)	2.08 x 2.08 x 55(5.3 x 5.3 x 140)
No. of plates per assembly	15
Clad, material	304 stainless steel
Clad, thickness, in. (cm)	0.005 (0.0127)
Dimensions, plate (active portion), in. (cm)	0.070 x 2 x 24(0.178 x 5.08 x 61)
Heat transfer surface, ft^2 (m^2)	10 (0.93)
Channel width, in. (cm)	0.066 (0.168)
Channel area per assembly, $in.^2$(cm^2)	1.99 (12.8)
UO_2 content (93% enriched), gm/plate	126.28
Central Fuel Temperature, °F (°C)	
Maximum without hot channel factors	990 (532)
Maximum with all hot channel factors	1200 (649)
Coolant	
Primary system	Na
Vol % in core	34
Flow rate, gpm (m^3/sec) (normal)	
total through core and loops	26,200 (1.65)
output main coolant pumps	25,400 (1.60)
through core excluding loops	22,400 (1.41)
through reflector	1,400 (0.088)
through one open loop	200 (0.013)
through one closed loop	200 (0.013)

Table I (Cont'd.)

Coolant (Cont'd.)	
Velocity in core, fps (cm/sec)	33 (1010)
Average reactor temperature, °F (°C)	
inlet	600 (316)
outlet	800 (427)
during fuel transfer	280-300 (140-150)
Secondary System	NaK
Flow rate, gpm (m^3/sec)	32,100 (2.02)
Average temperature in heat exchanger, °F (°C)	
inlet	648 (342)
outlet	448 (231)
Air cooled heat exchanger temperature °F (°C)	
inlet, air	100 (38)
outlet, air	500 (260)
Flow rate, lb/hr (m^3/sec)	7.1×10^6 (965)
Physics	
Burnup per cycle (30 days), 3.5 weeks at 200 Mw, kg	6.6
Burnup per year, kg	~80
Max total flux, n/(cm^2)(sec)	8×10^{15}
Max flux > 0.9 Mev, n/(cm^2)(sec)	1.5×10^{15}
Thermal fissions, %	≤ 1
Fissions below 100 ev, %	~8
Control Rods	
Type	magnetic jack
Location	bottom mounted
Experimental Facilities, (no. of each)	
Closed loops	4
Open loops	8
Capsule locations in core	~40
Capsule locations in reflector	32

III. REACTOR DESIGN CRITERIA

The design of the FFTR has been so oriented as to give it the following characteristics, not all possessed by any single existing reactor:

(1) a neutron energy spectrum that will assure acceptably uniform burnup rates in fast reactor fuel subassemblies of reasonable size;

(2) a typical fast reactor environment of sodium at high temperature to simulate engineering conditions for the test samples of fuel and structural materials;

(3) ready accessibility of fuel and test samples;

(4) provision for experimental test leads and instrumentation;

(5) flexibility, particularly in the location of the experiments and methods for increasing or decreasing test fuel loading permitted by adjusting coolant flow rates in the open and closed test loops;

(6) inclusion of closed test loops in which experimental irradiations can include release of fission products, or use of coolants other than sodium; and

(7) adequately high specific power in the test fuel.

Fuels for fast reactor normally contain high concentrations of fissile atoms because of the relatively low fission cross section of U^{235} and Pu^{239} for fast neutrons. For specimens with high fuel concentrations and of reasonable diameter, for example 0.3 cm, irradiated in a thermal reactor, almost all of the fissions will be concentrated in the outer layers. This makes interpretation of fuel-irradiation experiments difficult since the temperature and particularly the fission product distributions in the samples are quite different from what they would be in the actual fast reactor. The irradiation in thermal test reactors of fast reactor fuels based on plutonium is particularly complicated by the fact that a plutonium isotope of low cross section comparable to U^{238} is not available to lower the "enrichment" of the fuel. One cannot dilute such fuels without adding some element other than plutonium, and this would result in altered metallurgical characteristics. Thus, irradiations of even single specimens of fast reactor plutonium fuels in a thermal test reactor must necessarily be performed under conditions for which burnup is concentrated in the outer layers of the specimen. Because of their greater size, irradiations of fast reactor plutonium fuel subassemblies in a thermal test reactor would be even more subject to excessive flux-depression effects. Hence, experimental fuels with high fissile atom concentration cannot be effectively evaluated in thermal test reactors.

Fuel materials are usually evaluated by first irradiating relatively small samples of the material of interest. If the results are promising, prototype or full-scale fuel elements are often then fabricated from the material and then tested in loop or core facilities. It is expected that the majority of investigations in the loops of the proposed reactor would be carried out with sample sizes of the order of 20 fuel pins, which would correspond to a sample diameter without container of about 2.5 cm. Final proof tests of complete subassemblies would probably be desired occasionally, which would require a sample diameter of perhaps as much as 8 to 10 cm for large reactor subassemblies. A core height of 2 ft (61 cm) is desirable in order to prevent an excessive axial flux gradient. The radial power variation in the samples should not exceed about 25%.

The maximum specific power of the fuel for the first core loadings of EBR-II and the Fermi reactor is <1 kw/gm of U^{235}.

Alloys and ceramic fuels now under development will in all likelihood permit significantly higher specific powers before thermal conditions become limiting. Accordingly, the FFTR was designed to provide experimentally obtainable specific power ranging up to 1.5 kw/gm Pu^{239}. This relatively high specific power will enable irradiation testing of ceramic and refractory alloy fuels near their capability limits. It will also permit accelerated burnup tests on present fuels for reactors such as EBR-II and the Fermi Reactor. A more detailed discussion of desired burnup rates is given in Appendix B.

Experience at test reactors such as MTR has indicated that fuel materials can profitably be studied experimentally in instrumented capsules and in loops. Both types of facilities are usually located in or near the core for maximum burnup rates. Every effort has been made in the design of the FFTR to have as many capsule and loop facilities as possible throughout the core and reflector to provide a wide choice of sample specific powers. Because fuel elements will be used in the idle loops, through loops will be constructed as permanent parts of the reactor structure. Since the loops are an integral part of reactor operation, experimenters will be free of many of the problems usually associated with the construction and installation of loop-type experiments.

A major requirement is that the fuel samples be accessible for installation of experimental leads, such as thermocouples. Although this requirement presents a difficult technical design problem, irradiation temperature determinations are indispensable in fuel test experiments.

Although the fuel in most other liquid metal-cooled reactors is loaded remotely, it was considered essential that the FFTR core be loaded with fuel and that experiments be under full visual observations. This latter requirement arises mainly from the necessity of handling of the experimental

specimens, including leads, such as thermocouple wires. However, the opacity, chemical activity, and radioactivity of the sodium coolant greatly complicate the provision of visual access to the top of the core lattice. The requirements are met in the FFTR design by installing an argon-filled shielded cell over the reactor. After core decay heating has diminished to a sufficiently low value, the sodium can be lowered to expose the top of the fuel lattice. It is then possible to view the entire loading manipulation through shielding windows.

IV. SELECTION OF REACTOR CORE FEATURES

The emphasis in this report has been directed mainly toward a Be-moderated reactor with a neutron energy spectrum partially degraded into the hard intermediate region. It is believed possible to obtain higher fuel-sample specific powers in such a reactor than in a fast reactor of the same core size and total power without encountering excessive sample spatial power variations. With a fast reactor such variations are almost completely eliminated. Since one would prefer not to have these variations at all, it would seem desirable to incorporate enough flexibility into the detailed design so that operation as a fast reactor would be possible at times when the higher specific powers of the intermediate reactor were not necessary.

A UO_2-stainless steel plate was selected as the reactor fuel because this fuel element is commercially available at known cost. This in turn suggested the square grid layout that is proposed for the core. It was felt desirable to have the Be moderator separate from the fuel so that it would not have to be removed every cycle. It was therefore placed in the interstices between the square fuel subassemblies.

The approximate size of the core is dictated by the desire to have a minimum height of 61 cm for experimental reasons and by the U^{235} concentration possible in the proposed fuel element. Two core sizes have been considered for the FFTR, a smaller one with a volume of 238 liters corresponding to 97 subassemblies, and a larger one of 298 liters corresponding to 121 subassemblies. Actually, the physics calculations were carried out for core radii of 34.3 cm and 40 cm, corresponding to volumes of 226 liters and 306 liters, respectively, for the 61-cm core height. These slight differences have been neglected in applying the results of the physics calculations to the two core sizes. In any case, the uncertainties in the physics calculations make significant the range of the results rather than the exact values.

While it is the parameters for the larger core size that have been given in the summary of design conditions in Table I, the smaller size was the one being considered during most of this study. The reasons for now favoring the larger size are discussed below.

It is pointed out in Section VI-E that with the UO_2-stainless steel plates currently being considered for reactor fuel, operation of the FFTR with the smaller core as a fast reactor would be impossible because a sufficiently high concentration of fuel could not be attained. Operation as an intermediate reactor would hardly be feasible because of the limited excess reactivity available.

If UN-stainless steelfuel (see Section X-B) becomes available, operation with a core of smaller size might become possible by employing a heavier loading in the outer part of the core than in the center, to avoid excessive power densities. It would be a rather marginal operation, from the standpoint of available reactivity, however. This size of core is also rather cramped with regard to the location of test loops and control rods.

With the larger core, operation as an intermediate reactor seems possible with the UO_2-stainless steel fuel, although as discussed in Section VI-E the available reactivity may be slightly low. The reactivity loss occasioned by Li^6 buildup in Be would require an enlargement of about 10% over a period of about a year. Operation as a fast reactor would probably require use of the UN-stainless steel fuel.

In selection of a core size, the added capital and operating cost of a larger core must be balanced against the saving in fuel cost possible if the fuel can be used for more cycles. Radiation-damage data for the UO_2-stainless steel plates indicate that operation for at least six or seven cycles would be possible.(2) To take at least partial advantage of this, one could start with a core size of approximately 300 liters and increase the size with increasing exposure of the fuel. It is desirable to keep the sample specific powers as constant as possible by increasing the total reactor power during this process. The flux at sample positions in the outer part of the core and in the reflector would change with the variation of core size, which might be a fatal objection to this method of operation.

In Sections VI-D and VI-E it is shown that an intermediate reactor of approximately 300-liter core volume with a Be/U^{235} atom ratio in the range from 20 to 30 should allow the desired maximum sample specific power of 1.50 kw/gm Pu^{239} to be attained with a total reactor power of 154 Mw plus up to 10 Mw for samples. Since the heat transfer equipment has been sized to allow up to 250 Mw, there is ample capacity available for core enlargement to the maximum of 405 liters provided for Section V-A. The core composition listed in the design data given in Table I of 37.4 vol % matrix and structural steel, 34% sodium, and 28.6% Be would correspond approximately to the 30 Be/U^{235} atom ratio case of Tables V and VIII.

While radial power variation in the samples for this core composition has not been determined with certainty, it is not likely to be large enough to cause trouble. It is believed that an appreciably higher $beryllium/U^{235}$ ratio would degrade the spectrum too much.

To obtain the desired maximum specific power of 1.5 kw/gm with a fast reactor using the proposed fuel element, one would probably need a core size in excess of 300 liters. An increase in size to about 400 liters would increase the value given in Table VIII for a 306-liter core for 1.17 Mw/liter power density from 1.17 kw/gm Pu^{239} to 1.29 kw/gm. At this

size an increase in power density would still be necessary to meet the desired specific power. Allowing 10% overloading of the regular reactor fuel elements to provide operating excess reactivity, the necessary maximum power density would be about 1.5 Mw/liter. One might be able to reach this with the UN-stainless steel fuel by increasing the sodium concentration in the core. This would correspond to a total reactor power of about 300 Mw.

The fission rate for a given flux level in a fast reactor for samples containing Pu^{239} and U^{238} can be increased by substituting U^{235} for U^{238}, so that effective sample specific powers would be higher than indicated in Section VI-D if such a substitution were made. It is for samples with Pu^{239} or U^{235} and without U^{238} that the intermediate reactor would have the greatest advantage. Examples of such specimens are mentioned in Appendix B.

The selection of a 2.5-in. (6.35 cm) grid spacing for the reactor core was governed by the necessity of having sufficient subassembly positions available to accommodate the desired experimental facilities and to allow a sufficient number of control rods. The normal size available for loops of a 2.1-in. (5.33 cm) square could be designed to a 2.9-in. (7.36 cm) square by removing adjacent Be. It is felt that this would accommodate practically all experiments. If occasional testing of a larger size is desired, the detailed design could allow for use of four adjacent positions.

V. DESIGN DESCRIPTION

A. Reactor

1. Fuel Plate

The basic fuel plate (Fig. 1) is a section 0.070 in. (0.178 cm) thick and 2 in. (5.08 cm) wide. The fuel is UO_2 dispersed in a 304 stainless steel matrix which is metallurgically bonded to 304 stainless steel cladding material over a 2 ft (61 cm) length. The ends of the plate are of solid stainless steel and form part of the top and bottom reflector section. Thus the reflector regions above and below the core may be readily and concurrently fabricated with the fuel section. The sides of the plates are flanged to provide for the correct spacing between adjacent plates. The flanged sides are notched to equalize fluid pressure between adjacent channels. The top 12 in. (30.5 cm) portion of the fuel plate is more extensively notched to permit lateral flow of the coolant during refueling operations.

The active section of the fuel plate consists of a stainless steel matrix, 0.060 in. (0.152 cm) by 2 in. (5.08 cm) by 2 ft (61 cm) long, containing approximately 32 wt % UO_2 enriched 93% in U^{235}.

The application of this plate design has been based on the premise that stainless steel-UO_2 plates are obtainable from commercial suppliers at reasonable costs without additional fabrication development.

2. Fuel Subassembly

The fuel subassembly measures 55 in. (140 cm) long and weighs approximately 50 lb (23.7 kg). Pertinent design data are shown in Table I. The assembly (Fig. 2) consists of 15 fuel plates contained within a thin metal sheath. The plates are spot welded to the sheath at the bottom only, so that individual plates are free to expand upward and thereby avoid large thermal stresses caused by the temperature rise over the axial length of the core. The sheath provides for (1) the support of the fuel plates and (2) the channeling of the sodium.

Openings are made in the sheath at the top in the reflector region for lateral flow of sodium during the recharging operation. Thus the sodium level can be dropped to expose the fuel element tops without reducing the removal of decay heat. This method makes it possible to view the core configuration and the entire manipulation of fuel. The sheath is also perforated along the whole length to equalize static pressures and prevent collapsing conditions.

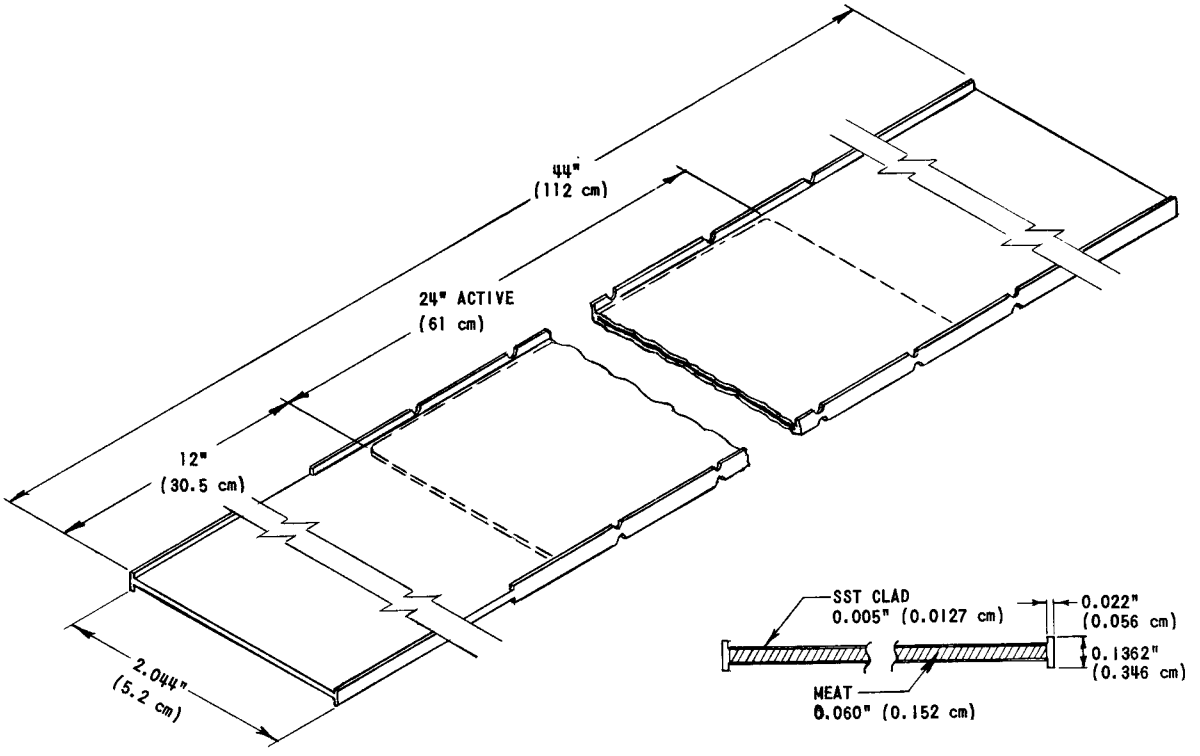

FIG. 1
FUEL PLATE

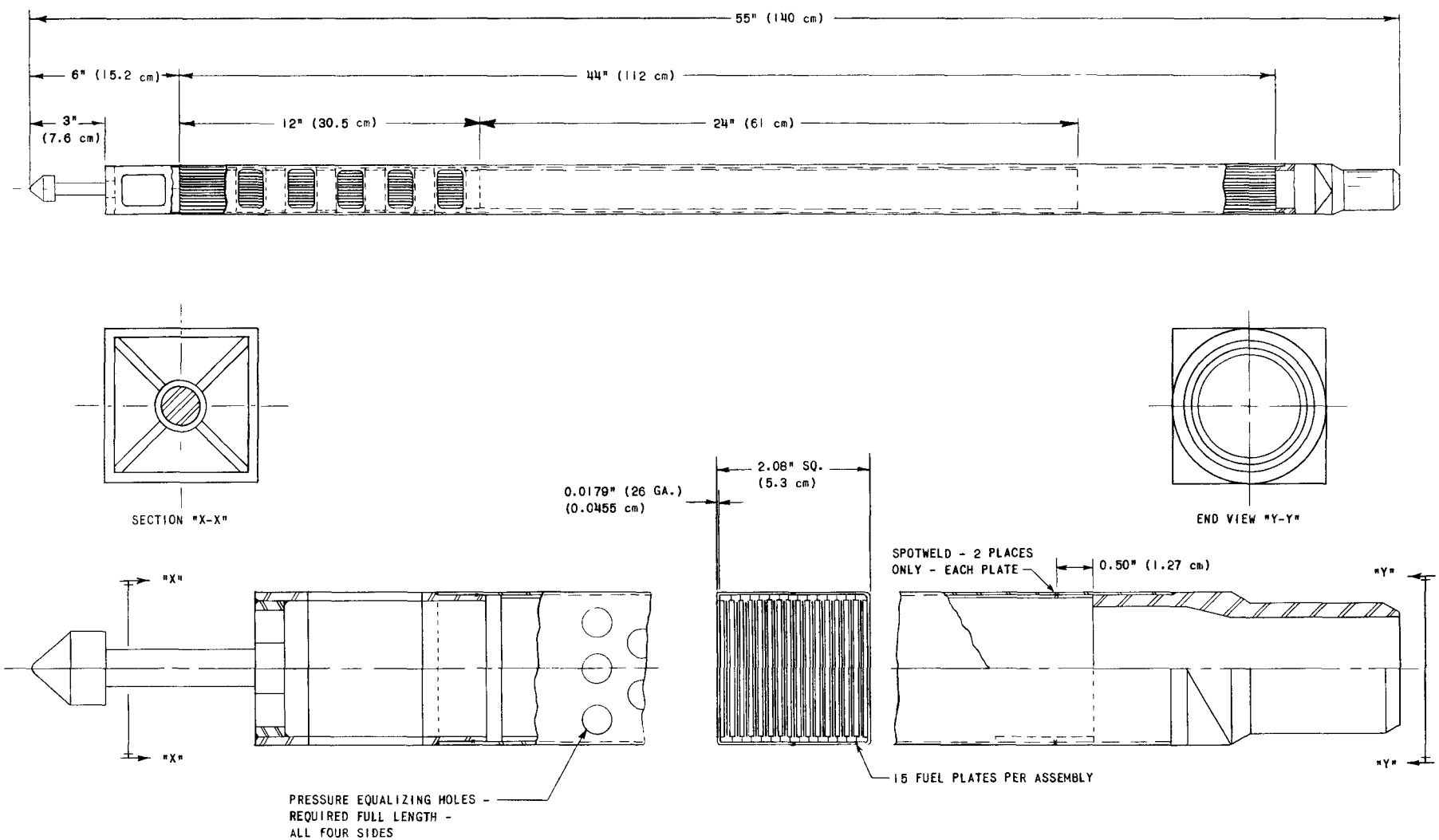

FIG. 2
FUEL ASSEMBLY

3. Core Description

The core consists of the fuel and reflector regions as shown in Fig. 3. The fuel region has 165 lattice openings, the centerlines of which measure 2.5 in. (6.35 cm) square. Of the 165 openings, 121 presently constitute the core proper; the surrounding and remaining 44 spaces are reserved for experiments, additional fuel, or reflector elements. The configuration of 121 lattice openings results in a core of approximately 2.58 ft (79 cm) equivalent diameter and a core volume of 298 ℓ. Use of all of the 165 lattice openings results in a core diameter of approximately 3 ft (91 cm) and a core volume of 405 ℓ.

Within the core proper there are eight movable elements that have extended poison sections to hold down excess reactivity. These

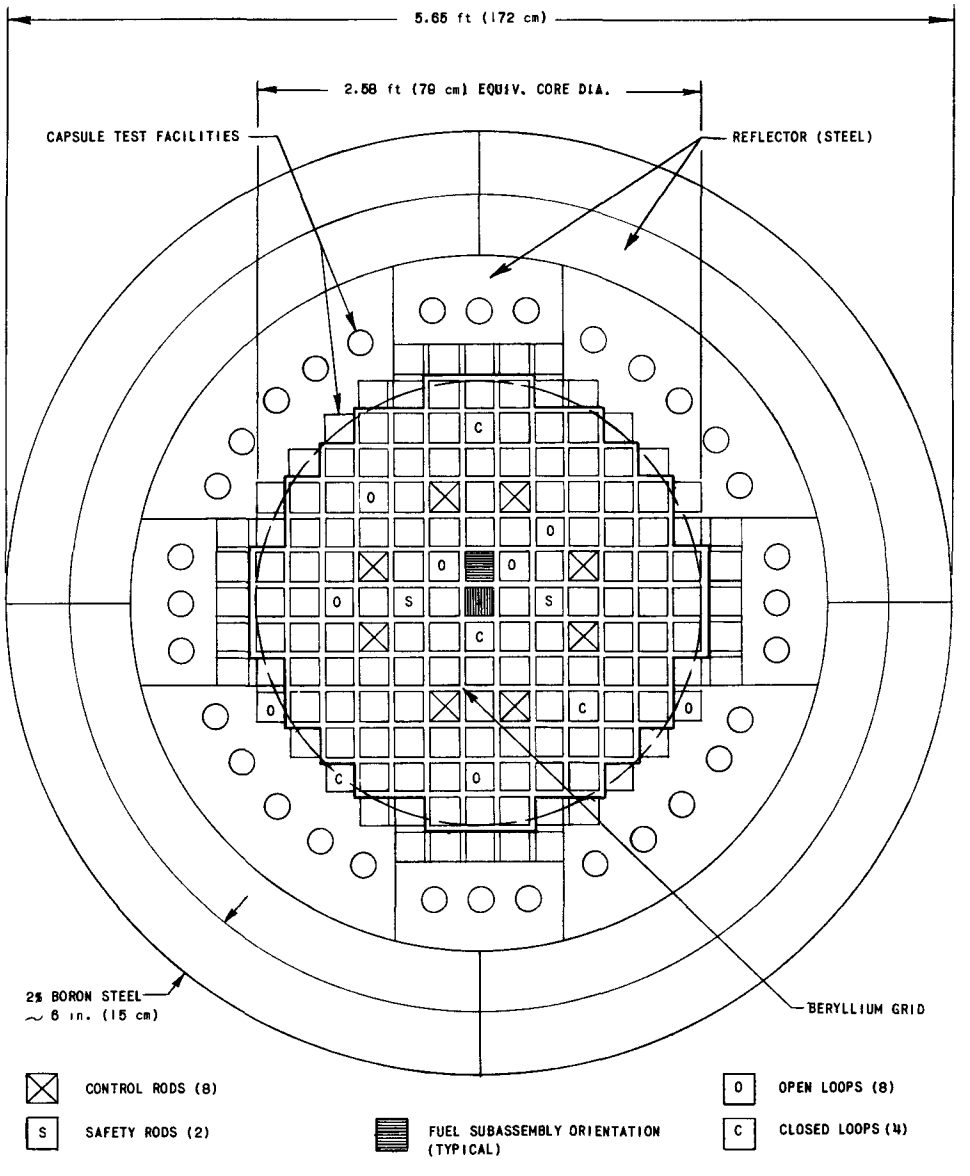

FIG. 3
FAST FUEL TEST REACTOR CORE PLAN

elements will be partially withdrawn during reactor operation. Two other like assemblies are safety rods which will be fully withdrawn during reactor operation. The two safety assemblies (fully withdrawn) and the eight partially withdrawn control assemblies may be released to effect rapid reactor shutdown. Also, there are four lattice openings that are completely enclosed within individual pipes or "closed loops," and eight that have individual supply pipes or "open loops." Thus, there are a total of 155 lattice openings, including those occupied by the loops, that may be used for loading of normal fuel elements, but any or a number may be occupied by specially fabricated fuel elements or test sections.

The fuel assemblies are separated by a grid of beryllium metal, 0.4 in. thick, and extending over the full two ft (61 cm) of core height. It is planned that the Be would be left in place during refueling. Actual tests conducted on beryllium in sodium at 1100°F (590°C) have shown satisfactory corrosion resistance for reactor service by additions of calcium.(3) Reference 4 reports good corrosion resistance up to 1300°F (700°C).

4. Reactor Vessel and Cover

The reactor vessel (Fig. 4) is 6 ft (183 cm) in diameter, has a 0.75 in.(1.9 cm) thick wall and is 21 ft (6.4 m) high. The material is stainless steel or stainless-clad low alloy steel. The lower head is dished to distribute stresses and is penetrated by control rod guide tubes. Three main inlet pipes and three main outlet pipes of 16 in.(40 cm)diameter are shown for the circulation of the sodium coolant upward through the core. In addition, there are three outlet pipes of 4 in. (10 cm) diameter located just above the core for the purpose of circulating sodium at a low flow rate and at a lower sodium level during fuel transfer.

The vessel is surrounded by a secondary containment shell. The function of this shell is twofold: (1) it serves as a container if sodium should leak from the vessel, and (2) it provides an insulating space, thus limiting the heat transfer to the shielding components. An atmosphere of inert argon gas is maintained in the secondary vessel to prevent rapid enlargement of a leak with O_2 present. Leakage may be detected by means of electrical contacts located within the lower part of the containment vessel. These contacts would be shorted out to effect an alarm signal when covered with conductive sodium.

The reactor vessel and containment vessel are supported from a flange held at the floor level. Thus, expansion is downward, which is consistent with that of the other major primary components that are floor level supported. Since it is conceived that differential expansion will occur between containment and reactor vessel, an expansion joint is provided in the containment vessel so that the relative positions between containment vessel nozzles and pressure vessel nozzles can be maintained.

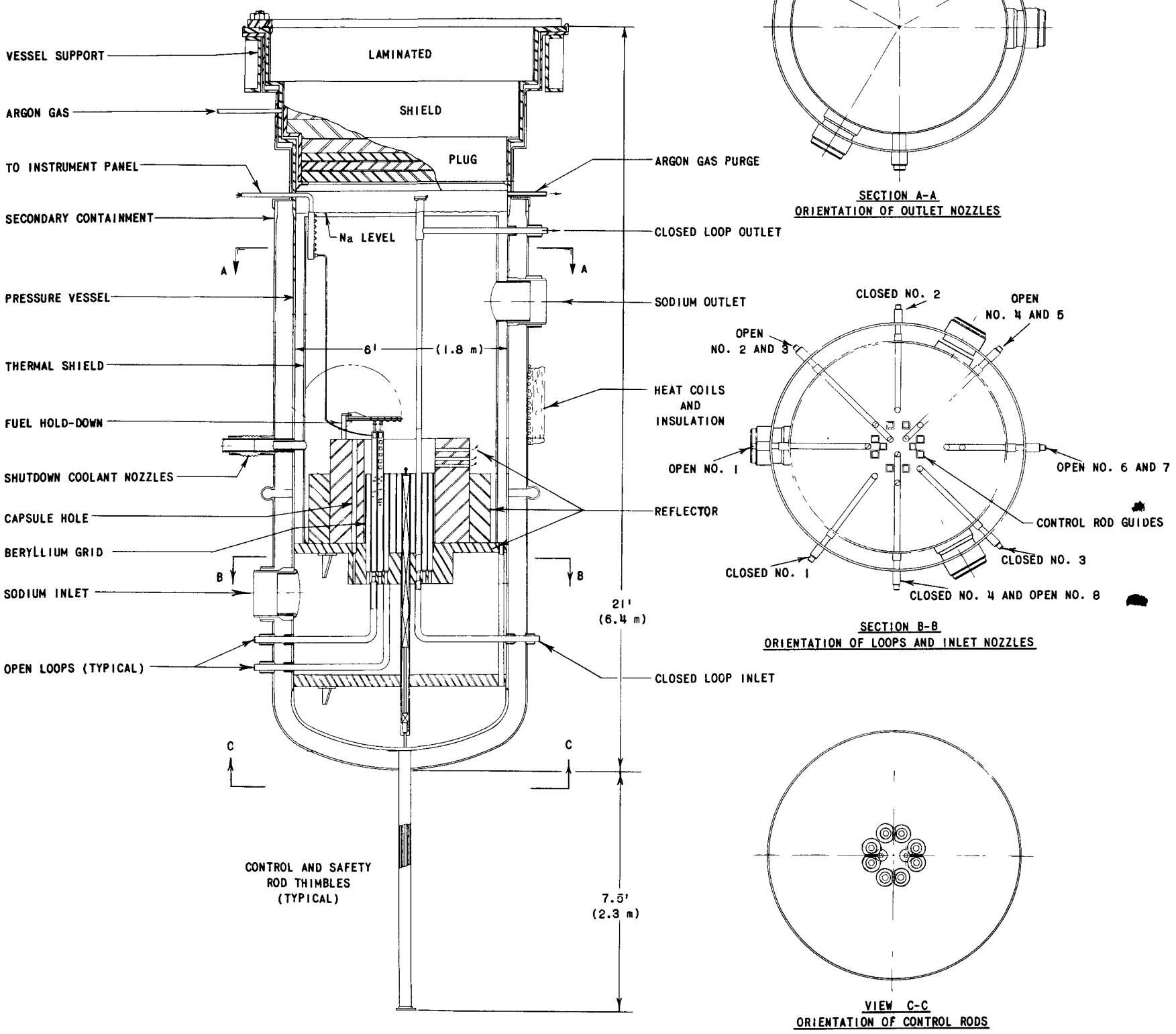

FIG. 4
PRESSURE VESSEL AND INTERNALS

satisfactorily. In addition, bellows connections are recommended at the nozzles of the containment vessel. The final joint between reactor and containment shell is seal welded so that interchange of gas between containment and fuel-transfer cell is excluded.

The reactor vessel closure is a simple cover,5 ft (152 cm) thick, consisting of laminated steel plates and some magnetite concrete. Cooling of the plug may be provided by means of argon gas circulation through the laminations between the steel plates. The gas gaps between plates would also prevent significant axial heat flow. The cover is bolted to the reactor vessel and a suitable gasket prevents leakage of blanket gas. A continuous supply of inert gas is introduced at the annulus between the plug and reactor vessel. Interchange of this gas and reactor blanket gas would be restricted by a metal labyrinth seal between pressure vessel and cover, as indicated in Fig. 4.

The shielding cover plug is raised by remotely operated jack screws and moved aside within the cell for complete observation of the reactor vessel during the refueling operation. Because of the absence of penetrations through the head, a reasonable cover thickness could be specified. If later studies should indicate that instrument connections or the like are to penetrate through the plug, it is proposed that this be done through a semipermanent annular ring. This would result in a cover of smaller diameter, which would probably make the refueling operations more difficult. At first a trough was visualized for the passage of experimental instrumentation leads into the fuel-transfer cell. These leads would connect with standard fittings to the shielding wall penetrations and then with the control panels. However, such a trough would make it possible for the hot gas within the reactor to leak into the fuel-transfer cell, particularly since the blanket gas in the reactor vessel is at the higher pressure (0.54 atm while the cell is maintained slightly below atmospheric pressure). The development of a suitable device for the sealing of leads within a trough was thought to be difficult. Therefore, the present instrument connections pass through the reactor shell. Appropriate union types of screw fittings are used inside the reactor vessel to connect the instrument with recording equipment in the test panel area. The leads may be pressurized with argon to eliminate the possibility of sodium entering the connectors. Placement of the screwed fitting manifold in the argon-filled portion of the vessel should also be considered.

Normally, the top of the vessel is at a temperature below the operating temperature of the reactor. Heating coils may be required around the pressure vessel at the plug location for the purpose of melting sodium should the sodium enter this cavity inadvertently or in the event that sodium vapors have deposited.

a. Core and Reflector Support

The core and reflector are supported by the lower grid section. This section is supported by brackets on the pressure vessel wall and is considered as a permanent assembly within the pressure vessel because of the loop attachments. The grid openings are for the insertion and support of the fuel elements. Control rod guides, cylinders and dashpots are a part of the grid section.

The reflector is fastened to the lower grid section and forms the core perimeter. Interlocking, but removable, beryllium plates are spaced in the core to form the 6.35 cm square lattice openings for the fuel elements and capsules.

b. Hold-down Grid

The hydraulic force on a fuel assembly due to the sodium flow is greater than the weight of the assembly. To prevent the fuel assemblies from lifting out of their support sockets, suitable hold-down devices must be used. The hold-down grid shown in Fig. 4 consists of several hinged sections containing spring members that fit over the ends of the fuel elements. The spring members allow for thermal expansion and contraction, and other minor dimensional variations. During the refueling operation, the hold-down grid is swung out of the way for removal of the fuel elements and also for the removal of the steel reflector plates located between the fuel element assemblies.

c. Reflector

The axial reflector region is formed above and below the core by the steel fuel plate extensions and a steel grid between the fuel assemblies. The radial reflector region is formed by solid steel or laminated sections to avoid high thermal stresses. There is a reflector approximately 30 cm thick above and below the core and 46 cm in the radial direction. Vertical holes for capsule irradiation are provided within the reflector. Provisions would be made for coolant flow through the reflector and through or past the capsules. The coolant flow through the capsule facilities may be regulated by orifices that are an integral part of the capsules. The outer 15 cm of this reflector contains steel with $\sim$2 wt % natural boron to limit the secondary capture gamma heating in the pressure vessel wall.

5. Control and Safety Rod Drives

The control rods for the FFTR are bottom mounted to improve viewing of and access to the core during the reloading operations. Thus, there are no penetrations through the top plug that could present difficult shielding and mechanical problems.

There are two types of control rods particularly adaptable for bottom mounting. One is the conventional rack and pinion, for which a suitable seal or canned motor and speed-reducing device is required. The second device is the magnetic jack type, an actuator which can be completely canned. It is considered that this latter device offers good possibilities for success in this application. The number of moving parts within the sodium is reduced to a single vertical rod for each drive which is actuated by externally located magnets. Clean sodium, coming from the cold trap, could be admitted to the control rod thimbles and heated by the magnet coils. In this manner, precipitation of oxides and impurities may be held to a minimum to insure satisfactory rod operations.

The control and safety rods consist of a fuel and poison section. Upon de-energizing of the electrical circuit of the magnetic jacks, the poison section of the rods will be inserted in the core. The speed of each rod is reduced at the bottom of the stroke by means of a dashpot. Preferably, the dashpots should be designed so that they can be replaced in the event of malfunction. The safety rods are identical in configuration to the control rods. Normally, the safety rods will be fully withdrawn during operation. Eight control rods and two safety rods are shown.

The control and safety rods should be hydraulically balanced to reduce upward hydraulic force. This may be accomplished by a balance piston at the lower end of the control rod assembly (see Fig. 4). For reactor shutdown, it should be possible to insert a balanced control rod within 0.5 sec. The balanced control assemblies may be inserted more rapidly during a reactor shutdown if the sodium in the lower portion of the pressure vessel is allowed to flow to a container at a lower pressure or by additional spring devices.

6. Biological Shield

The biological shield above the reactor is of essentially two parts, i.e., the shield cover plug and the walls of the fuel transfer cell. Both sections are 152 cm thick. The cell walls are constructed of magnetite concrete (density of 3.6 gm/cm^3). The shielding in the radial direction is compartmentalized by a 152 cm primary shielding wall surrounding the reactor to reduce secondary sodium activation. A 152 cm shielding wall placed through the reactor building separates the radioactive components from the test operational area of the building. Access to the main system and open test loop components can be made only after extended shutdown periods of approximately 17 days, at which time the sodium radiation level is 10 mr/hr. Dumping the sodium from some of the components may be used as a means of reducing activity levels for purposes of access. In any event, access to these areas should be made

only after sufficient ventilation and health survey procedures have been completed. For the closed loops, shielding walls should be provided for personnel access during reactor operation.

7. Experimental Facilities

The facilities for the irradiation of experimental fuel have been designed toward the following three objectives:

(1) sodium cooling as an integral part of the facility;

(2) accessibility of fuel specimens for thermocouple leads or similar devices; and

(3) loading and unloading of test samples to be performed from the top of the reactor.

a. Capsule Facilities

With the illustrated core configuration, it is possible to test at least 40 core capsules. Making the core capsule configuration identical to a fuel subassembly would provide sufficient flexibility so that any fuel location can also be used to hold a short core capsule. Also, short fuel assemblies may be installed above and below a short core capsule to maintain the required core loading. It is expected that mainly structural materials would be in the core capsules, but some fuel samples could be introduced as well. It is visualized that the core capsules might typically contain a total of 1 kg of Pu^{239} plus several kg of miscellaneous structural materials.

If the reactor operates at a flux equivalent to 1×10^{16} fast, some experiments might be located in the reflector to avoid too high a power density. There are presently 32 full-length capsule facilities within the reflector (Fig. 3); these are round holes to which sodium would be admitted for cooling purposes. The clearance around a capsule of a suitable orifice at the inlet to a capsule may function to allow a predetermined flow rate of sodium coolant. A stainless steel plug could be inserted within the reflector of facilities that are not in use.

There is sufficient reflector material to permit more or varied shaped test holes if such is desired. Further, a complete reflector section might be removed and substituted by another desired configuration.

All facilities are accessible from the top to accommodate both sample and reactor fuel insertion. A central manifold has been included for connecting the experimental sheathed thermocouple leads

to associated test control stations (see Fig. 4) in order to permit measurement of specimen temperatures. These connections will be screwed tight; since they are below the sodium level, this instrument device could also be pressurized with argon to prevent inleakage of sodium.

It is expected that most fuel irradiations would be performed in loops that enable coolant flow control with consequent temperature control for the specimen during irradiation. Both open and closed loops have been included as part of the reactor structure. Figure 5 illustrates the manner in which the loops are installed in the reactor core.

b. Open Loop Facilities

Most of the irradiations could be performed in open loops. In this type of loop, a portion of process sodium from the main inlet is bypassed to the inlet of the test section. A schematic flow sheet for this loop is shown in Fig. 6.

An electromagnetic booster pump is used to control flow. Also, suitable throttle valves, electric heaters and measuring devices would be parts of this loop. Control of specimen temperature would be accomplished by varying sodium flow, or by adding heat to the coolant stream. Sodium discharge from this loop or test section would mix with the sodium above the core, hence the notation of "open loop." The most attractive features of the open loop are:

(1) Samples may be readily changed.

(2) Thermocouple leads can be readily incorporated.

(3) Additional facilities to remove sample-generated heat are not required.

(4) Access to the core is relatively unrestricted.

Eight open loops are provided, six of which are in the core and two in the reflector (see Fig. 3).

A typical loading might be an average of 20 EBR-II-type pins per loop. For the eight loops, this would amount to a total of perhaps 3 kg of Pu^{239}. Control of flow in the loop should tie in with the reactor operating panel. For example, failure of the electromagnetic booster pump should shut the reactor down, although a reduced flow rate of sodium would be maintained through the test section, since the open loop is a take-off from the discharge of the main pumps.

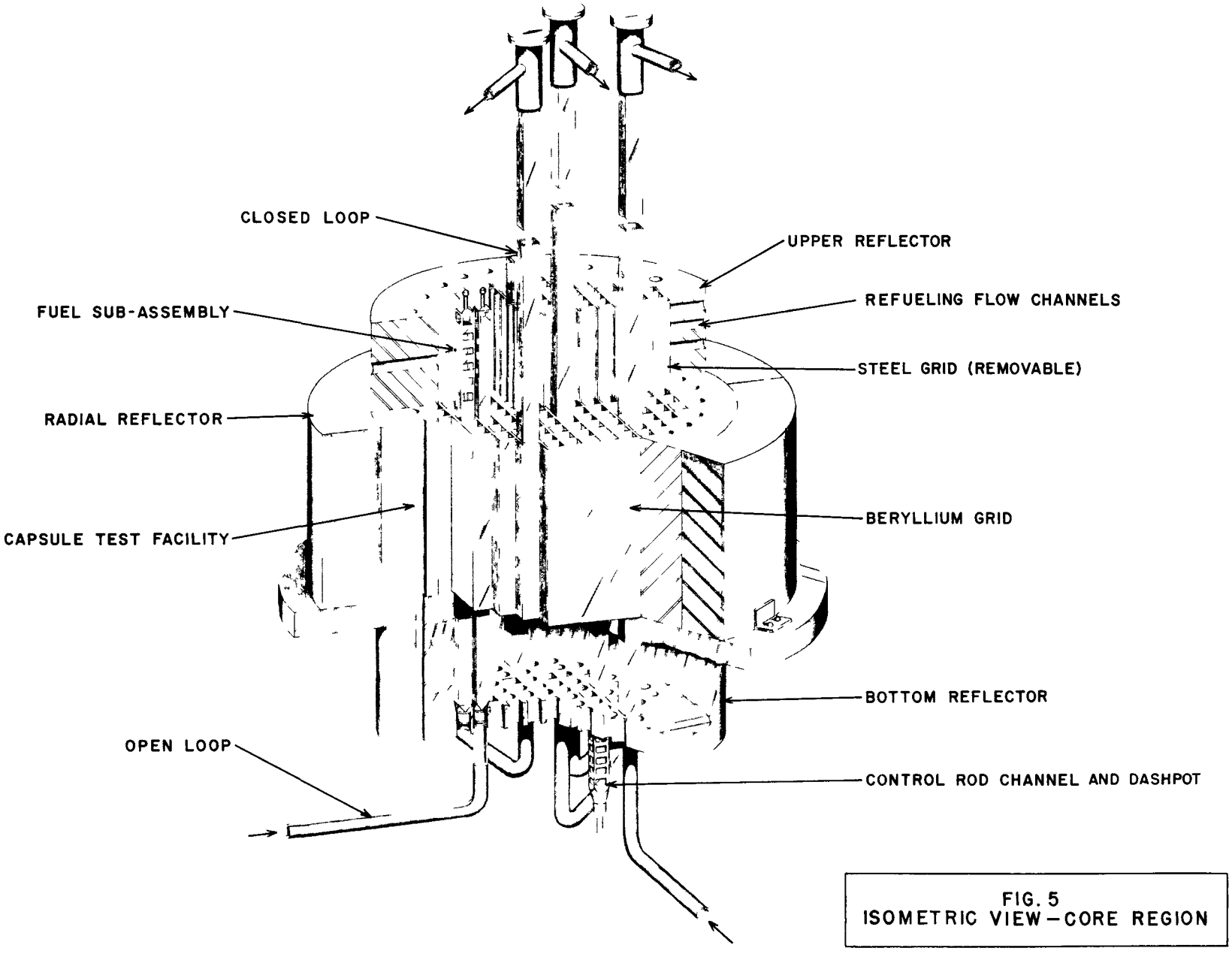

FIG. 5
ISOMETRIC VIEW—CORE REGION

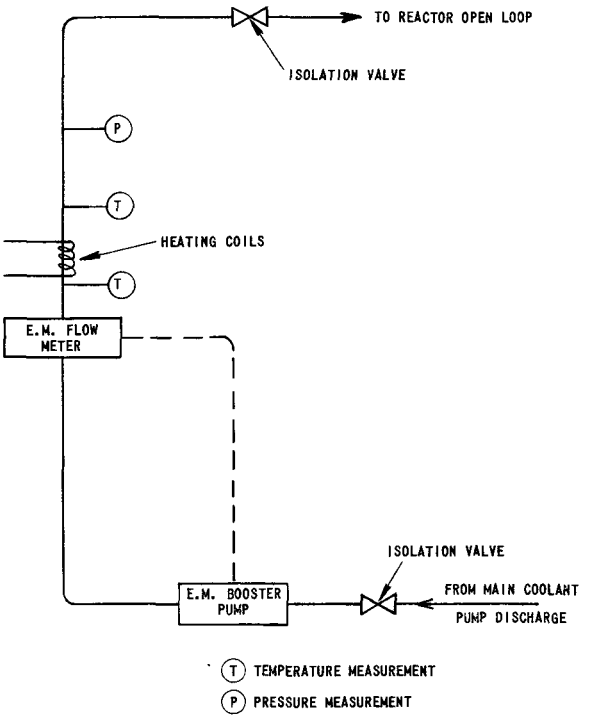

FIG. 6
OPEN LOOP FLOW DIAGRAM

For the case in which only FFTR fuel would be in the open loops, the open loops would form an essential part of the reactor cooling operation and this phase should be transferrable and controllable from the main control panel.

c. Closed Loop Facilities

A closed loop is shown schematically in Fig. 7. Three closed loops are provided within the core and one in the reflector. These loops are designed for more advanced types of experiments. For example, the irradiation of vented fuel assemblies and the release of radioactive products into the coolant stream may be separately investigated. Also, other metallic coolants could be used.

As in the case of the open loops, the closed loops are designed as part of the reactor structure. The top of the test section terminates in a tee to permit horizontal exit of the discharge line and normal vertical loading of samples. When in full operation, the closed loops might typically contain a total of 2 kg of Pu^{239}.

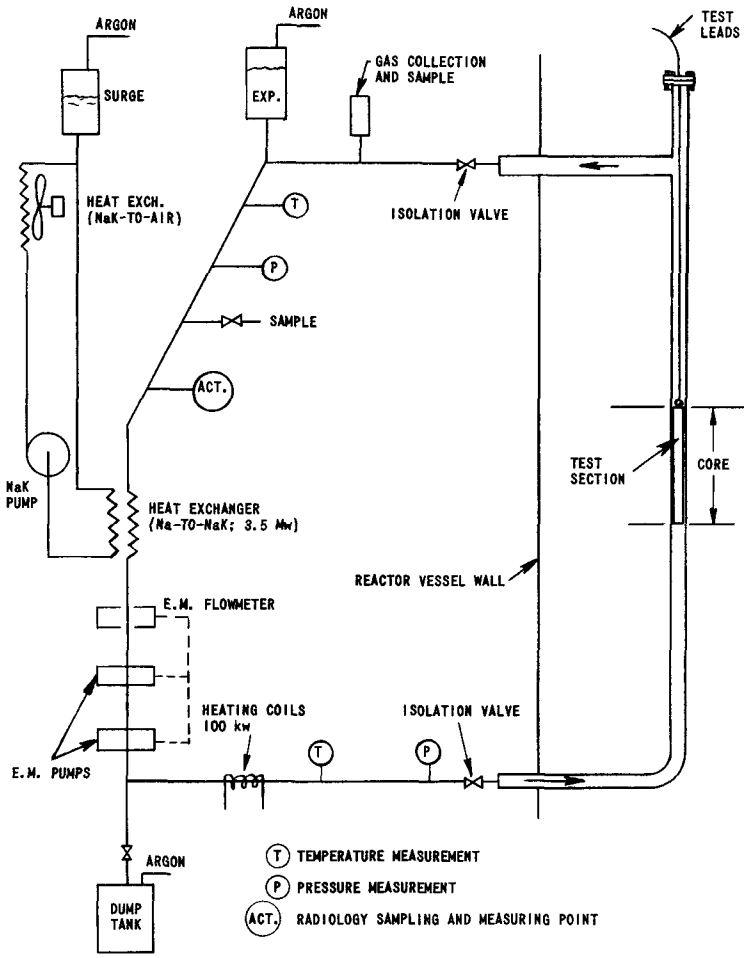

FIG. 7
CLOSED LOOP FLOW DIAGRAM

B. Cooling Systems

1. Primary System

Molten sodium is employed as the coolant in the primary system. The selection of sodium over the sodium-potassium alloy of lower melting point was dictated by improved heat transfer characteristics, lower chemical activity and lower cost.

Three primary coolant loops are provided as shown in Fig. 8. The normal system flow rate is 25,400 gpm (1.60 m^3/sec). At a reactor power level of 200 Mw(t) the sodium temperature rise would be 200°F (110°C).

Heat from the reactor is transferred in an intermediate heat exchanger to NaK in each of the three primary loops. As shown in Fig. 9, the flow path will be upward through the reactor, downward on the tube side of the intermediate heat exchanger, and then to the pump tank.

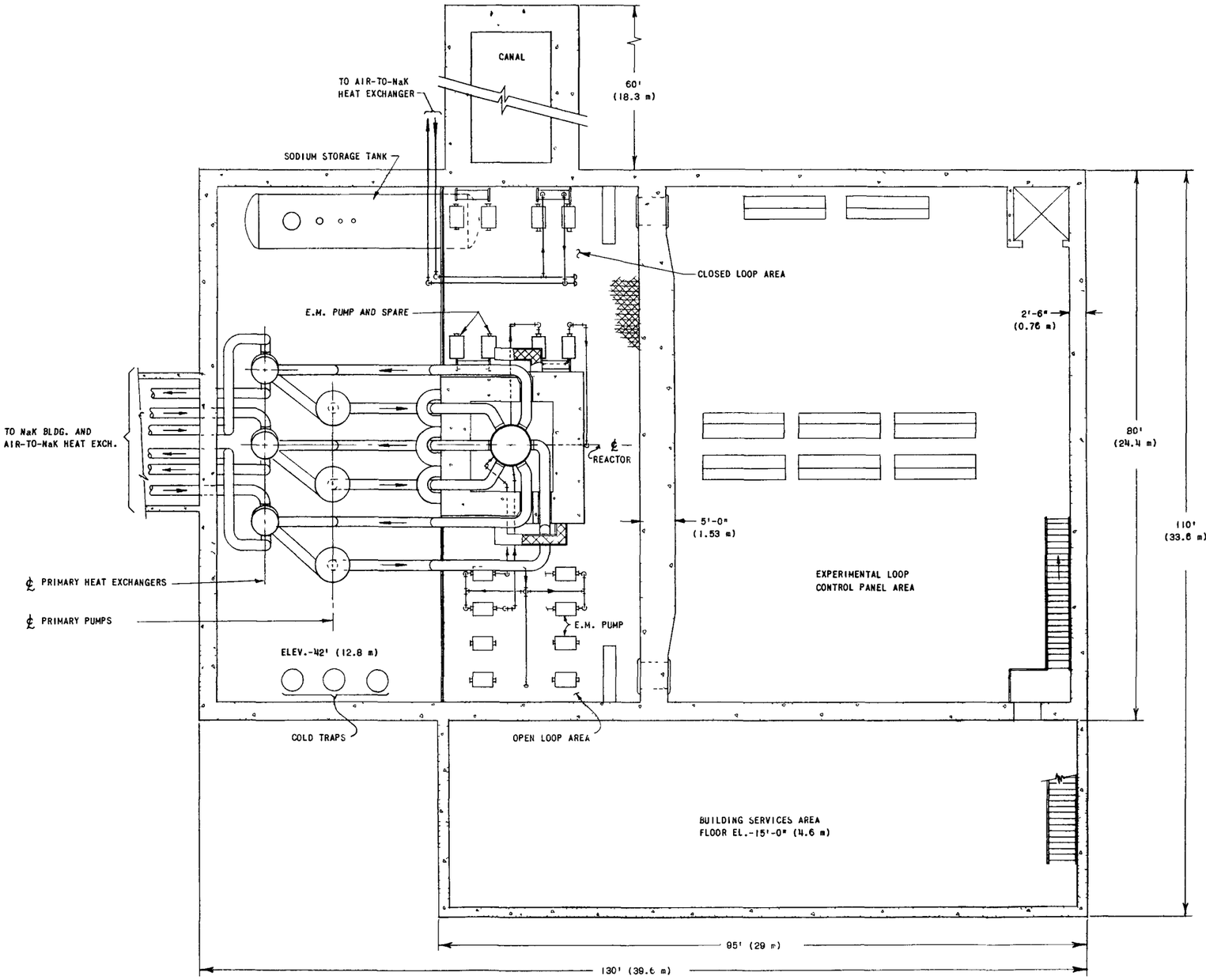

FIG. 8
PLAN BELOW OPERATING FLOOR
REACTOR BUILDING

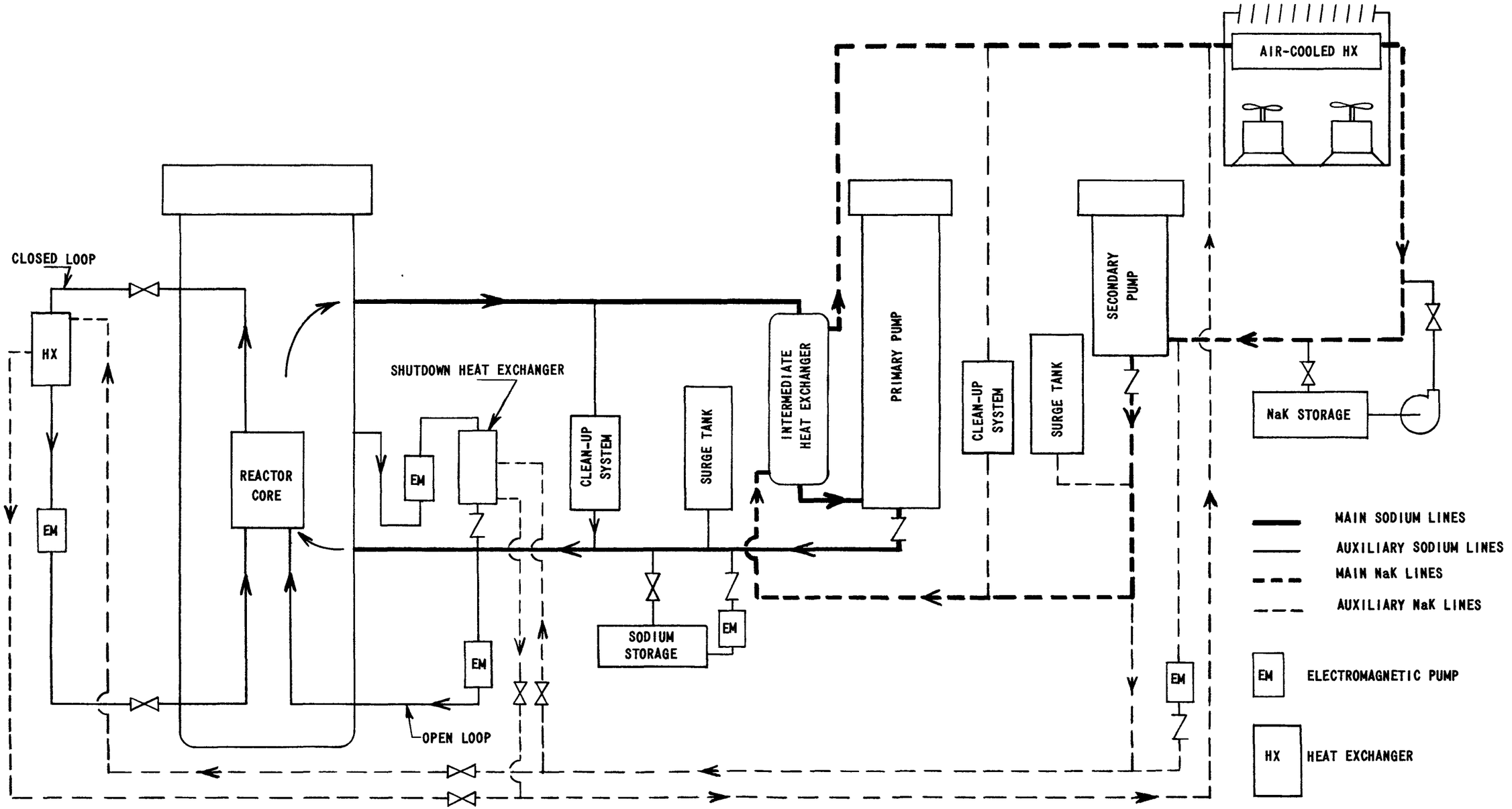

NOTE: ONLY ONE OF THREE MAIN CIRCUITS SHOWN.

FIG. 9
PLANT FLOW DIAGRAM

The intermediate heat exchangers are planned as shell-and-tube type with nonremovable tube bundles. It is believed that satisfactory designs are commercially available for this application. In order to effect some natural convection flow for shutdown cooling, the intermediate heat exchangers would be elevated with respect to the reactor core. It is proposed that the exchangers be positioned vertically to avoid problems of thermal stress, which could arise during low flow rates in horizontal or inclined heat exchangers.

In the preliminary study, consideration was given to a heat exchanger design with size characteristics as given in Table II. The exchanger is designed for operation at 83 Mw in anticipation of increased reactor power capabilities, a procedure which also provides some allowance for 67-Mw operation at lower sodium temperatures.

Table II

INTERMEDIATE HEAT EXCHANGER DESIGN DATA

(1) Description

Shell-side fluid	NaK
Tube-side fluid	Na
Number of tubes	918
Tube length, ft (cm)	10 (305)
Tube OD, in. (cm)	$\frac{5}{8}$ (1.6)
Surface area, ft^2 (m^2)	1,500 (139)

(2) Operating Conditions at 200 and 250-Mw Reactor Power

Heat transferred, Mw	67	83
Na flow rate, gpm (m^3/sec)	8,470 (0.535)	8,470 (0.535)
Na inlet temperature, °F (°C)	800 (427)	800 (427)
Na outlet temperature, °F (°C)	600 (316)	550 (288)
NaK flow rate, gpm (m^3/sec)	10,700 (0.675)	10,700 (0.675)
NaK outlet temperature, °F (°C)	648 (342)	610 (321)
NaK inlet temperature, °F (°C)	448 (231)	360 (182)
Heat transfer rate, Btu/(hr)(ft^2)(°F)[watts/(cm^2)(°C)]	990 (0.56)	990 (0.56)

Calculated exchanger conditions are given for three loop operation with reactor power level at 200 and 250 Mw. Heat transfer coefficients used in these analyses were obtained from Ref. 5 and 6.

The main piping is nominally 40 cm in diameter, and the material is stainless steel. All primary components have surrounding sheathing for the purpose of leakage containment. The primary component sheathing is of a magnetic steel material so that 60-cycle induction heating coils may be used for preheating the system and for maintaining the sodium in a liquid state.

The main coolant pumps are of the centrifugal sump type and each pump is capable of circulating 0.55 m^3/sec at a total head of 56 m. These pumps supply all of the reactor coolant (including the open experimental loops) with the exception of the four closed experimental loops. Each closed experimental loop has individual electromagnetic pumping equipment to circulate its coolant independently of, but concurrently with, the main system pumps. The design of the main coolant pump would allow removal for repairs without draining sodium from the system and without cutting the main piping. It is considered essential that means for controlling the main coolant flow rate should be provided such as a variable frequency power supply or hydraulic or electrodynamic coupling.

The sodium levels in the reactor vessel and primary pump tank are controlled by argon gas under pressure (see Fig. 10), thus avoiding the problems of sealing sodium directly. Although a surge or expansion tank is shown in Fig. 9, future studies may indicate that the space above the sodium levels in the reactor vessel and pump tank can be used effectively to accommodate surges and thermal volume changes of the sodium.

2. Secondary System

The secondary coolant is a sodium-potassium (NaK) alloy consisting of 56 wt % sodium and 44 wt % potassium. This coolant represents a compromise between heat transfer properties and low freezing point (19°C as compared with -11°C for eutectic NaK and 98°C for sodium). Since the secondary system heat is dissipated to the atmosphere in a NaK-to-air heat exchanger, the low freezing point of the NaK would give a better margin in avoiding freeze-up in the air-cooled heat exchanger at low load and low ambient temperature conditions. However, it is felt that a reliable air-cooled heat exchanger system may be designed to circumvent freeze-up conditions so that sodium could also be selected for use in the secondary system. The air-cooled heat exchanger is composed of several sections or banks of finned tubes. Air is circulated across the tubes by blowers or fans. The exchangers are equipped with a short stack

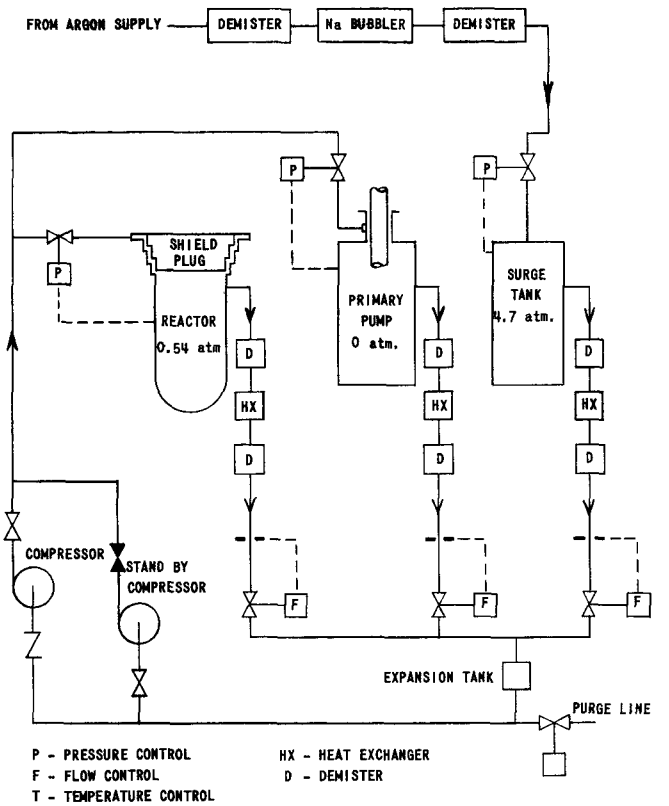

FIG. 10
ARGON GAS PRESSURIZING AND FLOW DIAGRAM FOR PRIMARY SODIUM SYSTEM

to assist natural circulation and to prevent recirculation of the exhaust air. Temperature control could be achieved by means of dampers and/or motor-speed variation to regulate the air flow rate during power operation and by additional heating devices during extended idle periods. Characteristic data for an air-cooled heat exchanger section are shown in Table III.

There is one section for each of the three secondary loops. Heat transfer, fluid friction and dimensional data for the exchanger surface were obtained from Ref. 7. The installed blower capacity would be considerably greater than the requirements indicated in Table III, to allow for possible operation at lower reactor temperatures.

There are three sump-type centrifugal pumps capable of circulation of approximately 32,100 gpm (2.02 m^3/sec), one pump for each of the three loops. These pumps, surge tanks, and most of the NaK service equipment would be housed in a separate building structure apart from the reactor building. This equipment should be readily accessible for routine inspection.

Table III

AIR-COOLED HEAT EXCHANGER DESIGN DATA

(1) Description

Tube diameter, OD, in. (cm)	1.0 (2.54)
Number of tube rows	6
Number of fins per in. (cm)	8.8 (3.5)
Finside surface area, ft^2 (m^2)	114,000 (10,600)
Fin material	aluminum

(2) Operating Conditions at 200 and 250 Mw Reactor Power

Heat transferred, Mw	67	83
Air flow rate, lb/hr (kg/sec)	2.37×10^6 (299)	3.91×10^6 (493)
Design air inlet temperature, °F (°C)	100 (38)	100 (38)
Air outlet temperature, °F (°C)	500 (260)	400 (204)
Pressure drop over tube bank, H_2O in (cm)	0.6, 1.5	1.3, 3.3
Required fan power, (kw)	(72)	(270)
Heat transfer rate, Btu/(hr)(ft^2)(°F) (watts(cm^2)(°C))	9.4 (5.3×10^{-3})	12.1 (6.8×10^{-3})

3. Shutdown Systems

For refueling the core, the primary sodium inlet temperature will be reduced to approximately 280°F (138°C) and the level in the reactor vessel will be lowered until the tops of the fuel elements are visible. During this procedure it is proposed to dissipate decay heat to a shutdown cooling system. Gravity flow of primary sodium would take place from the reactor through smaller nozzles in the vessel (placed slightly below the top of the fuel assemblies) to one of three auxiliary cooling loops. Each of these loops would contain an electromagnetic pump and intermediate heat exchanger. During refueling, the primary flow rate would be approximately 500 gpm,(0.03 m^3/sec) limiting the average sodium temperature rise to 20°F (11°C) (at 0.2% of full power).

The secondary side of this system would also use a NaK coolant, electromagnetic pump, and an air-cooled heat exchanger. Since it is desirable that the air side of the system operate satisfactorily by natural convection, and because of the relatively low temperatures desired in

the primary system, it is expected that extensive heat transfer area will be required. It is therefore proposed that a portion of the regular NaK-air heat exchanger serve on the secondary side of the shutdown cooling system.

It is conceivable that long-term shutdown cooling can be accomplished by natural convection in the present cooling system. However, where certain shutdown conditions produce sodium or NaK temperature patterns which prevent stable convection circuits from being established, the refueling cooling system may be used effectively. Pumps in this system would require an auxiliary power supply for use during loss of normal power.

4. Cleanup Systems

The cleanup system for the primary and secondary cooling systems will be similar, except that provision must be made for the radioactivity of the primary system. Basically, both systems will use a cold trapping system. However, because of the restrictions imposed by the beryllium metal in the core, the maximum effectiveness of the cold trap of 6 ppm sodium oxide equilibrium is probably inadequate. It is visualized that conditions of <1 ppm sodium oxide equilibrium are desirable to reduce the beryllium corrosion rate.* In order to obtain these conditions additional hot trapping facilities or the utilization of gettering agents, such as calcium metal, are required. Acceptably low corrosion rates of beryllium can be obtained by suitable cold trapping followed by calcium deoxidation of the liquid metal.[3]

The cold trapping system would essentially consist of a cooled section, in which the oxides and hydrides are precipitated out on filtering media, such as screens and steel wool, and a plugging indicator to monitor the effectiveness of the cold trapping operation.

C. Auxiliary Systems and Components

1. Fuel and Test Specimen Handling

One of the significant features of the FFTR is the fuel-transfer cell which is located directly above the reactor and contains shielded windows (see Fig. 11) through which the handling of the spent fuel can be visually followed. The viewing may be done with the aid of mirrors and/or binoculars. In this way, the location of fuel and test specimens can be seen after the level of the sodium within the reactor vessel is lowered below the top sections of the fuel assemblies.

Commercially available manipulators are used within the shielded cell and these are operated from the outside of the cell.

---

* Personal Communication, V. Rutkauskas, Argonne National Laboratory

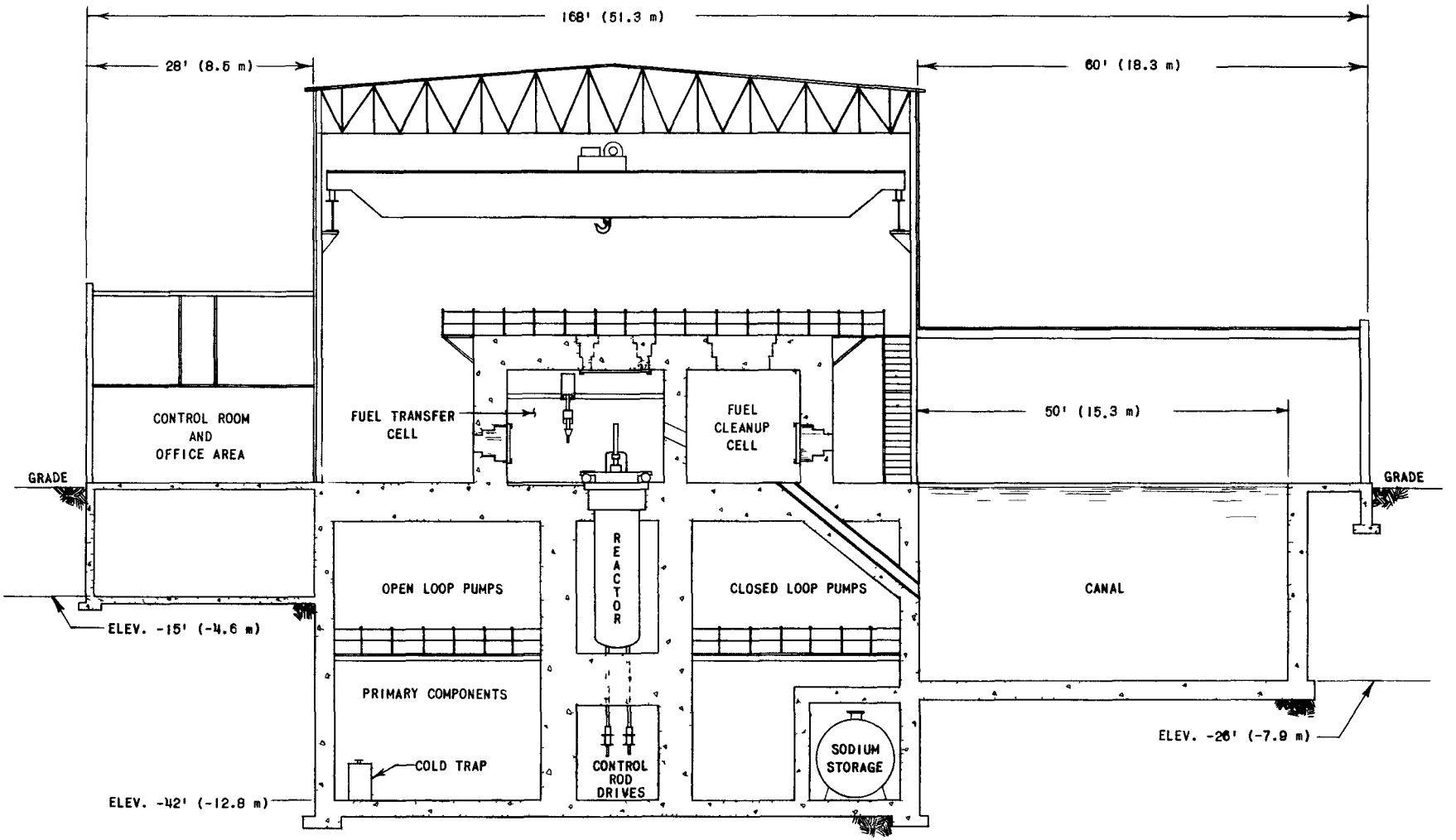

FIG. 11

TRANSVERSE SECTION-REACTOR BUILDING

The inside surface of the shielded cell is covered with a welded and sealed steel surface which serves as a hermetically sealed membrane. Argon gas of high purity is circulated within the fuel-transfer cell and its pressure will be maintained slightly below atmospheric. This is to prevent escape of gas, which may include fission products, to the atmosphere should a defect develop in the sealed membrane. Accidental inleakage may cause excessive oxidation of the sodium; for this reason, the cell membrane should be of exceptional integrity. The cell could be tested by a tracer technique and slight pressurization during the reactor operation or just prior to reactor startup.

It is recognized that the transfer of spent fuel with an argon atmosphere is complicated by the poor heat transfer characteristics of the argon gas. However, decay times of the order of 12 hours can be allowed for the FFTR fuel to reduce the heat transfer problem within the cell (see Section VII-E).

Spent fuel is transferred directly to the adjacent air-filled cleaning cell through an argon-filled transfer lock. The air pressures within the cleaning cell and the transfer lock could be independently adjusted to preclude the possibility of air passing from the cleaning cell into the fuel-transfer cell.

A transfer chute leads directly from the cleaning cell to the water canal which permits direct transfer of the spent fuel into the canal, thus avoiding the use of a mobile transfer coffin at this point.

A convenient reactor operating cycle from the standpoint of the users would be an integral number of weeks. For example, the reactor could be started up every fourth week with a cycle of $3\frac{1}{2}$ weeks of operation and a half-week shutdown. The fuel could probably be used for several such cycles and would presumably be replaced partially at each shutdown. However, because the operation of a high-temperature, sodium-cooled plant is considered more complex than a water-cooled reactor, such as MTR or ETR, the cycle may be extended. The shutdown procedure could involve the following steps, typically:

(1) Reduce the reactor power and lower coolant temperatures. Reduce pumping rates.

(2) When a primary coolant inlet temperature of 280°F(138°C) is reached after approximately 12 hr of radioactive decay, and the balance of the system and test loops are regulated consistent with the decay power operation, the pumping operation is transferred to the electromagnetic refueling pump.

(3) The sodium levels and argon gas pressures are adjusted in the system components to permit equalization of cell and reactor pressure.

(4) Unbolt the reactor cover with remote tools.

(5) Raise the reactor cover and move cover over to side of the cell on its wheel tracks.

(6) Lower the sodium level to uncover fuel element hold-down devices and grip-ends. (Note: Sodium circulation is maintained at all times to remove decay heat.)

(7) Loosen the hold-down devices of those elements to be transferred.

(8) Lower the manipulator and grasp the desired fuel element.

(9) Remove and raise the element and, after reaching the cell, start argon circulation through the element. Replace removed element with new or dummy element.

(10) Transfer the fuel element through transfer lock to the cleanup cell (air atmosphere).

(11) Direct a stream of superheated steam over the element to remove sodium traces.

(12) Lower the element onto transfer mechanism and into water canal.

(13) Place the element into suitable racks in the canal to await further handling.

Additional steps would be required if the element is instrumented. In that case the instrument connection would have to be unscrewed and the instrument lead would have to be cut off close to the element prior to transfer. The leads could be rolled up on a suitable jig and also transferred through the fuel-element lock.

Removal of a fuel element or test section from a closed loop would require a reduced flow rate of sodium for removal of the closure and extraction of the element. A wire or a long sectional rod may be attached to the element to permit removal from the long loop tubes.

Access to the cell for the purpose of transfer of fresh fuel, capsules, tools, manipulator parts, etc., would be through conventional gas locks.

2. Inert Gas System

For both the primary and secondary cooling systems, argon gas is used for the purpose of maintaining an inert atmosphere over the coolant to prevent oxidation. Gas purity, pressures and operating

temperatures will be maintained consistent with the operating conditions in the various parts of the system. A schematic diagram showing the principal components and operating conditions for this system is shown in Fig. 12.

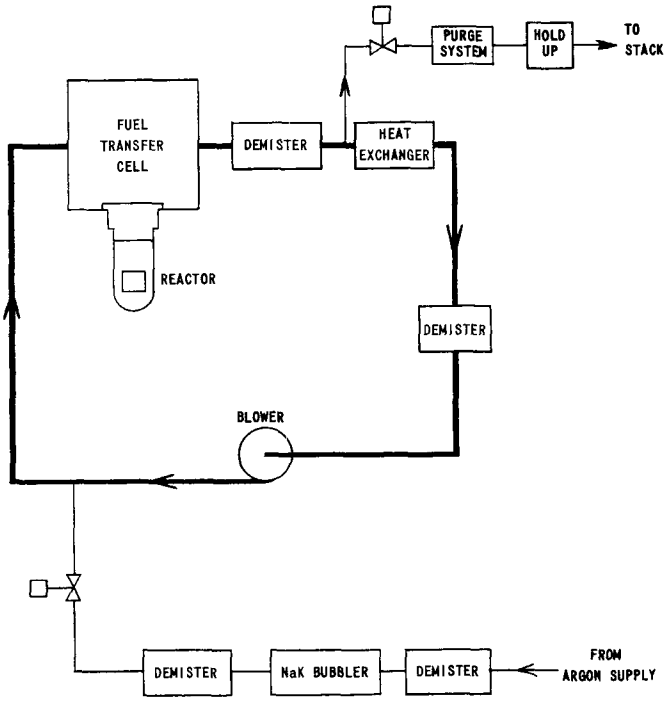

FIG. 12
ARGON GAS FLOW DIAGRAM
FOR FUEL TRANSFER CELL

The gas may be purged occasionally or at continuous flow rates, if necessary. The purged gas is monitored in the gas-treatment system and disposal area and contained if contaminated by fission products or discharged directly or diluted to the atmosphere.

3. Water Canal System

The canal location is shown in Figs. 8 and 11. The dimensions of the canal are 50 ft long, 12 ft wide and 26 ft deep (15.3 x 3.7 x 7.9 m). A transfer chute is to connect with the cleanup cell so that spent fuel elements, test capsules and other activated test devices may be readily transferred to the canal. To maintain desired water purity, a demineralizing system will be required. A stainless steel lining is thought desirable for minimum maintenance. After cooling for a sufficient time, the elements may be removed from the canal and transferred into shipping coffins.

4. Auxiliary Power System

Normally, the electrical load is supplied by the local public utility company. For the case where this power supply is interrupted, an emergency diesel generator provides reduced standby power. This diesel machine should have a generating capacity of 300 kw or sufficient to operate the plant in a shutdown condition. In addition, there should be battery standby power for operating essential instruments and devices in any event of malfunction.

D. Instrumentation and Control

The control and instrumentation systems are visualized as designed for essential central control (control room) of the reactor plant and auxiliary systems. If practical, control of individual processes are best handled locally. For example, control of the waste products would be a function which could be separated from the plant control. However, some of these systems may be represented by indicating or alarm systems within the control room for centralized information.

E. Electrical System

The electrical system has been estimated to supply roughly 7,000 kw to the plant during normal operation. It would consist of two 13-kv transmission lines, transformers, switchgear, etc., of the normal variety. In addition, rectifiers will be required for operating the dc magnetic pumps. Electrical heating coils are used on sodium and NaK equipment and piping to prevent freezing of the liquid metal coolants.

F. Buildings and Site Development

The building layout for the reactor site is shown in Fig. 13.

The reactor building structure measures 80 ft by 180 ft (24 x 55 m) and includes a service area accessible to the main building crane. Attached to the reactor building is a fuel-handling canal. Since water is used in the canal and humid atmospheric conditions may at times exist above the canal, a separate but attached building was specified. Because of the nature of the test fuels, special ventilation may be necessary for the canal area. A control room and office complex is shown immediately adjacent to the reactor building, thus utilizing the main building wall.

The reactor building is divided into two parts below the operating floor, separated by shielding (see Fig. 8). One-half of the building houses the reactor system and the other half is designated for experiments and tests (see Fig. 14). The operating floor is open for the most part for

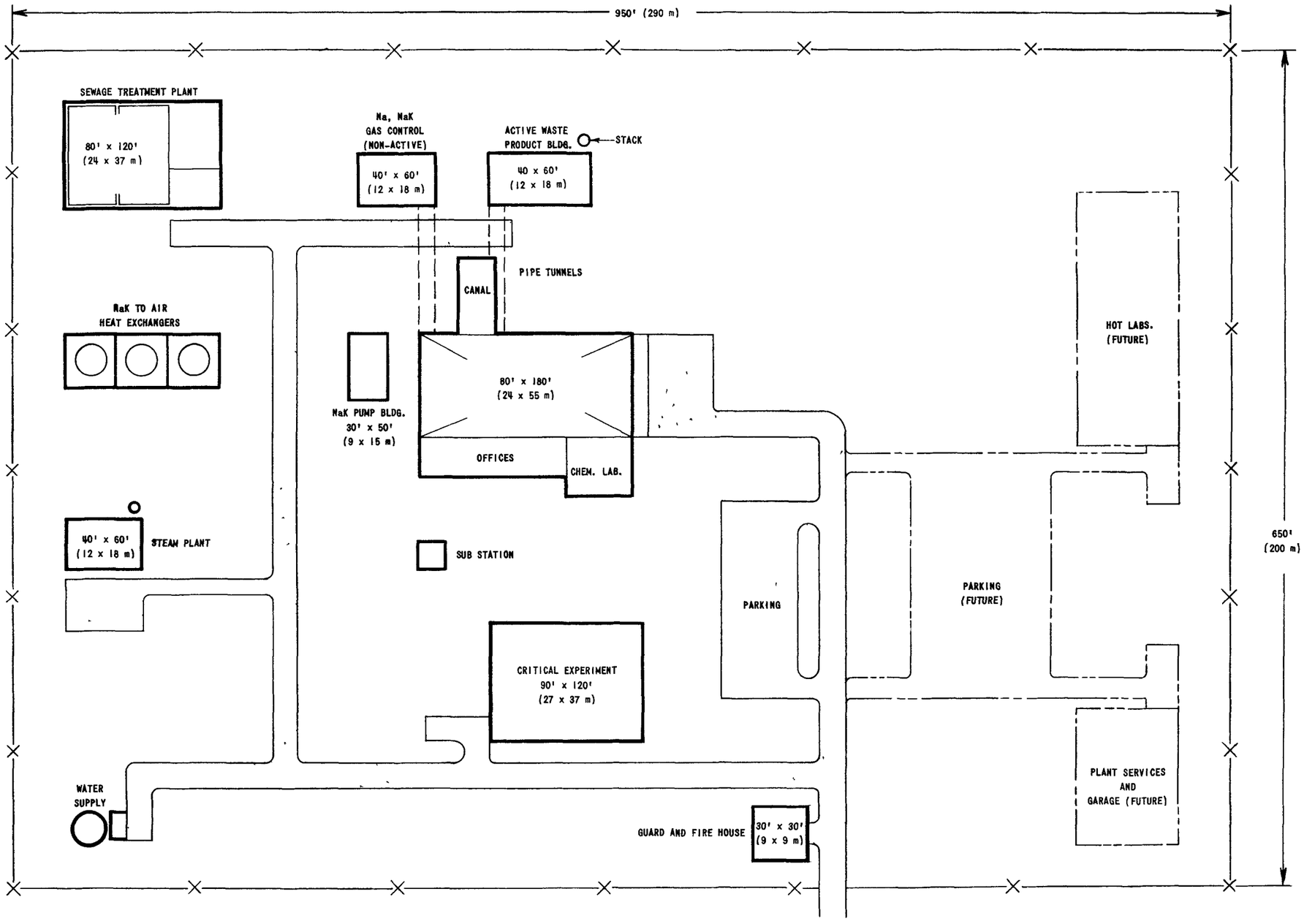

FIG. 13
BUILDINGS AND SITE PLAN

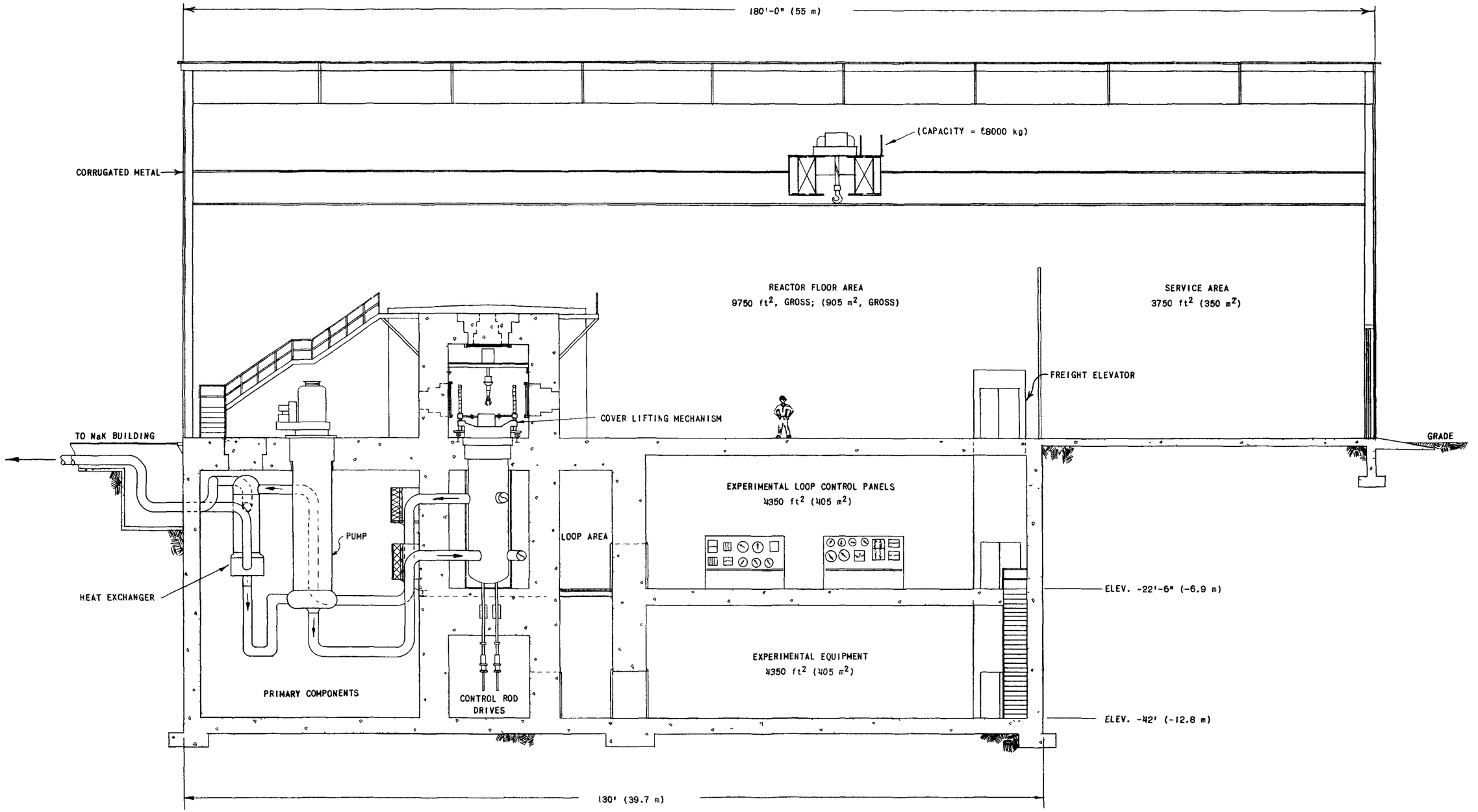

FIG. 14
LONGITUDINAL SECTION – REACTOR BUILDING

work area and service to the reactor, system components and experiments (see Fig. 15). Logically, removable plugs in the operating floor would provide access to the primary components should repair or removal be necessary.

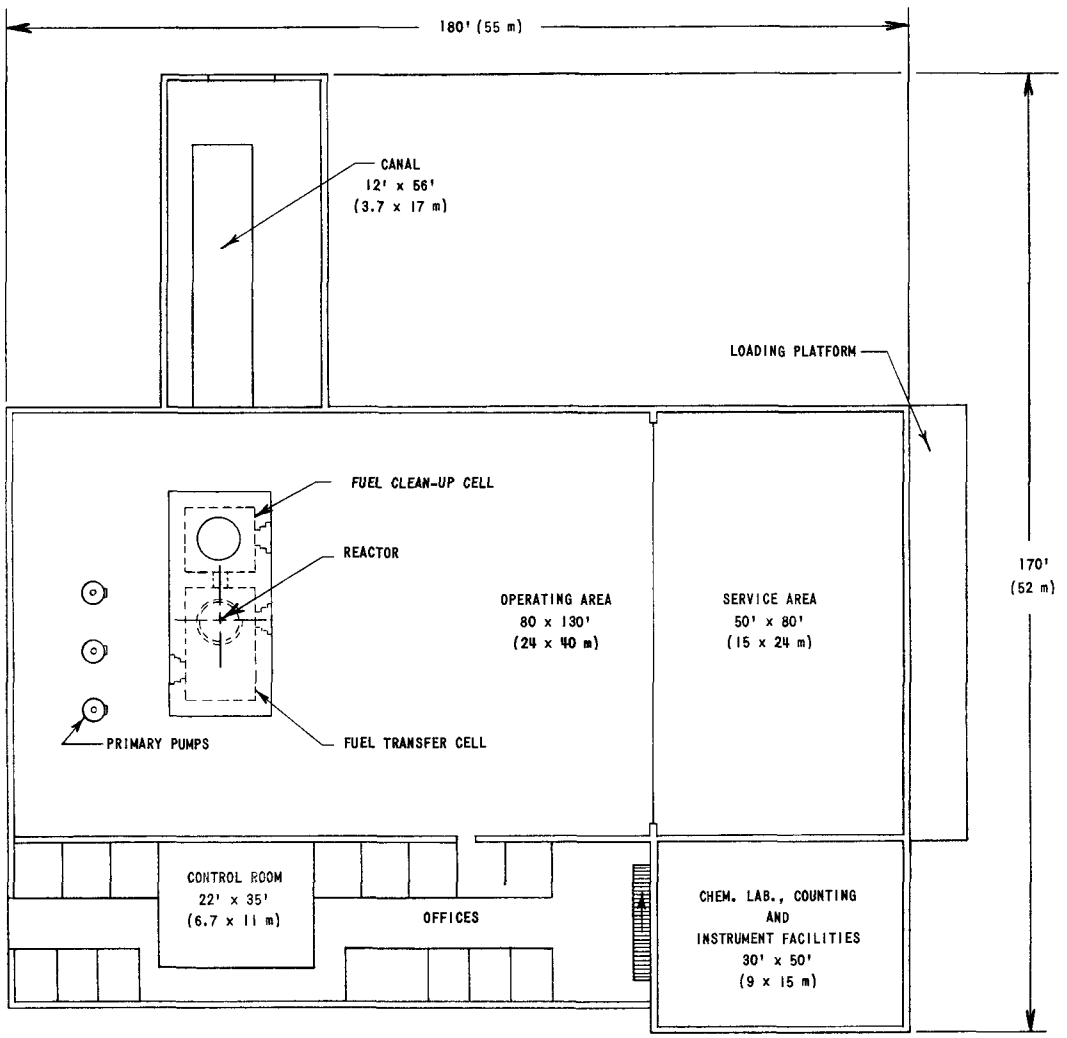

FIG. 15
FIRST FLOOR PLAN-REACTOR BUILDING

All the experimental loops are located behind the main shielding wall. Two levels are provided in the test area. A total of 8700 ft^2 (810 m^2) is available for work and instrument setup.

Since the reactor operation must be closely tied to the experiments and since the experimental elements are an essential part of the core loading, criticality experiments will be conducted on a continuous

basis. Thus a critical facility is visualized as an essential part of the reactor building complex. Construction experience at the Argonne National Laboratory has been applied in sizing and cost appraisal of this building.

An essential part of the inventory control of liquid metal and argon gas is one of storage and handling. It was thought that this operation could best be handled separately from the reactor building in a nonactive Na, NaK and gas-control building.

The control of waste (gaseous and liquid metal) is also considered to be a separate function from the reactor control. Operations such as filtering, compressing, venting, storage, processing and disposal were thought to be most effectively handled in a separate building. A tunnel has been shown as a convenient and safe means to house connecting piping which may contain radioactive gases or fluids. Released quantities are discharged into the stack as a part of the disposal operation.

The NaK pump building is shown separately from the main reactor building. The distance between these buildings serves as additional shielding for eliminating secondary sodium activation. Thus the NaK pump system is readily accessible for surveillance and maintenance. It was also thought that a separate pump building could be more economically constructed than a similar addition to the reactor building.

Other buildings and facilities that complete the plant complex are items such as water supply, steam plant, NaK-to-air heat exchangers and sewage treatment plant.

Also, an area has been included in the building layout for the addition of hot laboratories and a plant service garage, but these have not been considered as part of the most essential plant cost.

VI. PHYSICS

A. Cross Sections

Two principal sources of uncertainty in reactor statics calculations for the FFTR occur in the characteristics of the (n, 2n) reaction in beryllium and in the effective fission and capture cross sections of fissile materials in the intermediate energy region. The former uncertainty affects mainly the criticality of the system, while the latter is mainly important in determining the energy spectrum in the intermediate energy region and the sample power level and distribution. The uncertainties in the effective cross sections of intermediate energy fissile materials are caused by lack of knowledge of resonance parameters above 19 ev for U^{235} and above 53 ev for Pu^{239}, by the fact that the resonances are so closely spaced that they interfere with each other so that a single-level description is often inaccurate, and by computational difficulties associated with the latter fact and with the complexity of attempting to calculate spatial effects in resonance absorbers. Lack of information on resonance parameters handicaps calculation of the Doppler effect.

Two different sets of cross sections have been employed. One of these, given in Table XXI of Appendix A and hereafter denoted as Set I, was already available at ANL.[8] The cross sections for U^{235}, U^{238}, and iron above 0.009 Mev are the same as those given in Ref. (9) and were known to give reasonable results for fast reactors. The beryllium cross sections were based on the work of Ref. (10) with the elastic removal cross section for Group 1 adjusted to give the correct age when used in a calculation by multigroup diffusion theory. The intermediate energy cross sections in this set were not prepared with consideration of the special characteristics of FFTR and, thus, did not take into account self-shielding corrections or correction to elastic removal cross sections caused by deviation of the reactor neutron spectrum from $1/E$. The other set of cross sections, referred to as Set II and given in part in Table XXII of Appendix A, is identical with one given by G. Hansen and W. Roach of LASL[11,12,13] except for minor additions and alterations as explained in Appendix A. In this case, self-shielding of U^{235} and U^{238} on the basis of the homogeneous medium narrow resonance approximation was available. When using the Set II cross sections, the deviation of the reactor spectrum from $1/E$ was taken into account. The beryllium cross sections for Set II yield the correct age when a $1/E$ intermediate energy spectrum is assumed.

B. Tests of Cross Sections

The time and manpower available for this study did not permit extensive evaluation and readjustment of cross sections. In any event, the limited availability of experimental information would limit the amount of evaluation that could be done. It is believed that the resulting uncertainties

will not raise any serious questions about the feasibility of the concept. As discussed in a later section, there are critical experiments one would want to do before proceeding with the final design of the reactor.

Some checks of cross sections for the fast region have been discussed in Section A above. The most useful integral data for cross-section evaluation for the intermediate FFTR concept are those obtained on the KAPL critical assembly PPA-5.[14,15] In this assembly, the Be/U^{235} atom ratio was 33, corresponding to a beryllium concentration of 54.6 vol % and a U^{235} concentration of 3.1 vol % (based on ρ = 18.7 gm/cm^3). The reflector consisted of a thin beryllium region followed by thick natural uranium. The core of the reactor was a hexagonal cylinder with a volume of 85 liters. The geometrical arrangement of the reflector was rather complex, which introduces uncertainty into criticality calculations. In Ref. (15) an equivalent spherical model is given which represents the reactor approximately; it was suggested that this model should give a k of 1.05 to 1.10 for the actual critical reactor. It was found that the Set I cross sections with the suggested spherical model gave a k of 1.07, and the Set II cross sections with the suggested spherical model gave a k of 1.04 when used in diffusion theory calculations. It thus appears that the calculated criticality results with either set using diffusion theory are in a reasonable range, with the Set II results possibly giving slightly too low a reactivity. The Set II cross sections used in an SNG calculation gave a k of 1.07.

Another measurement made on PPA-5 is a rough determination of the core spectrum in the lower intermediate energy region using manganese, gold, and indium detectors. This was found in Ref. (15) to agree well with age theory calculations. Accordingly the "age theory" result for the center of PPA-5 as given in Ref. (15) was used here as a representation of the PPA-5 data, which are presumably the most reliable spectral information available. In Fig. 16 are given the "age theory" curve from Ref. (15) together with the calculated spectra for the center of PPA-5 using cross sections of Sets I and II. It is seen that the spectra calculated from Sets I and II are not greatly different, both giving less flux than the "age theory" curve below 100 ev (u = 11.5).

C. Criticality Calculations

A comparison of critical U^{235} concentrations for the 221-liter core for a range of Be/U^{235} atom ratios is given in Table IV using cross sections from Sets I and II. The calculations are not strictly comparable because of minor differences in assumed compositions and dimensions. The fact that the required fuel concentration is found to be slightly larger using Set II would be expected from the reactivity calculation comparison for PPA-5. Because the criticality results obtained using Set II are more conservative and because these cross sections contained a U^{235} and U^{238} self-shielding correction in the intermediate energy range, they were used in further work.

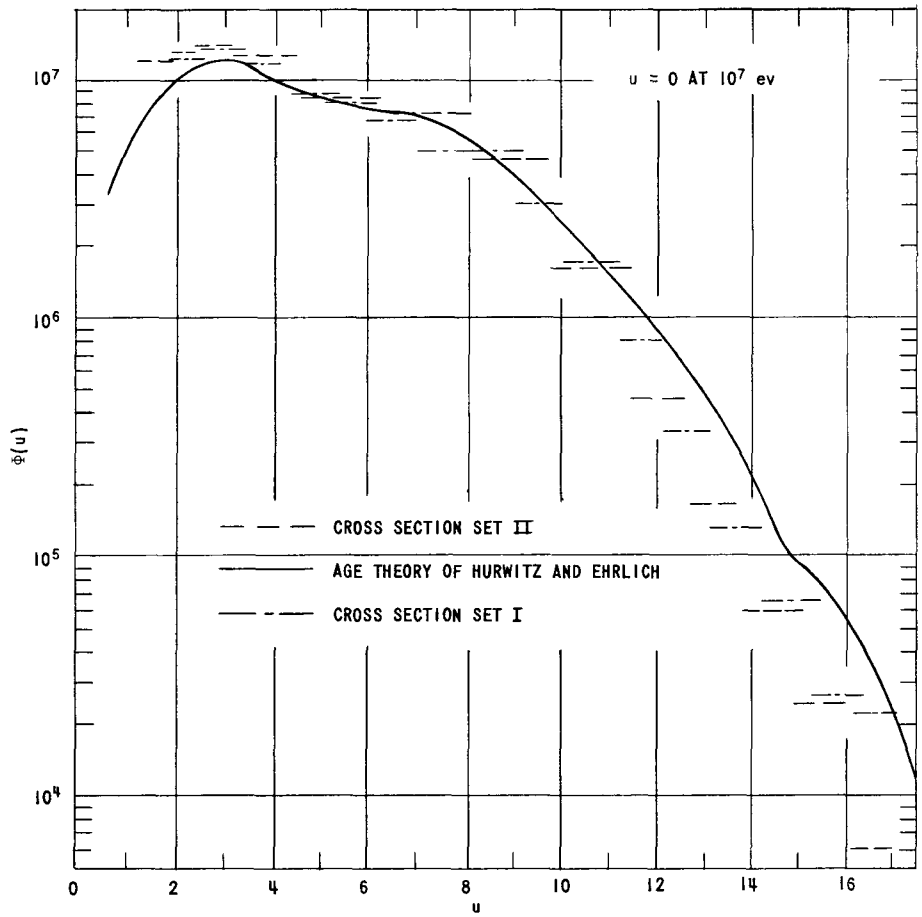

FIG. 16
FLUX PER UNIT LETHARGY FOR
CENTER OF PPA-5 CORE

Better criticality results could have been obtained by using two-dimensional calculations instead of the one-dimensional ones used to obtain the results of Table IV. This refinement did not seem justified for the present study.

A value of 86-cm bare height was found to be a more precise approximation for a 61-cm core height and a one-foot thick axial reflector consisting of 65 vol % iron and 35 vol % sodium than the 90 cm usually assumed. A corresponding adjustment as well as an allowance for sodium in the inner part of the radial reflector is reflected in the calculation given in the final line of Table IV. Also, results of criticality calculations for a 306-liter core using Set II are given in Table V.

Table IV

CRITICALITY CALCULATIONS FOR A 221-LITER CORE[a]

Be/U^{235} Atom Ratio	Set I[b]		Set II	
	Vol % U^{235} (ρ = 18.7 gm/cm^3)	Vol % Be	Vol % U^{235} (ρ = 18.7 gm/cm^3)	Vol % Be
0			6.80	0[c]
10	4.09	16.0		
15	3.41	20.0	3.58	21.0[c]
20	2.97	23.0	3.10	24.2[c]
33	2.26	29.0	2.34	30.0[c]
28.6			2.70	30.0[d]

[a] One-dimensional cylindrical geometry calculation. Equivalent bare height 90 cm. Core radius 34.3 cm. Cold clean core with fuel distributed homogeneously.

[b] Radial reflector of full-density Fe, 30 cm thick. Core also contains 30 vol % Fe and sufficient Na to fill void space.

[c] Radial reflector of full-density Fe, 40 cm thick. Core also contains 25 vol % Fe and 40 vol % Na, with sufficient U^{238} and O_2 to correspond to UO_2 fuel 93% enriched in U^{235}. There is a slight inconsistency in the total volume occupied, which would be adjusted by altering Fe or Na volumes.

[d] Equivalent bare height of 86 cm. First 5.7 cm of radial reflector 65% Fe, 35% Na. Otherwise same as for footnote (c).

Table V

CRITICALITY CALCULATIONS FOR A 306-LITER CORE

Core radius 40 cm. Equivalent bare height 90 cm.
First 5.7 cm of radial reflector 65% Fe, 35% Na.
Outer reflector 100% Fe, outer radius 85 cm.

Be/U^{235} Atom Ratio	Vol % U^{235}[a] (ρ = 18.7 gm/cc)	Vol % Be	Vol % Fe	Vol % Na
0	5.59	0	46.1	40.0
20	2.75	21.3	32.5	40.0
33	2.12	27.1	28.1	40.0
30	2.30[b]	27.1	27.8	40.0

[a] U^{235} present as 93% enriched UO_2. Cold clean core with fuel distributed homogeneously.

[b] Estimated value for 86-cm bare height; believed more accurate than 90 cm.

D. Sample Irradiation Rates and Flux Depression in Samples

1. Irradiation Rates for Small Samples

The calculation of intermediate energy fission in Pu^{239} samples is made uncertain by uncertainties in the fission cross section and lack of information about resonance parameters as well as by computational difficulties. Below 100 ev considerable self-shielding of resonances will occur in the samples. The extent of this self-shielding was estimated for the Pu^{239} resonances up to 52.6 ev, for which resonance parameters are available using the resonance capture theory of Wigner[16] as extended by others.[17-20] It appears that for most samples of interest, consisting of on the average of about 20 pins of about 0.15-in. diameter, the shielded cross sections for these resonances will be in the range from one-third to one-half of the infinitely dilute fission resonance integral. This integral has been calculated to be 250 barns above 2 ev.[21] The cross sections in Table XXII give an integral of about 126 barns to 2 ev, of which 81 barns is below 100 ev, where most self-shielding will take place. Then sample fission rates calculated with these cross sections will include a reasonable allowance for self-shielding. Although there is a considerable amount of uncertainty in this calculation, it is probably not enough in error to make any important difference. In addition to the uncertainty in cross sections, there is a question about the accuracy of the calculated reactor spectrum below 100 ev in view of the comparison in Fig. 16. This indicates that the calculated reactor spectrum for a given Be/U^{235} ratio may be too hard.

Total neutron fluxes at the horizontal central plane of a 306-liter core for various radii are summarized in Table VI. Also given are fluxes above 0.9 Mev. These are normalized to a maximum core power at the center of 1.17 Mw/liter. Average fission cross sections based on the calculated reactor spectra and the cross sections of Table VII are given in Figs. 17 and 18. The radius of 40.0 cm corresponds to the core boundary in these calculations, while the results at a radius of 28 cm are reasonably close to an average for the core. Specific powers for Pu^{239} samples based on these fluxes and cross sections are given in Table VII.

The flux integrals in the central part of the core for Be/U^{235} atom ratios in the range from 20 to 30 have 85 to 90% of their total value in the fast range (~10 kev). The median fission energy at the center of the core in Pu^{239} samples corresponding to the curves in Fig. 18 falls in Group 6 with energy limits of 17-100 kev, while the median fission energy in the U^{235} fuel falls in the range 1-10 kev. This difference is due to the fact that the variation with energy of the Pu^{239} fission cross section in the region between 1000 ev and 500 kev is much less pronounced than it is for U^{235}. This is reflected also in the behavior of the curves in Figs. 17 and 18, in which it is seen that the relative increase in fission cross sections in going from a fast to an intermediate spectrum is much less for Pu^{239} than for U^{235}.

Table VI

FFTR FLUXES AT HORIZONTAL MIDPLANE AS A FUNCTION OF RADIUS[a]

Axial Max/Ave = 1 21
Central Power Density = 1.17 Mw/liter
Core Radius = 40.0 cm
Core Volume = 306 liters

Be/U^{235} Atom Ratio	Vol % U^{235} ($\rho = 18.7$ gm/cm^3)	σ_f (U^{235}), barns (R = 0)	ϕ Total (R = 0)	ϕ Above 0 9 Mev(R = 0)	ϕ Total R = 28 cm	ϕ Total R = 40 0 cm	ϕ Total R = 45.7 cm
0	5.59	1.55	9.3×10^{15}	$2\ 3 \times 10^{15}$	6.1×10^{15}	4.1×10^{15}	3.3×10^{15}
20	2.75	2.82	10.4×10^{15}	2.1×10^{15}	7.1×10^{15}	4.4×10^{15}	3.4×10^{15}
33	2 12	3 54	10.7×10^{15}	$2\ 0 \times 10^{15}$	7.3×10^{15}	4.4×10^{15}	3.4×10^{15}
30	2 30	3.37	10.4×10^{15}	$2\ 0 \times 10^{15}$	7.2×10^{15}	4.4×10^{15}	3.4×10^{15}

[a]Maximum values based on homogeneous fuel loading of cold clean core. See discussion in Section VI-D and VI-E It is believed that for reasonable operating conditions the fluxes and the specific powers given here should be divided by 1 3.

Table VII

FFTR SPECIFIC POWER FOR Pu^{239} SAMPLES AT HORIZONTAL MIDPLANE[a]

(kw/gm Pu^{239})
Axial Max/Ave = 1 21
Central Power Density = 1 17 Mw/liter
Core Radius = 40.0 cm
Core Volume = 306 liters

Be/U^{235} Atom Ratio	Small Sample				Large Sample
	R = 0 cm	R = 28.0 cm	R = 40 cm	R = 45.7 cm	R = 0
0	1 29	0 95	0.68	0 65	1 29
20	1.88	1 33	0 94	0.90	1 58
33	2 32	1 60	1.10	1 01	1 72
30	2 16	1 53	1.07	0 99	1 72

[a]Maximum values based on uniform homogeneous fuel loading of cold clean core See discussion in Section VI-D and VI-E It is believed that for reasonable operating conditions the fluxes and the specific powers given here should be divided by 1.3.

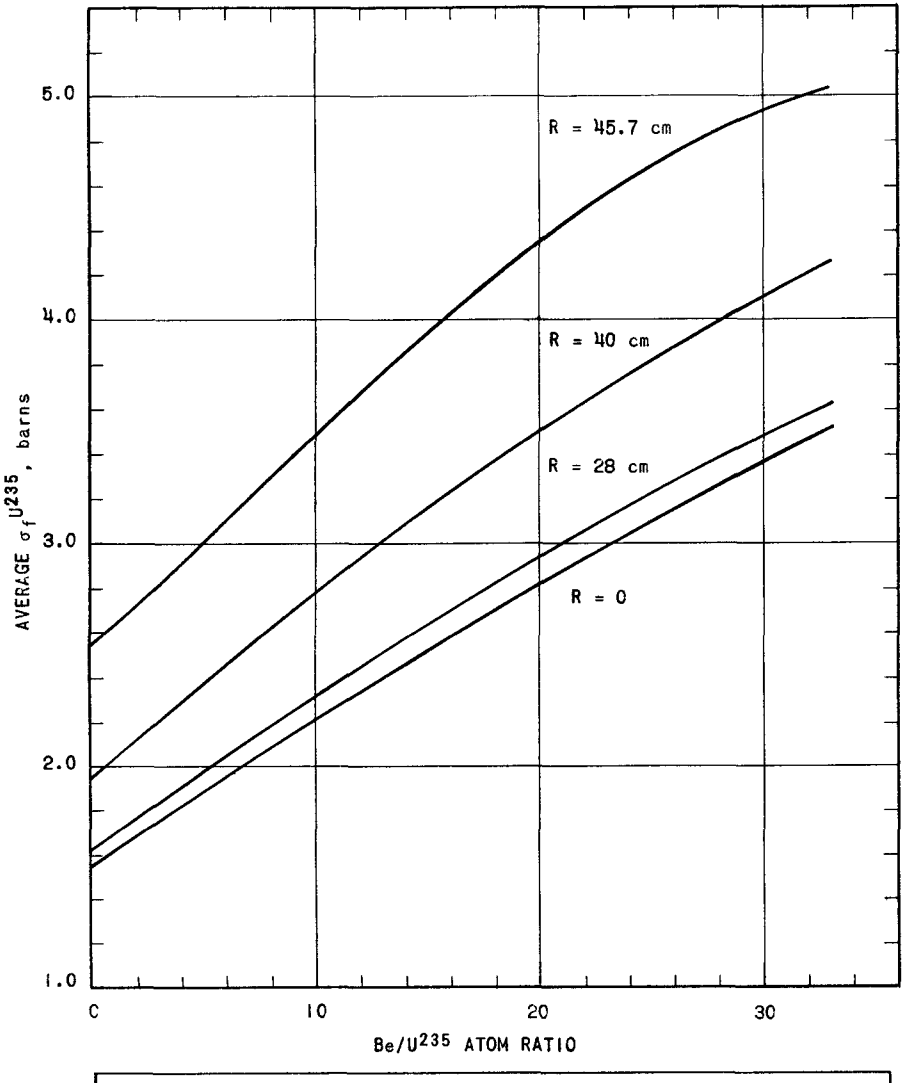

FIG. 17
AVERAGE FISSION CROSS SECTION OF U^{235} vs Be/U^{235} ATOM RATIO AT VARIOUS RADII (R) IN REACTOR FOR CORE RADIUS=40 cm.

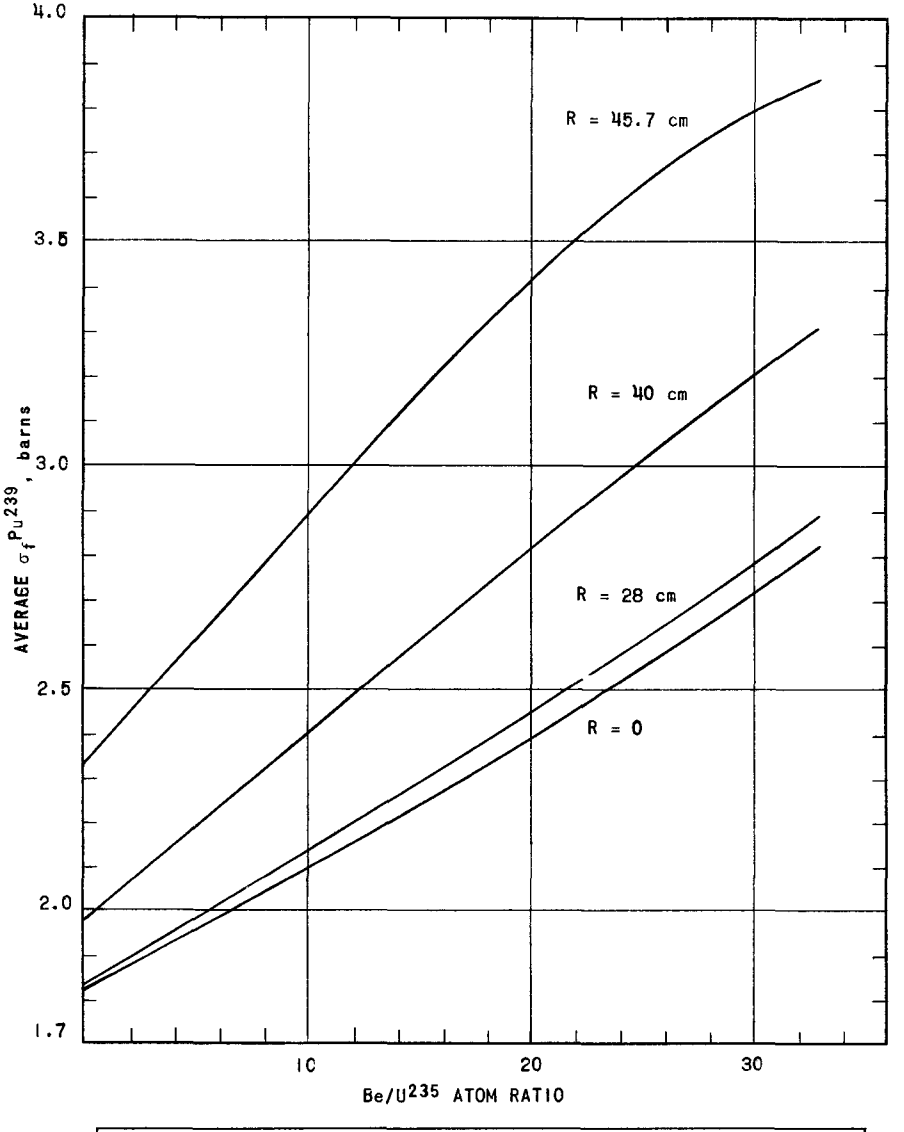

FIG. 18
AVERAGE FISSION CROSS SECTION OF Pu^{239} vs Be/U^{235} ATOM RATIO AT VARIOUS RADII (R) IN REACTOR FOR CORE RADIUS = 40 cm.

The results of the specific power calculation carried out for the center of a 34.3-cm radius core are given in Table VIII. The radial dependence has not been plotted for this case but is similar to that for the 40-cm case except for a change of radial scale in the core corresponding to the change in core radius.

The results given in Tables VI, VII, and VIII are maximum values which are based on the critical fuel concentration of the uniformly loaded cold clean reactor. As discussed in Section VI-E, because of the necessity of providing excess reactivity to take care of temperature coefficient, burnup reactivity loss, and loss of fuel in sample regions, the normal reactor fuel elements must have a higher concentration than would correspond to the average core compositions indicated in Tables IV and V. This reduces the reactor flux that corresponds to a given maximum power density, the exact amount of the reduction depending upon how the reactor is loaded. As discussed in Section VI-F, operation of the 298-liter core reactor with the UO_2-stainless steel fuel should be possible with a reduction of 30% in the fluxes and specific powers indicated in Table VIII. This would allow the design objective of a maximum sample specific power of 1.5 kw/gm Pu^{239} to be met for small samples. For large samples the maximum specific power would be 1.3 kw/gm Pu^{239}.

It should be noted that the flux above 0.9 Mev, which is most important for neutron damage, does not vary greatly from the fast to the intermediate reactor for the same power density. If one used a fast reactor with lower power density compensated for by using samples containing more fissile material, which is possible in certain cases, the total flux would of course be proportionately lower.

The fraction of total sample fissions occurring below 100 ev is given in Fig. 19. It is seen that this fraction is quite small in the core, so that an error in estimating the fissions below 100 ev would not affect calculated specific powers greatly. It is these fissions which would be most likely to exhibit strong spatial variation in the samples. No attempt has been made to calculate what the spatial distribution of fissions in the small samples would be, but this distribution should not present a severe problem, at least in the core, because of the small fraction of total fissions affected. It is noted that in PPA-5 in a slab of pure U^{235}, 0.16-in. (0.4-cm) thick, the edge-to-center fission ratio was found to be 1.23.[15] This is probably representative of the behavior that would be encountered in the FFTR, although, of course, one is concerned here with Pu^{239} instead of U^{235}.

Table VIII

FFTR SPECIFIC POWER FOR Pu^{239} SAMPLES AT CENTER OF CORE[a]

Axial Max/Ave = 1.21
Central Power Density = 1.17 Mw/liter
Core Radius = 34.3 cm
Core Volume = 226 liters

Be/U^{235} Atom Ratio	Vol % U^{235} (ρ = 18.7 gm/cm^3)	$\sigma_f(U^{235})$, barns (R = 0)	ϕ Total R = 0	Specific Power, kw/gm Pu^{239}	
				Small Sample	Large Sample
0	6.8	1.55	7.6×10^{15}	1.06	1.06
15	3.58	2.52	8.9×10^{15}	1.52	1.36
20	3.10	2.82	9.2×10^{15}	1.67	1.40
33	2.34	3.54	9.7×10^{15}	2.10	1.55
28.6	2.70	3.30	9.0×10^{15}	1.84	1.45

[a] Maximum values based on homogeneous fuel loading of cold clean core. See discussions in Sections VI-D and VI-E.

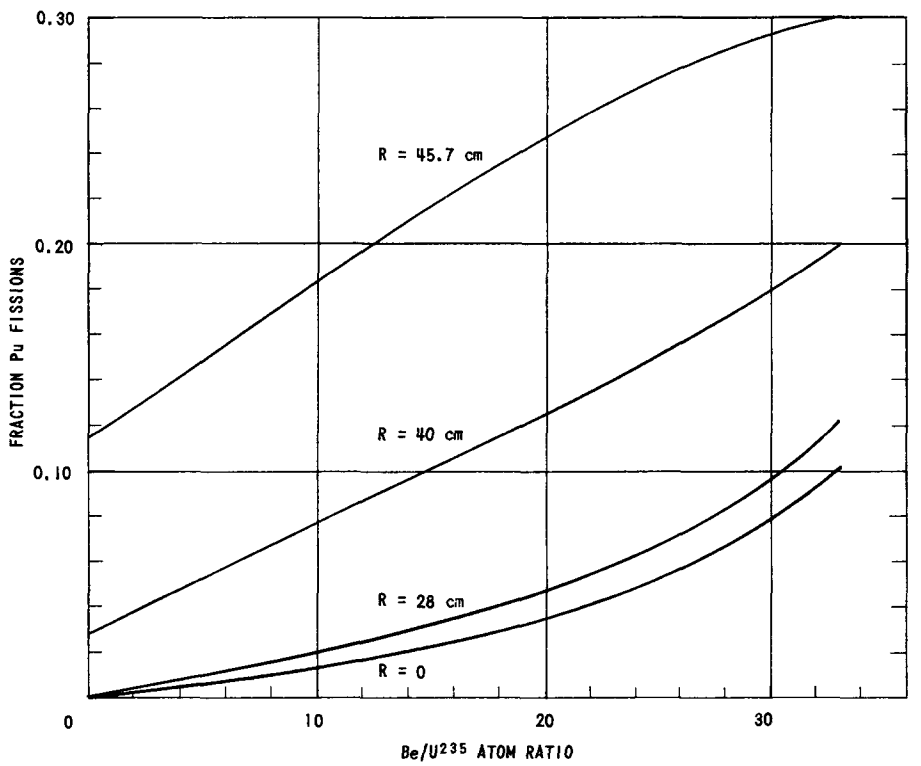

FIG. 19
FRACTION OF Pu SAMPLE FISSIONS BELOW 100 ev VERSUS Be/U^{235} ATOM RATIO AT VARIOUS RADII (R) IN REACTOR FOR CORE RADIUS = 40 cm

2. Flux Depression in Large Samples

The extent of the power depression for large samples was investigated by using SNG calculations in one-dimensional cylindrical geometry for a sample located at the center of the core. Calculations were made for 3-cm and 5-cm radius samples, the former corresponding approximately to the area of a normal 5.33 cm by 5.33 cm hole and the latter to the area of a 7.36 cm by 7.36 cm hole that would be obtained by removing the beryllium pieces adjacent to a normal hole. The sample was assumed to have a composition of 50% sodium, 20% iron, and 30% fuel by volume, the fuel being 20 at % Pu^{239} and 80 at % U^{238}.

The calculations gave a very flat radial power distribution in the samples, the variation for the 33 Be/U^{235} atom ratio being only about 5%. This flatness was due to the fact that, although neutrons below 100 ev were found to be attenuated very rapidly in the samples by resonance fission and capture, their contribution to the total power was quite small because of depression of the low-energy flux in the vicinity of these large samples. Also, there was some increase in the high-energy fission source in the interior of the samples. However, because of the lack of low-energy flux in the large samples, the Pu^{239} fission cross section was found to be not more than 2.1 barns. The "large sample" specific powers based on these calculations are given in Tables VII and VIII.

The SNG calculations discussed above were somewhat unrealistic in that they did not take proper account of the capture of resonance energy region neutrons undergoing collision in the sample after having undergone a previous collision in moderator, as there is a mismatch in spectrum between the two regions. This is not likely to be important for large samples because of the flux depression effect previously referred to and would probably not amount to more than 5 or 10% in radial power variation.

E. Burnup and Control - Sample Reactivity Effects

1. Reactivity Requirements for Burnup and Temperature Coefficient

The burnup by fissions of U^{235} at 200-Mw operation for a 3.5-week cycle is 5.1 kg. Assuming a capture-to-fission ratio of 0.30, the destruction of U^{235} per cycle is 6.6 kg. Estimation of the fission product poisoning effect using the Moldauer cross sections[22] leads to the conclusion that a reasonable assumption is that the products from a fission exert a negative reactivity equal in magnitude to one-half[a] the positive reactivity of the fissioned fuel. The average worth of fuel for the 238-liter core is about 0.29% k per kg U^{235}. For the 298-liter core, assuming that the worth of U^{235} varies inversely as the critical mass, the worth per kilogram is

[a] A more accurate calculation gives three-fourths instead of one-half. This adds slightly more than 1 kg of U^{235} to the burnup reactivity loss per cycle.

about 0.24% k. Taking account of nonuniformity of burnup raises the worth of fuel burned about 7% over this. With these assumptions the reactivity effect of U^{235} burnup for one cycle at 200-Mw total power is estimated to be equivalent to 10 kg of uniformly distributed U^{235}.

The high-energy (n,α) capture of neutrons in Be leads to the formation of Li^6, which can introduce an appreciable poisoning effect after sufficient time.[22,23] An estimate of the reactivity loss in kg of U^{235} for a 238-liter core with 165-Mw total power as a function of exposure time is given below.

Exposure of Be, yr	Reactivity Loss, kg U^{235}
1	8.4
2	13.6
3	16.6
Saturated	20.8

For the 298-liter core the reactivity loss numbers would be increased by 25%.

Neutron captures in Li^6 cause production of tritium, which decays with a 12.5-year half-life to He^3, which by neutron capture goes back to tritium. If these gases do not escape from the beryllium, the negative reactivity effect keeps building up and becomes important over a period of 5 to 10 years. The reactivity effects in the Li^6 and He^3 poisoning are large enough that periodic replacement of the Be,perhaps every year or two might be necessary, depending on the available reactivity margin in the reactor. It seems probable that swelling from gas production in the beryllium would require its replacement in a shorter time.

The overall temperature coefficient of the reactor has not been calculated, but it is estimated from results from other fast and intermediate reactors that the necessary control would be about 1% k, equivalent to about 4 kg of U^{235}. The sodium void coefficient is strongly negative, the total worth of the sodium in the core being about 4% k for the 238-liter core. The Doppler effect is discussed in Section VI-F.

2. Preliminary Control Rod Calculations

Calculation of the relative worth of a central control rod and its fuel follower for a 238-liter cylindrical core with an equivalent bare height of 90 cm gave the following results:

N^B = atoms/cm^3 of normal boron x 10^{-24}	Normal Boron (gm/cm^3)	%Δk Compared to Fuel Follower
0.0025	0.0415	-1.24
0.005	0.083	-1.77
0.010	0.166	-2.44

These numbers should be multiplied by 0.8 to allow for the fact that an equivalent bare height is used and by about 0.5 to give the off-center worth of the rod. For the 298-liter core a further reduction of about 20% would occur. It appears then that temperature effects and burn-up for one cycle can probably be controlled with five or six rods having the maximum boron content indicated above, although a more detailed study is obviously necessary. The effect of the rods on reactor power distribution is shown in Fig. 20. It is desirable to use rods as lightly loaded as possible for reactivity shimming in order to reduce changes in reactor flux distribution during operation. The power perturbation for the heaviest boron loading in Fig. 20 is about the strongest one would want to have. It appears that the use of more rods or of a harder spectrum, if possible, would be desirable to reduce perturbation of the sample flux by the rods. The B^{10} contents indicated above could be obtained in boron steel by using enriched boron. For shutdown rods, larger boron contents could be used, so that 2%Δk per rod should be feasible. This would give adequate shutdown with three rods.

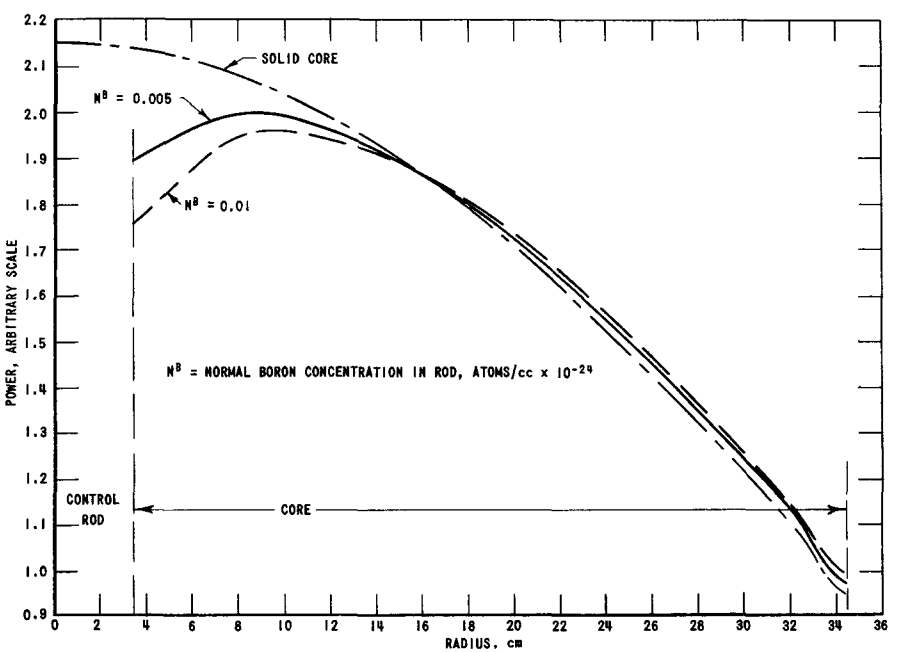

FIG. 20
POWER VS RADIUS FOR BORON CONTROL RODS IN CORE WITH Be/U^{235} RATIO = 33

3. Reactor Loading and Sample Reactivity Requirements for a 238-Liter Core

The critical U^{235} concentration for the uniformly loaded 238-liter core with 30 vol % beryllium, 25 vol % iron, and 40 vol % sodium is estimated to be 2.7 vol % U^{235} (ρ = 18.7 gm/cm^3), which corresponds to a critical mass of 120 kg and a Be/U^{235} atom ratio of 28.6. For 97 subassemblies this corresponds to a uniform loading of 1.24 kg U^{235}/subassembly. The nine loops in the core would correspond to a normal loading of 9 x 1.24 = 11 kg U^{235}. It is assumed that the normal sample loading will be 3 kg Pu^{239} and that Pu^{239} is equivalent to U^{235}, leaving a reactivity deficit of 8 kg of U^{235}. It may be desired to insert 40 capsules containing little or no fuel which would occupy the center one-fourth of various fuel elements. It is estimated that this will correspond to 13 average elements, giving a reactivity deficit of 13 x 1.24 = 16 kg. The total reactivity deficit over the uniformly loaded core expressed as uniformly distributed U^{235} is then as follows:

	U^{235}, kg
Burnup and fission product poisoning (one cycle at 165 Mw)	8
Temperature coefficient	4
Loops	8
Capsules	16
	36

This deficit must be made up by loading the normal part of the core with more than 2.7 vol % U^{235}. With the UO_2-stainless steel plates, the maximum average loading is 3.41 vol % U^{235}. The total normal subassemblies available, excluding 8 control and safety rods which would probably have to have a light loading to allow for guides, is

$$97 - (13 + 9 + 8) = 67 \text{ subassemblies.}$$

If these are loaded at an average of 3.41 vol % U^{235}, the excess fuel over that for the 2.7 vol % loading is

$$\left(\frac{3.41 - 2.70}{2.70}\right) \times 1.24 \times 67 = 22 \text{ kg } U^{235} \quad .$$

The reactor then could not operate under these conditions without elimination of a large part of the allowance for loops and capsules.

The use of the 3.41 vol % U^{235} fuel throughout the core would correspond to a reduction by a factor of 2.70/3.41 = 1/1.26 in the fluxes and specific powers given in Tables IV and VII for the 28.6 Be/U^{235} atom ratio case, since the maximum power density remains the same.

If the UN-stainless steel fuel were used, a 40% increase in average U^{235} concentration to 4.76 vol % would be possible. If the normal reactor fuel elements were given such a loading throughout, the core excess U^{235} would be

$$\frac{4.76 - 2.70}{2.70} \times 1.24 \times 67 = 63 \text{ kg } U^{235} \quad .$$

However, this would require a reduction in flux and specific power for the 28.6 Be/U^{235} atom ratio cases of Tables IV and VII of 2.70/4.76 = 1/1.77, which would lead to an unacceptably low specific power. This situation could be alleviated somewhat by confining the heaviest loading to the outer part of the core. It is estimated that if one uses a nonuniform loading of this type and accepts a reduction by a factor of 1/1.30 in maximum power density and sample specific power, perhaps half of the excess reactivity of 63 kg of uniformly distributed U^{235} calculated above could be realized. This excess reactivity of some 30 kg of U^{235} would make operation more nearly possible. The nonuniform fuel loading would represent an added expense and inconvenience, however.

It has been implicitly assumed that the inhomogeneity caused by heavier loading of the fuel in some subassemblies to compensate for lack of fuel in others will have no effect of reactivity. This may be too optimistic, and also there may be significant spatial variation of the neutron energy spectrum caused by this inhomogeneity. The sample power depression effect associated with the energy spectrum variation might force the use of a lower Be/U^{235} ratio than would otherwise be necessary. Evaluation of these effects can best be done in a critical experiment.

For a fast reactor with a 238-liter core, assuming a composition of 34 vol % sodium, 9% structure, and 57% UO_2-stainless steel meat, the maximum possible vol % UO_2 is 57 x 26.75 = 15.2. At 93% enrichment, this corresponds to 15.2/2.27 = 6.7 vol % U^{235} (ρ = 18.7 gm/cc). Since the homogeneous critical composition given in Table IV is 6.8 vol % U^{235} (neglecting the effect of the difference in sodium and steel vol % and also the correction to equivalent bare height made for the intermediate case), the reactor could not operate under these conditions. With the UN fuel, the possible U^{235} concentration would increase to 9.4 vol %. In this case, the reactivity deficit in kg of U^{235} would be as follows:

Loops and capsules	66
Temperature coefficient	10
Burnup (1 cycle at 165 Mw)	8
	84

With the UN-stainless steel fuel, a gain of 80 kg over the average core composition is possible by a heavy loading of 67 subassemblies, so that operation would be possible with a slight reduction in the assumed loop and capsule reactivity deficit. If the maximum power density were assumed to remain at 1.17 Mw/liter, the reduction flux and specific power over the values given in Tables IV and VII for a Be/U^{235} ratio of 0 would be by a factor of $6.8/9.4 = 1/1.38$. The maximum power density has not been evaluated for this configuration but would be somewhat higher than for the intermediate reactor if a higher temperature rise in the sodium could be permitted, because of the lower power density in the fuel.

4. Reactor Loading and Sample Reactivity Requirements for a 298-Liter Core

In the case of the 298-liter, 121-subassembly core, the critical uniform reactor loading is estimated to be 2.3 vol % U^{235} for 30 vol % beryllium, corresponding to a critical mass of about 130 kg U^{235}. Under these conditions the total deficit in terms of kg of U^{235} is as follows:

Capsules	14
Loops	7
Temperature	5
Burnup and fission product poisoning (1 cycle at 200 Mw)	10
	36

The subassemblies available for heavy loading, assuming 12 control and safety rods, are now

$$121 - 34 = 87 \text{ subassemblies.}$$

If these are loaded with the UO_2-stainless steel fuel at an average concentration of 3.41 vol % U^{235}, the excess fuel over that for a 2.3 vol % U^{235} loading is 45 kg of U^{235}.

The reduction in flux and specific power over the values given in Table VIII would be by a ratio of $2.3/3.41 = 1/1.48$, which is probably more than could be tolerated. A uniform loading of 3.0 vol % U^{235} in

the normal subassemblies would correspond to a reduction in the Table VIII values by a factor of 1/1.30, which is more acceptable. This would correspondingly scale down the total reactor power to 154 Mw plus that in loops and capsules, which would be at most about 10 Mw. The burnup loss would be reduced to about 8 kg of U^{235}. This loading would correspond to an available excess reactivity of 28 kg of uniformly distributed U^{235}, which is still slightly below what is needed unless the assumptions have been too pessimistic. The accuracy of the calculations is not such that one can regard this discrepancy as significant. One could gain reactivity by expanding the core volume by an estimated 4 liters per kg of uniformly distributed U^{235}. The core size could be expanded farther to use the fuel for more cycles or to compensate for reactivity loss from Li^6 production.

For a fast reactor with a 298-liter core, with the volume percent of sodium and structural material and meat assumed the same as for the 238-liter core, the critical composition given in Table V is now 5.6 vol % U^{235}. A calculation made as before for the reactivity deficit now yields 77 kg of U^{235}, while with uniform heavy loading of the 87 normal subassemblies out of the 121 total, one could gain 44 kg at the expense of a decrease by a factor of 5.6/6.7 = 1/1.20 in the flux and specific power for the Be/U^{235} atom ratio case in Table VIII. Operation would then be possible for the UO_2-stainless steel fuel only by paring the loop and capsule reactivity requirements considerably. Again, it might be possible to increase the maximum power density over the 1.17 Mw/liter calculated for the intermediate reactor case. As in the 238 liter core case the loading could be increased by use of the UN-stainless steel fuel at the expense of a further decrease in sample specific power. A fuel loading corresponding to 7.6 vol % U^{235} which would correspond to reduction by 1/1.35 in the flux and specific powers of Table VIII, would give an excess reactivity of 77 kg.

F. Doppler Effect

A negative Doppler effect in the FFTR would be an important safety asset because of the finite time required for heat to pass from the fuel particles to the stainless steel matrix of the fuel plates, while, of course, a positive one could be a serious liability. No attempt has been made to calculate the Doppler effect in the FFTR. Sufficient measurements have been made on fast reactors[24] to establish that it would be small and positive in a highly enriched fast reactor, so that a lowering of enrichment might be desirable from a safety standpoint. Measurements were made in PPA-5 (33 Be/U^{235} atom ratio)[15] at an early stage of the technique when the precision was not high. It was concluded from theoretical studies[15] that the Doppler effect in PPA-5 would contribute a reactivity effect not exceeding $\pm\frac{1}{3}$% k if the U^{235} absolute temperature were double that of room temperature. All that could be concluded from the experiments was that the Doppler effect was small and did not exceed the theoretical estimate, with the sign again uncertain.

More recent measurements have been made[24] in Be-moderated intermediate reactors with median fission energies of 50 and 125 ev, as opposed to the 1500 ev of PPA-5. Negative Doppler effects were observed for 93% enriched U^{235} fuel. It was concluded that half the negative effect was due to the U^{235} and half to the U^{238}. It seems hopeful from this that a negative effect could be obtained in the intermediate FFTR, perhaps with a slight lowering of the enrichment of the fuel. This would be more feasible with development of the UN-stainless steel fuel because of difficulty of incorporating enough U^{235} in the UO_2-stainless steel fuel even at 93% enrichment.

G. Shielding

1. During Operation

a. Neutron Fluxes

A 19-group diffusion theory using the Set I cross sections in Appendix A was used to determine the neutron flux distributions in the core and reflector regions. The RE-34 shielding code with six energy groups was used to extend the distribution through the outside regions.

A total of 8 ft (244 cm) of magnetite concrete is needed outside the radial reflector and vessel to provide the necessary biological shielding. The primary shielding wall constitutes the first 5 ft (152 cm) of this thickness. In the axial direction a 5 ft (152 cm) thick vessel cover and a 5 ft (152 cm) cell top structure provide 8 ft (244 cm) of magnetite concrete and 2 ft (61 cm) of steel above the sodium. The shielding neutron flux distributions are given in Figs. 21 and 22.

b. Core Gamma-ray Fluxes

The core gamma-ray calculations were based on the following assumptions and procedures:

(1) The gamma rays were grouped into 1, 2, 4, 6, and 8-Mev energy groups.

(2) The source is uniformly distributed in the core.

(3) Prompt fission and fission product gamma rays,

8.61 Mev/fission of 1-Mev photons
4.822 Mev/fission of 2-Mev photons
1.357 Mev/fission of 4-Mev photons
0.256 Mev/fission of 6-Mev photons

(4) Secondary gamma rays from neutron capture by iron in the core were determined by calculating an effective iron absorption rate in the core from the multigroup fluxes and multiplying by N_γ(Mev/capture). The effective iron neutron absorption rate in the core is calculated to be 1.8×10^{12} capt/(cm^3)(sec).

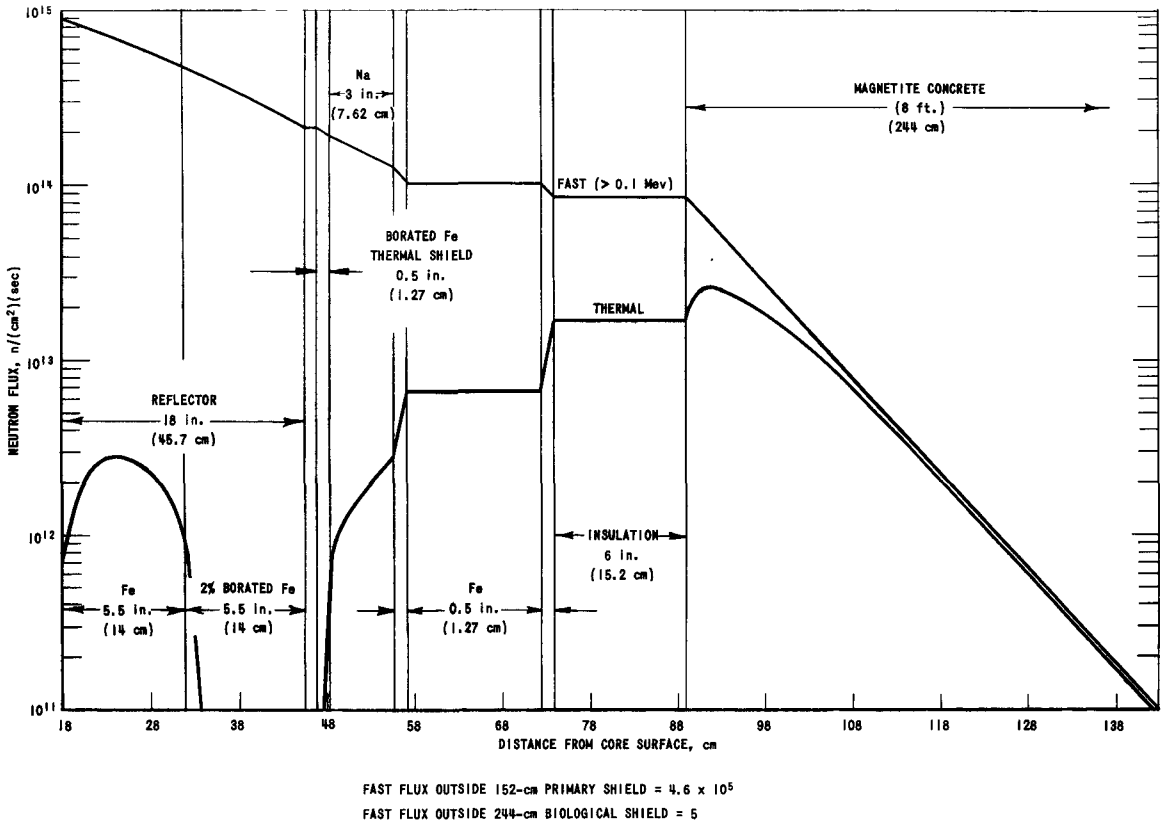

FIG. 21
RADIAL NEUTRON FLUXES USED IN SHIELDING CALCULATIONS

(5) Secondary gamma rays from neutron capture by sodium in the core were determined by calculating an effective sodium absorption rate in the core from the multigroup fluxes and multiplying by N_γ (Mev/capture). The effective sodium neutron absorption rate in the core is calculated to be 1.5×10^{11} capt/(cm^3)(sec).

Table IX lists the gamma-ray absorption cross sections used in gamma-ray flux calculations.

The total core volumetric source strength, Q_3, in Mev/(cm^3)(sec), for each energy group was estimated for a 250-Mw power level.

$$\frac{\text{Core Fissions}}{(\text{cm}^3)\ (\text{sec})} = \frac{2.5 \times 10^8 \text{ watts} \times 3.29 \times 10^{10} \text{ (fissions)/(watt)(sec)}}{2.98 \times 10^5 \text{ cm}^3}$$

$$= 2.76 \times 10^{13}$$

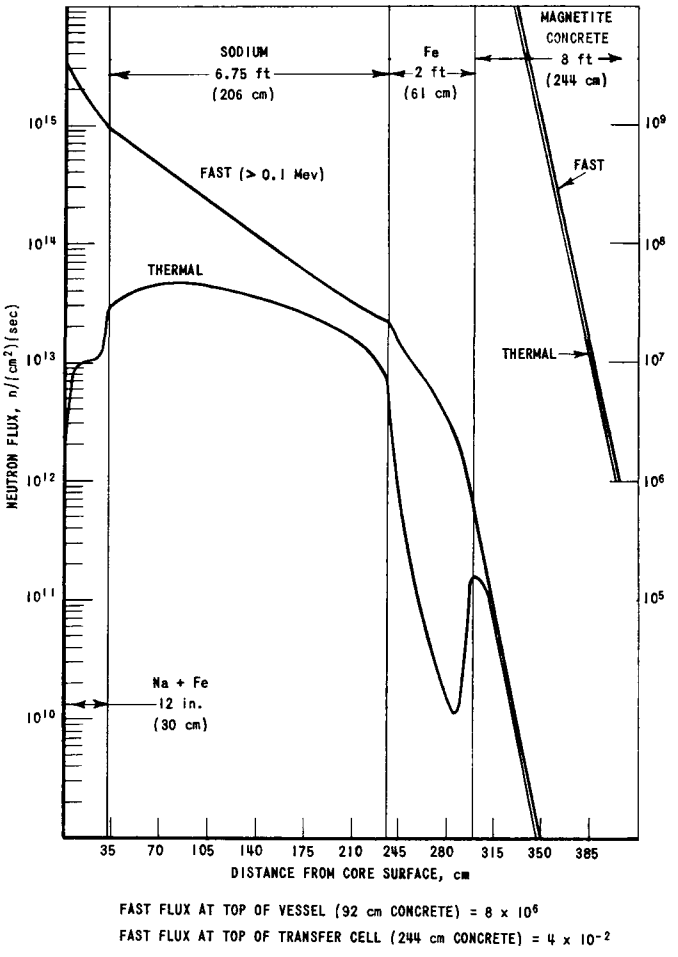

FIG. 22
AXIAL NEUTRON FLUXES USED IN SHIELDING CALCULATIONS

Table IX

GAMMA-RAY CONSTANTS

Linear Absorption Cross Section (μ), cm^{-1}

E (Mev)	Core	Fe	Na		Magnetite Concrete
			Core	Bulk	
1	0.220	0.468	0.051	0.052	0.216
2	0.153	0.333	0.0359	0.0365	0.155
3	0.130	0.284	0.0293	0.0297	0.130
4	0.120	0.259	0.0255	0.0259	0.115
6	0.111	0.239	0.0214	0.0217	0.102
8	0.108	0.232	0.0192	0.0195	0.096

Total Volume Strengths in Core

E, Mev	Q_3, Mev/(cm^3)(sec)
1	2.38×10^{14}
2	1.34×10^{14}
4	3.9×10^{13}
6	8.8×10^{12}
8	7.0×10^{12}

The core gamma-ray flux in the regions outside the core was determined by the following formula, which effectively includes a linear buildup factor:

$$\phi_\gamma\left(\sum_{i=1}^{i} t_i\right) = \frac{Q_2}{2}\sqrt{\frac{r}{r_0}}\exp\left(-\sum_{i=1}^{i}\mu_i t_i\right) ,$$

where μ_i = gamma-ray linear absorption coefficient for i'th region, cm^{-1}

$\frac{Q_2}{2}$ = radiating surface source
[flux at the surface of the core, Mev/(cm^2)(sec)].

r = radius of cylindrical source

$$r_0 = r + \sum_{i=1}^{i} t_i$$

t_i = thickness of i'th region, cm .

c. Capture Gamma Rays from Regions Other than the Core

The thermal neutron flux was represented by an exponential shape or a constant, and the appropriate equations from Ref 25 were used to calculate the capture gamma-ray flux at either surface of each source region and through specified exterior shields. Table X shows constants used in the capture gamma-ray source calculations.

The gamma-ray flux distributions (Figs. 23 and 24) include core gamma rays and capture gamma rays calculated for four energy groups.

Table X

CONSTANTS FOR CAPTURE GAMMA-RAY CALCULATIONS

$N\gamma$ (Mev/Neutron Capture)

	1 Mev	2 Mev	4 Mev	6 Mev	8 Mev
Steel	-	0.55	0.82	0.84	0.378
Sodium	0.80	1.83	1.05	1.16	-
Magnetite	-	0.77	1.01	2.24	2.80
Concrete (ρ = 3.62 gm/cm^3)					

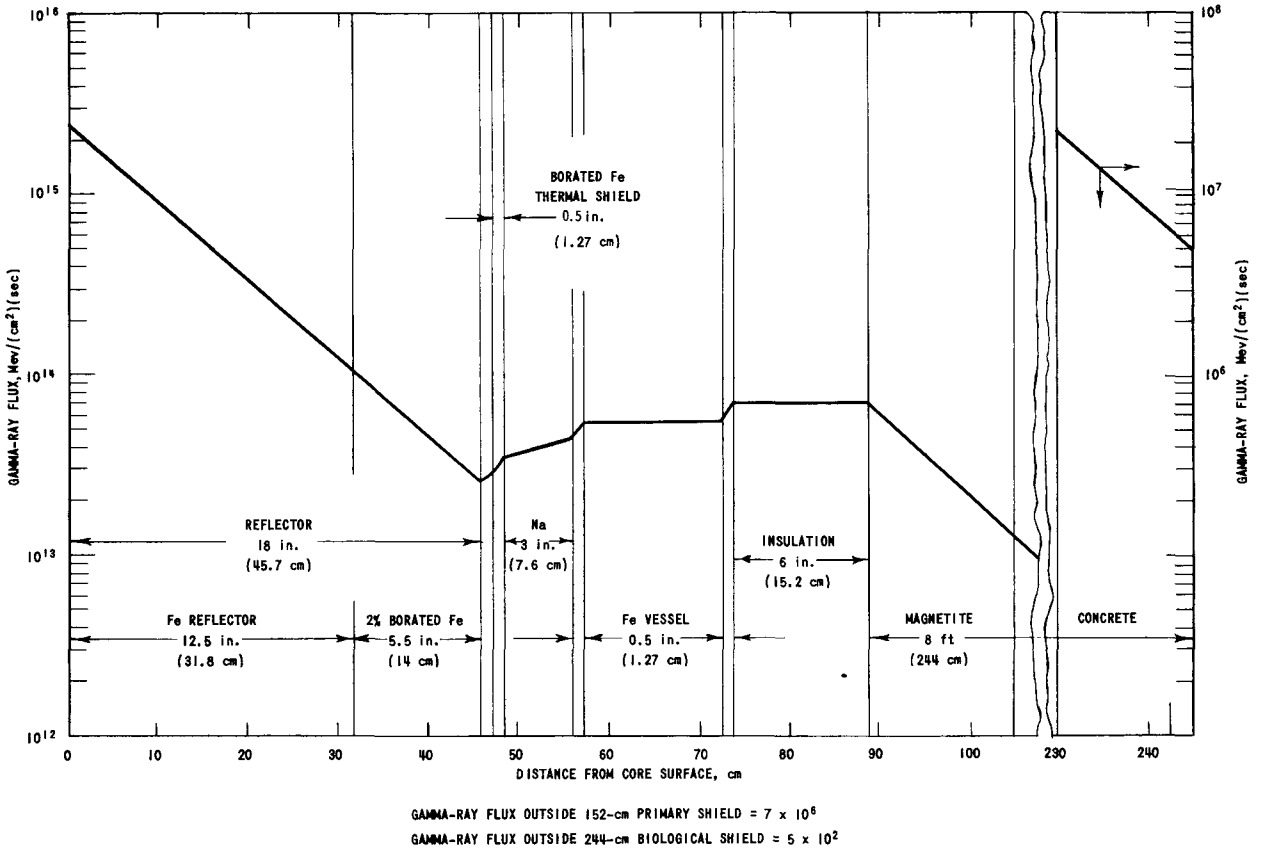

FIG. 23
TOTAL RADIAL GAMMA-RAY FLUX AT CORE MIDPLANE

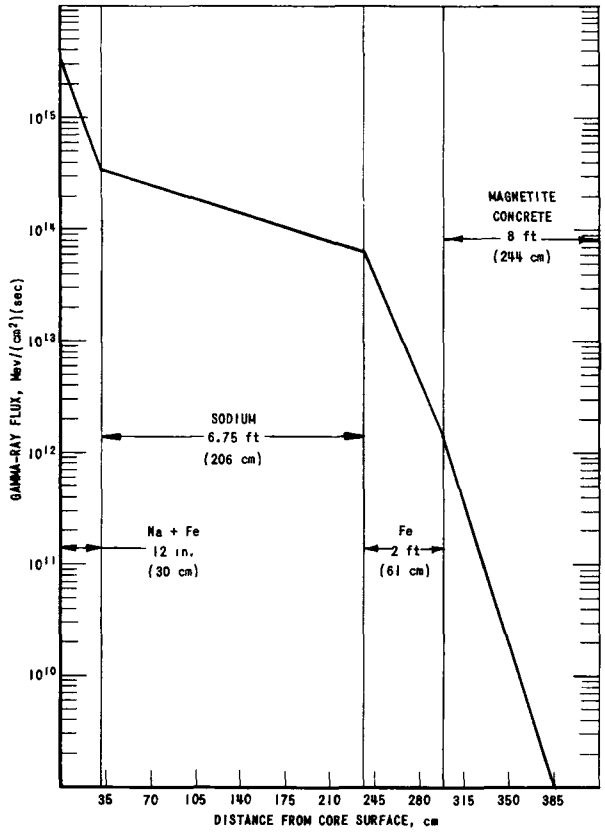

FIG. 24
TOTAL AXIAL GAMMA-RAY FLUX

2. During Shutdown

The fission product activities were determined using seven energy groups.[26] The values after infinite operation are listed in Table XI.

Table XI

FISSION PRODUCT GAMMA RAYS

(Mev/sec per watt of operating power)

Energy (Mev)	Time after Shutdown	
	12 hr	24 hr
0.1 - 0.4	1.4×10^9	1.3×10^9
0.4 - 0.9	8.5×10^9	7.4×10^9
0.9 - 1.35	2.9×10^8	1.2×10^8
1.35 - 1.8	3.1×10^9	3.0×10^9
1.8 - 2.2	2.1×10^8	8.1×10^7
2.2 - 2.6	2.8×10^8	2.7×10^8
2.8	1.5×10^6	7.7×10^4

For convenience, the values for 12 hours of cooling were combined to give the values shown for three energies, developed from collapsing the 7-group sources:

Mev	Mev/(sec)(watt)
1	1.02×10^{10}
2	3.3×10^{9}
3	2.82×10^{8}

After 250-Mw operation and 12 hr of cooling, the fission product gamma-ray flux at the top of the fuel subassemblies is

Mev	Mev/(cm^2)(sec)
1	8×10^{7}
2	2×10^{9}
3	7×10^{8}

After the sodium has been lowered to the top of the subassemblies, the total gamma-ray flux at the surface of the sodium from fission products and from sodium that has cooled 12 hr is

Mev	Mev/(cm^2)(sec)
1	8×10^{7}
2	3×10^{11}
3	8×10^{11}

Five feet of magnetite concrete shielding at the top of the fuel handling cell will reduce this flux to a dose of about 1 mr/hr on top of the cell.

In the radial direction, the reflector and vessel shield the fission product gamma rays so that 61 cm of magnetite concrete would reduce the dose to below tolerance. However, the flux from the sodium requires the shielding provided by the vessel and five feet of magnetite concrete to reduce the dose to about 1 mr/hr.

3. During Fuel Transfer

Based on calculations that convert the subassembly to an equivalent line source, the maximum flux inside the fuel-handling cell from ten subassemblies that have cooled 12 hours is estimated to be 4.5×10^{13} Mev/(cm^2)(sec).

For ten subassemblies, representing an operating power of 20 Mw, the five-foot magnetite concrete shielding wall of the cells will limit the dose on the outside to less than 0.1 mr/hr. This will make it possible to place all subassemblies in the cell if necessary and still be well below a tolerance of 7.5 mr/hr.

The line source values for a single subassembly with 2 Mw of operating power after 12 hr of cooling are

Mev	Mev/(cm^2)(sec)
1	3.3×10^{14}
2	1.1×10^{14}
3	9.2×10^{12}

With no shielding this gives a flux a few inches away of about 4×10^{12} Mev/(cm^2)(sec), or about 8×10^{6} r/hr.

4. Heat Exchanger and Secondary Coolant Shielding

The sodium in the heat exchangers will produce an estimated radiation of 2×10^{6} r/hr in this area. Since Na^{24} has a half-life of 15 hr, one week of cooling will reduce this radiation to 9×10^{2} r/hr. Seventeen days of cooling should make the area accessible in a radiation field of about 10 mr/hr.

Without any cooling time the heat exchanger region must be shielded by 5 ft (152 cm) of magnetite concrete to give a dose of less than 7 mr/hr on the outside.

Calculations indicate that the NaK coolant from the heat exchangers will have an activity of 8×10^{2} Mev/(cm^3)(sec) due to the neutron flux outside the primary shielding wall of magnetite concrete. The activity will consist mainly of 2.76 and 1.38-Mev photons from Na^{24}.

The secondary NaK coolant will produce a dose of approximately 7 mr/hr at 30 cm from the surface of a 40-cm diameter pipe. Consequently, no shielding of the pipes should be necessary.

VII. REACTOR FLUID FLOW, HEAT TRANSFER, STRESS ANALYSIS

A. System Pressure Losses

Calculated values for pressure loss in primary system components are shown in Table XII. The major loss, occurring in the reactor core, was calculated using McAdams' smooth pipe friction factor relationship.[27] A flow rate of 26,200 gpm (1.65 m^3/sec) was assumed to pass through the primary system. The results indicate that at 75% efficiency, the pumping work required for each primary loop will be 475 horsepower (350 kw).

Table XII

PRIMARY SYSTEM PRESSURE LOSSES

Region	Pressure Loss, psi (atm)
Pump to reactor core inlet	9.6 (0.65)
Reactor core	47.5 (3.24)
Core outlet to heat exchanger	4.7 (0.32)
Intermediate heat exchanger	4.0 (0.27)
Heat exchanger to pump	3.6 (0.25)
Total loop pressure drop	69.4 (4.73)

The static pressures at various points in the system that correspond to the above pressure drops are indicated in Fig. 10. This shows that the argon gas pressure above the sodium in the reactor is 8 psig (0.54 atm), which is considered reasonably low for sealing of the blanket gas at the reactor cover plug.

The results of pressure loss calculations in the secondary system components and piping are shown in Table XIII.

Table XIII

SECONDARY SYSTEM PRESSURE LOSSES

Region	Pressure Loss, psi (atm)
Intermediate heat exchanger	7.2 (0.49)
Air cooled heat exchanger	0.3 (0.02)
Piping	18.7 (1.27)
Total loop pressure drop	26.2 (1.78)

Using the above pressure drop data and an efficiency of 75%, the calculated pumping work for each secondary loop will be 220 horsepower (165 kw).

B. Reactor Coolant Distribution

Because of the varied heat generation rates in different sections of the overall reactor core such as reflector, capsules, fuel elements, open and closed loops, the coolant must be distributed proportionately. It has been estimated that the flow rates would be distributed approximately as indicated by the values in Table XIV.

Table XIV

REACTOR COOLANT FLOW RATES, gpm (m^3/sec)

	Normal	Maximum
From main coolant pumps	25,400 (1.60)	26,200 (1.65)
To reflector, including capsules	1,400 (0.09)	1,400 (0.09)
To eight open loops	1,600 (0.10)	2,400 (0.15)
To 112 fuel element positions	22,400 (1.41)	22,400 (1.41)
To four closed loops (independent supply)	800 (0.05)	1,200 (0.08)

The average coolant velocity in a (0.168 cm) channel corresponding to the above flow rates is approximately 33 ft/sec (10.1 m/sec).

C. Hot Channel Factors

The hot channel factors anticipated for FFTR attempt to account for dimensional deviations, uncertainties in physical constants, operational uncertainties and empirical correlations, and were used to determine the maximum conceivable steady-state temperatures for the coolant and fuel plates. The factors have been formulated mainly from information reported by other reactor projects. For example, factors associated with fuel plate and assembly fabrication were influenced by those reported for the APPR core,[28] which has a plate configuration similar to that of the FFTR. A summary of the factors employed is shown in Table XV.

The factors apply to the following temperature differences calculated for nominal conditions:

$F_{\Delta T}$ - coolant temperature rise
$F_{\theta f}$ - film temperature difference
$F_{\theta c}$ - temperature drop through cladding
$F_{\theta m}$ - temperature drop through fuel matrix

Table XV

FFTR HOT CHANNEL FACTORS

Factor	$F_{\Delta T}$	$F_{\theta f}$	$F_{\theta c}$	$F_{\theta m}$
Distribution of coolant to channels	1.11	1.04	-	-
Dimensional deviations affecting flow	1.14	1.08	-	-
Flux distribution precision	1.10	1.15	1.15	1.15
Fuel concentration	1.00	1.01	1.01	1.01
Fuel thickness	1.01	1.03	1.03	1.06
Cladding thickness	-	-	1.10	-
Material property uncertainties	1.00	1.01	1.05	1.15
Heat transfer correlation accuracy	-	1.20	-	-
Power level measurement and control	1.08	1.08	1.08	1.08
Overall factor	1.53	1.74	1.50	1.53

D. Core Heat Transfer

The power output from a single subassembly at maximum power density is 2.36 Mw with a chopped cosine axial distribution. A peak heat flux of 975,000 Btu/(hr)(ft^2) [308 watts/cm^2] is obtained. Steady-state temperatures for the subassembly hot spot are shown in Table XVI for both nominal conditions and the adverse case (nominal conditions with the hot channel factors of Table XV applied). The nominal film coefficient was calculated to be 72,100 Btu/(hr)(ft^2)(°F)[41 watts/(cm^2)(°C)]from the recommended equation of Ref. 5. For the calculation of fuel temperatures, a thermal conductivity of 9.3 Btu/(hr)(ft)(°F) [0.16 watts/(cm)(°C)]was estimated for the fuel matrix.

Table XVI

SUBASSEMBLY TEMPERATURES
°F (°C)

	Nominal Case	Adverse Case
Coolant inlet temperature, T_c	500 (316)	600 (316)
Coolant temperature rise, ΔT[(a)]	258 (143)	396 (220)
Film temperature drop, θ_f[(a)]	10 (6)	17 (10)
Temperature drop in clad, θ_c[(a)]	25 (14)	38 (21)
Temperature drop in fuel, θ_m[(a)]	97 (54)	149 (83)
Fuel matrix temperature, T_m[(a)]	990 (533)	1200 (650)
Maximum coolant rise, ΔT_c	292 (162)	446 (248)
Maximum coolant temperature, T_H	892 (478)	1046 (564)

[(a)]at point of maximum fuel temperature.

Coolant flow capacity in the experimental loops would provide for 150% of the power output of the nonexperimental fuel assemblies. Actual flow rates used, however, would depend on the nature of the experiment and could be controlled by the electromagnetic pumps in the individual loops.

Heat generated in the beryllium moderator will be transferred to leakage sodium flowing outside the fuel assembly. The maximum beryllium temperature would exceed the peak coolant temperature by only a few degrees, reaching about 1050°F (566°C) in the worst case.

Approximately 5% of the core flow rate has been alloted for reflector and capsule cooling, in proportion to the fraction of heat produced in the reflector. However, the detailed arrangement of the reflector has not been established; hence this value is a first approximation.

E. Cooling of Spent Fuel

During refueling periods prior to removal from the core, the spent fuel assemblies will be cooled by sodium circulating through the refueling cooling system. Sufficient sodium flow would be provided so that bypassed flow through one open fuel assembly position could be tolerated. Sodium temperature during refueling would be kept to around 150°C, allowing some temperature potential for heat dissipation while maintaining a reasonable temperature environment for handling equipment.

It is estimated that operations prior to withdrawing fuel assemblies from the core could be completed approximately 12 hr after shutdown, at which time decay power would be about 0.22% of full power. The spent fuel assemblies would be lifted from the core through the argon atmosphere to a cleanup cell. Without external cooling, the temperature in the hottest subassembly could rise as much as 1°C/sec. The poor heat transfer properties of argon and the possibility of a low (radiant heat) emissivity film of sodium over the fuel-assembly surfaces makes this rate a fairly realistic approximation. Unreasonably long decay times would be required before a natural-convection cooling system would be adequate. These factors, coupled with the consequences of a meltdown into the sodium, make a positive cooling system mandatory for this operation. It is proposed that a cooling stream of argon be supplied to an assembly during the transfer. Approximately 0.05 m^3/min of 40°C argon should be adequate to maintain plate temperatures within 260°C.

After cleanup, the fuel assemblies will be placed in a storage canal where natural circulation of water should provide satisfactory cooling.

F. Stress Analysis

Stresses in several components of the system were calculated for steady-state conditions. The analysis of other classes of loadings, in particular of thermal shock, is important for this type of reactor but was beyond the scope of this study.

1. Fuel Element Stresses

Thermal stresses in the fuel plate have been estimated for a heat flux of 308 watt/cm^2. Three situations were considered: (1) nominal plate dimensions and operating conditions, (2) "hot spot" conditions obtained using hot channel factors, and (3) a condition approximating that which might result from a statistical analysis of hot channel conditions for a low order of probability of occurrence. Thermal stresses calculated on an elastic basis are as follows:

Case	σ_{Fuel}	σ_{Clad}
1	-1840	2860
2	-2450	4280
3	-2140	3820

where σ is the stress in kg/cm^2. The stresses were calculated assuming uniform heat generation and a symmetrical temperature distribution in the plate. Although the yield strength is exceeded, initial yielding at startup would relieve the stresses. Information presented in Ref. 29 indicates that at least 1000 thermal cycles can be experienced before failure under a stress of 4200 kg/cm^2 could occur (as calculated on the basis of elastic theory). Since the fuel will undergo only a few thermal cycles in its lifetime, this endurance appears to be adequate; however, possible distortion of the fuel element has not been investigated.

In the case of the end plate, the temperature distribution would be asymmetric about the plate centerline and some lateral pressure differences can occur as a result of unequal velocities in adjacent channels. These considerations would affect the tabulated values somewhat, as would stresses resulting from the interaction between the fuel plates and the relatively cool sheath.

The problem of critical velocities for plate collapse was considered. Where adjacent channels are nominally equispaced, a collapse velocity of 30 m/sec was determined for the case of simply supported plates with no pressure communication between channels. The equations of reference 30 were used, nominal dimensions and uniform strength through clad and fuel being assumed. This result, however, does not apply to the case of the end fuel plate where a lateral force will normally exist, the magnitude of which will depend on the effectiveness of the side slots in equalizing coolant pressures.

2. Moderator Grid Stresses

Steady-state thermal stresses were calculated for the beryllium grid. Treating the grid web as an infinite plate, a thermal stress of about 185 kg/cm^2 was obtained. This stress is easily within strength limits attainable from several fabrication processes and should provide sufficient margin for embrittlement due to radiation. The beryllium, however, must be guarded against severe thermal shocks. The extent to which the fuel-assembly sheath and operational practices can provide this protection must be determined.

3. Reactor Vessel Stresses

Stresses in the reactor vessel were calculated for 7 atm design pressure and 250-Mw operation. Reasonable stress levels were obtained for the thin-walled stainless vessel and are tabulated below. A maximum heating rate of 2 watts/cm^3 at the core midplane was calculated, leading to an average wall temperature of 13°C in excess of inner surface temperature.

Source of Stress	Stresses in Pressure Vessel Wall, kg/cm^2	
	Axial	Tangential
Coolant pressure	140	280
Thermal load	610	610
Weight on walls	28	-
Combined stress	778	890

VIII. COST ESTIMATE

As a basis for cost estimating, a hypothetical reactor site was assumed to be located at the Idaho Testing Station. Costs at other industrial sites that are closer to populated areas may be reduced because of available utilities, but this cost reduction may be partially offset by the possible requirement for a containment vessel.

There may also be a cost saving if the reactor is installed next to existing facilities, such as the MTR and ETR, if such facilities can readily accommodate additional requirements for increased utilities. A comparison can be more accurately determined after detailed engineering of the reactor and plant studies have been made.

A. Capital Costs

The capital cost of the FFTR (see Table XVII) was derived from costs of comparable equipment and buildings of facilities, such as ETR,

Table XVII

FFTR REACTOR COST ESTIMATE
(Thousands of Dollars)

Buildings		
Construction		
Land improvement		255
Reactor building structure (including canal, office, lab)		3,045
Critical experiment structure		1,310
Sodium, NaK, gas-storage building		97
NaK pump building		97
Waste products building		144
Tunnel		128
Guard and fire house		10
Outside utilities		1,047
Electrical (exterior and standby)		980
Miscellaneous equipment and systems		375
	Subtotal	7,488
Engineering, design, inspection (10%)		750
		8,238
Contingency (20%)		1,648
	Construction Total	9,886
Reactor Plant		
Pressure vessel and internals, plug		1,450
Control mechanisms		1,000
Primary piping and system (sodium)		2,700
Secondary piping and system (NaK)		2,400
Instrumentation		1,700
Fuel-handling cells and equipment		2,000
Test loop including power supply and instrumentation		4,700
Other systems, gas, storage, waste		2,400
		18,350
Engineering, design (15%)		2,750
		21,000
Contingency (25%)		5,275
	Components and Systems Total	26,375
	GRAND TOTAL	36,261

EBWR, EBR-II, existing critical facilities, and other general figures on cost of plant construction. Costs of several of the major components were established using manufacturers' cost estimates. Experience has shown such estimates to be low; hence, appropriate increasing factors were applied.

The concept of the FFTR is preliminary in nature and costs of many parts of the system could only be roughly estimated. A more detailed design must be developed to establish costs more accurately. However, it was recognized that the reactor systems will be complex and this thought is reflected in the cost estimate.

It must be realized that the cost of the experimental loops is $6,756,000 (including engineering and contingency), and this amount is included in the total cost estimate. These loops are considered a part of the reactor complex and must be tied in with the plant operation. Normally, for water-cooled test reactors, test loops are not a part of the first capital cost of the reactor.

It is believed that the building construction costs can be established somewhat more readily than the reactor system costs. Thus, 20% contingency has been applied to the building cost and 25% to the reactor system. Likewise, the design of the reactor system is thought to be more difficult as reflected in the 15% engineering fee for this system.

There are various cost items which have not been considered in the overall capital cost for the plant. In particular, the items that could increase the construction cost are: premium time, bus transportation, temporary water and power supplies, temporary lunchroom, cleaning quarters, ambulance and fire trucks, access roads, railroad spurs, transmission lines, development engineering, test, inspection and preoperational testing, building permits and miscellaneous fees, insurance and taxes, administrative cost (AEC and others), and escalation.

B. Core Cost

The core cost is estimated to be $200,000 for the beryllium grid, including material and fabrication, and $300,000 per core loading for the fuel fabrication.

The fuel cost on an annual basis is not included, but the following characteristic quantities and costs are listed in Table XVIII as a rough guide:

Table XVIII

ANNUAL CORE COST REFERENCE QUANTITIES
(200-Mw core)

Burnup U^{235}, kg	~80
Fabrication Cost, 4-6 Cores, dollars	1,200,000-1,800,000
Beryllium (2-year cycle), dollars	100,000

C. Operating Costs

The operating costs (Table XIX) include wages and salaries for 188 persons with an average annual allowance per person of $14,000 including indirect charges. The power cost is based on 7,000 kw/hr consumption at 10 mil/kw hr and 300 operating days per year. The operating costs for experiments are not included.

Table XIX

ANNUAL OPERATING COSTS
(Dollars)

Wages and salaries	2,630,000
Power	500,000
Na, NaK, gas make-up	100,000
Heating fuel	10,000
Demineralizer beds and filters	10,000
Maintenance supplies	50,000
Waste-handling supplies	30,000
Miscellaneous materials and supplies, special service, cafeteria, buses, first aid, telephone, telegraph	250,000
	3,580,000

The number of personnel (see Table XX) required for the operation of the FFTR is estimated on the basis of (1) the plant facilities requiring servicing and normal operation, and (2) the service, analysis and liaison activities associated with the experimental work. No allowance is made for personnel assigned directly to the experiments. Critical experiments are assumed part of the duties of this staff.

In the event that the facility would become integrated with existing plants, such as the ETR-MTR, the number of personnel might be revised downward.

Table XX

PERSONNEL REQUIREMENTS

Director	1
Assistant Director	1
Shift Supervisors	4
Facility Supervisors	4
Shift Foremen	4
Technicians	40
Waste Operators and Helpers	8
Engineering and Review Group	12
Physicists	4
Reactor Operators	10
Service Personnel including Janitorial	30
Health Physics Supervisor	1
Health Physics Shift Attendants	8
Plant Project Engineering Group	8
Plant Operation Group	13
Maintenance Supervisor	1
Assistant Maintenance Supervisor	1
Maintenance Foreman, Mechanic	1
Trades	20
Secretarial	4
Clerks	4
Radiochemist	1
Plant Protection	6
	188

IX. TIME SCHEDULE

A time schedule has been prepared to indicate dates at which the various stages of progress could be expected to occur. It should be understood that the schedule is based on a reasonable priority and early assignment of personnel, and of Architect-Engineer.

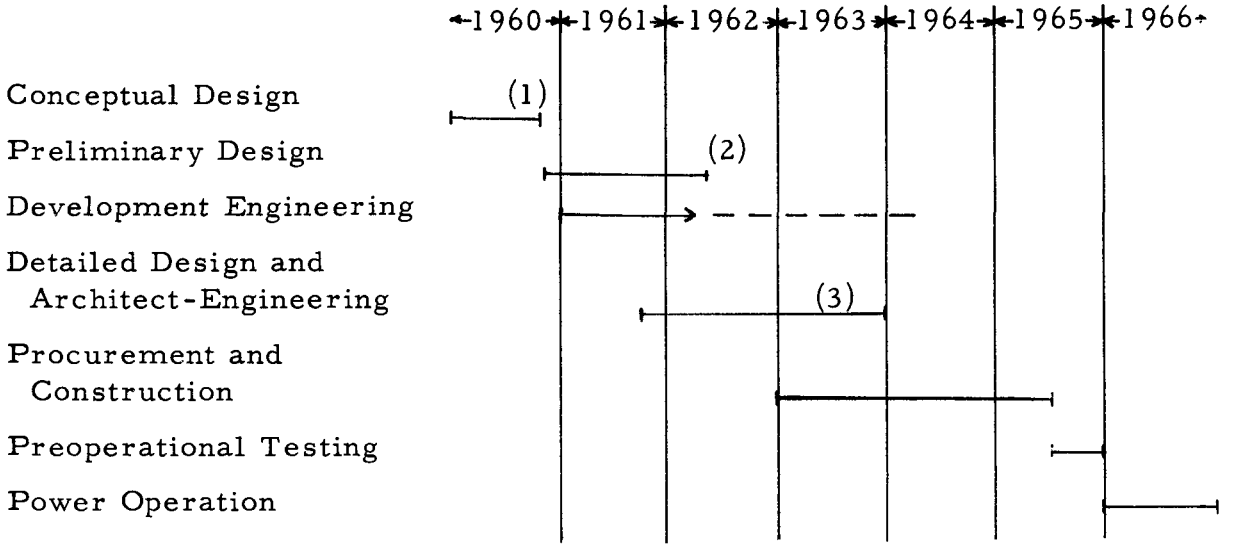

(1) Feasibility Report

(2) Design Report

(3) Hazard Report

It has also been assumed that a development program, particularly in the area of critical experimentation, component testing, heat transfer analysis and fluid flow simulated tests will receive early emphasis. Dates for three essential reports are also shown.

X. FUTURE STUDIES

Throughout the feasibility study, the objective has been to draw from existing technology, particularly that based on the EBR-I, EBR-II and the Fermi reactors.[31-34] Hence, future studies should include minimum development effort. Two important departures from the present breeder reactor designs are with respect to the fuel-handling system and the position of the control rod drive mechanism. Although both items have been developed, their application to the sodium-cooled test reactor will require further effort and test work.

A possible alteration is the use of a hexagonal rather than a square grid for the fuel elements. The square grid has been used primarily because of the commercial availability of the UO_2-stainless steel fuel plates, thus avoiding possible major additional fuel development cost. It is possible that circular fuel elements to be used in a hexagonal grid could be obtained at similar cost. The hexagonal grid would probably be more advantageous from the standpoint of sample shapes.

A suggested alternate core* is in the shape of a skewed arrangement similar to the arrangement adopted for the Belgian Test Reactor BR-2.[35] Conceivably, this arrangement may increase accessibility to the core for test specimen and control rods. Evaluation of the merits of this proposal is beyond the scope of the present report. The application of the intermediate reactor concept using beryllium in the interstices between the fuel elements would probably not be feasible with this design because of the necessarily large axial variation in beryllium thickness. Beryllium would probably have to be incorporated directly in the fuel elements, and some heavier material, such as steel, used to fill the interstices.

Another possible change would be the use of Pu^{239} as fuel instead of U^{235}. This would allow possibly an increase in sample fission rates for the same power and would tend to reduce surface flux depression effects in Pu^{239} samples. To evaluate the use of Pu^{239} one would need information about the cost of fuel fabrication, the value of the Doppler effect, and the value of the sodium void coefficient.

Exceptionally high purity of the sodium coolant is required for the protection of the beryllium. Since the degree of purification is above that obtained in currently operating or planned sodium-cooled reactors, development work should be directed toward the most satisfactory purifying system.

Some of the additional work that should receive early consideration in the next design study may be listed within the next categories.

---

* W. H. Jens, Atomic Power Development Associates - Private Communication

A. Design

(1) Further work of the FFTR concept should first be directed toward a more detailed design of the reactor vessel and internals, experimental loops, instrument connections, and plug design.

(2) The fuel-transfer facilities, including the cooling systems, lighting, manipulators, and handling tools, should be studied in greater detail. A mockup facility should be constructed for simulating the fuel-transfer operation.

(3) A detailed study should be made of the optimum component sizes for the primary and secondary coolant systems.

(4) The selection of the control rod drive system should preferably include an alternate system, and both drives should be developed. Such a program should include a test facility to conduct a control rod test at simulated reactor operating conditions of temperature and pressure.

(5) Alternate core designs should be studied. The geometric configuration of the control rods in the core is to be studied to obtain reasonable control rod centerline distances for installation of the drives.

(6) The beryllium grid design should be studied. It is now visualized that the grid will consist of sections, plates, or boxes, or a combination of these. The design of the grid should be closely tied to the fabrication technique that will be developed. Suitable fastening methods must be developed to maintain the required lattice openings and to permit periodic replacement.

B. Physics

A number of uncertainties in the physics have already been pointed out which it would be desirable to resolve by means of critical experiments before the final design of the reactor was attempted. The indicated measurements are summarized below:

(1) Doppler effect measurements;

(2) critical mass measurements; effect on reactivity of displacement of normal reactor fuel by samples; effect of spatial variation in reactor fuel loading;

(3) control rod worths; reactivity coefficients of fuel, structural material, coolant, and poisons;

(4) power distribution in samples and effective sample fission cross section; perturbing effect on power distribution of interaction among samples and of control rod insertion; optimum loop locations,

(5) energy spectrum measurements;

(6) study of effect of varying Be/U^{235} ratio and core size from standpoint of obtaining a suitable combination of sample irradiation rate, sample power distribution, total reactor power, and reactor fuel lifetime.

C. Heat Transfer, Fluid Flow, Stress Analysis

Analytical work to be performed in further detail design of the plant would require routine studies on items such as cell cooling, transient performance, fluid systems analysis, experimental loop design, pressure vessel and systems design analysis, emergency and shutdown cooling, insulation and heating coil design, and shield cooling.

In addition, special studies should be directed toward the following problems:

(1) A core arrangement similar to that in the EBR-II design was first considered for the FFTR in which the upward hydraulic force on a fuel element is partially offset by a hydraulic downward force on a lower fuel element extension. However, for the FFTR a mechanical hold-down scheme was selected which was thought to result in a shorter fuel element, lower cost, and better control over flow distribution. The subject of hydraulic and mechanical restraint of the fuel assemblies requires more detailed consideration.

(2) Down flow of coolant should be examined as a possible means for eliminating the need for fuel element hold-down devices.

(3) The pressure drop, vibration and deflection characteristics of the fuel element must be evaluated experimentally. A study of the combined effects of thermal and pressure loading on fuel-plate behavior should be undertaken.

(4) The calculated maximum fuel and beryllium temperatures, based on hot channel factors, impose limitations on the core power density with desirably high sodium temperatures. A re-examination of the hot channel factors using a statistical basis and a review of the temperature limitations of the materials involved may indicate capabilities for obtaining higher core power.

(5) The practicability of substituting sodium as the heat transfer fluid in the secondary system should be investigated.

(6) Spent fuel-element conditions during transfer from the core to the water canal and the various possible cooling methods should be further evaluated.

D. Metallurgy

It is quite likely, based on present development programs, that fuel materials with properties superior to UO_2-stainless steel will soon be available. For example, dispersions of UN in stainless steel are being developed; these permit fuel densities to be achieved that are much higher than those which are presently obtainable using UO_2 as the dispersed phase.(36)

It is further visualized that the fabrication technique for fuel elements and the beryllium lattice will need considerably more study. The literature on the corrosion of beryllium is somewhat limited and it has not been clearly demonstrated that beryllium is sufficiently corrosion resistant for the application, or that a satisfactory sodium environment of extremely low oxide content can be maintained. Support work in this category is advised.

Since the use of unclad beryllium under presently specified coolant temperatures and flow rates appears marginal, consideration should also be given to plating or cladding the beryllium.

The use of a lower coolant temperature may be advisable for the use of beryllium to reduce swelling due to helium production.(37,38) Further studies should be made in this connection.

XI. REFERENCES

1. W. A. Reardon and H. H. Hummel, Hotbox, A Fuel Element Test Reactor Transactions of American Nuclear Society, 1, (No.1), p. 61 (June 1958).

2. J. E. Cunningham and R. J. Beaver, A.P.P.R. Fuel Technology, Proceedings of the Second United Nations International Conference on the Peaceful Uses of Atomic Energy, United Nations, Geneva (1958), Vol. 6, p. 521.

3. F. L. Bett and A. Draycott, The Compatibility of Beryllium with Liquid Sodium and NaK in Dynamic Systems, Proceedings of the Second United Nations International Conference on the Peaceful Uses of Atomic Energy, United Nations, Geneva (1958), Vol. 7, p. 125.

4. Liquid Metals Handbook, Sodium-NaK Supplement, Report TID-5277, USAEC-Department of Navy (1955).

5. S. Lubarski, and S. J. Kaufman, Review of Experimental Investigations of Liquid Metal Heat Transfer, NACA Report 1270 (1956).

6. R. A. Tidball, et al, Final Report on the 1000-Kw Aircooled Liquid Metal Heat Transfer Loop, MSA-TR-39 (August 1955).

7. W. M. Kays and A. L. London, Compact Heat Exchangers, National Press (1955).

8. D. Meneghetti and H. H. Hummel, unpublished.

9. H. H. Hummel, et al, Experimental and Theoretical Studies of the Coupled Fast-Thermal System ZPR-V, Proceedings of the Second United Nations International Conference on the Peaceful Uses of Atomic Energy, United Nations, Geneva (1958), Vol. 12, p. 166.

10. D. Meneghetti and H. H. Hummel, Effect of (n, 2n) and (n, α) Reactions on Age Calculations for Beryllium, Nuclear Science and Engineering, 6, 57-62 (1959).

11. G. Hansen and W. H. Roach, Los Alamos Internal Memorandum N-2-753.

12. W. H. Roach, Nuclear Science and Engineering, to be published.

13. G. Hansen, Properties of Fast-Neutron Critical Assemblies, Proceedings of the Second United Nations International Conference on the Peaceful Uses of Atomic Energy, United Nations, Geneva (1958), Vol. 12, p. 84.

14. T. M. Snyder, The Critical Assembly - A Nuclear Design Tool, Proceedings of the International Conference on the Peaceful Uses of Atomic Energy, United Nations, New York (1955), Vol. 5, p. 162.

15. H. Hurwitz, Jr. and R. Ehrlich, Comparison of Theory and Experiment for Intermediate Reactors, Proceedings of the International Conference on the Peaceful Uses of Atomic Energy, United Nations, New York (1955), Vol. 5, p. 423, p. 534.

16. E. Creutz, H. Jupnik, T. Snyder and E. P. Wigner, Review of the Measurements of the Resonance Absorption of Neutrons by Uranium in Bulk, J. Appl. Phys., 26, 257 (1955).

17. J. Chernick and R. Vernon, Some Refinements in the Calculations of Resonance Integrals, Nuclear Science and Engineering 4, 649 (1958).

18. B. I. Spinrad, J. Chernick and N. Corngold, Resonance Capture in Uranium and Thorium Lumps, Proceedings of the Second United Nations International Conference on the Peaceful Uses of Atomic Energy, United Nations, Geneva (1958), Vol 16, p. 191.

19. J. Chernick, Studies of Neutron Capture in Uranium-238 Resonances Proceedings of the Brookhaven Conference on Resonance Absorption of Neutrons in Nuclear Reactors, BNL 433 (1956).

20. W. Rothenstein, Collision Probabilities and Resonance Integrals for Lattices, BNL 563, (1959).

21. R. L. Macklin and H. S. Pomerance, Resonance Capture Integrals, Progress in Nuclear Energy, Series I, Vol II, Physics and Mathematics, McGraw-Hill Book Co. (1956).

22. P. Moldauer, On the Estimation of Fast Neutron Cross Sections, Proceedings of the Conference on the Physics of Breeding, ANL, October 1959, ANL-6122, p. 67.

23. P. Benoist, et al., Critical and Subcritical Experiments on U-BeO Lattices, Proceedings of the Second United Nations International Conference on the Peaceful Uses of Atomic Energy, United Nations, Geneva (1958), Vol 12, p. 585

24. R. T. Frost, W. Y. Kato, and D. K. Butler, Measurement of Doppler Temperature Coefficient in Intermediate and Fast Reactors, Proceedings of the Second United Nations International Conference on the Peaceful Uses of Atomic Energy, United Nations, Geneva (1958), Vol 12, p. 79.

25. M. Grotenhuis, Lecture Notes on Reactor Shielding, ANL-6000 (March 1959).

26. F. H. Clark, Decay of Fission Product Gammas, NDA-27-39 (December 30, 1954).

27. W. H. McAdams, Heat Transmission, 3rd Ed. McGraw-Hill Book Co. (1954).

28. J. O. Brondel, APPR-1 Hot Channel Factors - Re-evaluation on the Basis of Manufacturing Experience and Zero Power Experiments, APAE Memo #96.

29. B. F. Langer, Design Values for Thermal Stress in Ductile Materials, ASME Paper 58-MET-1 (January, 1958).

30. D. R. Miller, Critical Flow Velocities for Collapse of Reactor Parallel-plate Fuel Assemblies, KAPL M DRM - 13 (August 12, 1958).

31. H. V. Lichtenberger, F. W. Thalgott, W. Y. Kato, and M. Novick, Operating Experience and Experimental Results Obtained from a NaK-Cooled Fast Reactor, Proceedings of the International Conference on the Peaceful Uses of Atomic Energy, United Nations, New York (1955), Vol. 3 p. 345.

32. L. J. Koch, et al., Summary Report of the Hazards of the EBR-II, ANL-5719. (May 1957)

33. L. J. Koch, et al., Construction Design of EBR-II, Proceedings of the Second United Nations International Conference of the Peaceful Uses of Atomic Energy, United Nations, Geneva (1958), Vol. 9, p. 323.

34. Enrico Fermi Atomic Power Plant, USAEC-APDA-124 (January, 1959)

35. A. W. Flynn, W. H. Jens N. R. Adolph, D. Rush, A Materials and Engineering Test Reactor (METR) for Belgium, paper presented at the Nuclear Congress, Chicago, Illinois, March 17-21, 1958. Nuclear Development Corporation of America, White Plains, New York.

36. J. E. Gates, el al, Experiments to Determine the Radiation Stability of UN Dispersions in Stainless Steel, BMI-1446 (June 14, 1960).

37. C. E. Ells and E. C. W. Perryman, Effects of Neutron-induced Gas Formation on Beryllium, Journal of Nuclear Materials, 1, 73-84 (1959).

38. J. B. Rich. G. B. Redding, and R. S. Barnes, The Effects of Heating Neutron Irradiated Beryllium, Ibid., 96-105.

XII. APPENDIX A

Table XXI

SET I. CROSS SECTIONS

(BARNS)

Note: σ_A is total group removal cross section

Group	E, Mev	β (Fission Spectrum Distribution)
1	1.353-∞	0.574
2	0.825-1.353	0.18
3	0.498-0.825	0.115
4	0.302-0.498	0.065
5	0.183-0.302	0.034
6	0.111-0.183	0.017
7	0.067-0.111	0.008
8	0.025-0.067	0.006
0	0.00912-0.025	0.001
10	1000-9120 ev	0
11	400-1000	0
12	120-400	0
13	47-120	0
14	16-47	0
15	6-16	0
16	2-16	0
17	0.7-2	0
18	0.4-0.7	0
19	thermal (316°C)	0

Table XXI (Cont'd)

U^{235}

Group J =	σ_A	$3\sigma_{TR}$	$\nu\sigma_F$	σ_{IN} (J→k)					
				k=/J+1	J+2	J+3	J+4	J+5	J+6
1	2 626	14 07	3 56	0 466	0 28	0 19	0 13	0 11	0 08
2	2 2	14 55	3 19	0 45	0 22	0 11	0 06	0 03	0 02
3	2 329	16 5	3 05	0 509	0 24	0 13	0 06	0 04	0 02
4	2 428	20 16	3 14	0 548	0 25	0 12	0 09	0 03	
5	2 255	25 02	3 46	0 356	0 13	0 09	0 03	0 01	
6	2 502	31 5	3 94	0 302	0 13	0 05	0 01		
7	2 623	34 8	4 43	0 223	0 02				
8	3 192	38 4	5 41	0 122	0 01				
9	4 281	42 3	7 38	0 081					
10	9 038	56 66	14 76	0 038					
11	20 124	90 27	32 79	0 094					
12	28 69	111 6	46 96	0 07					
13	48 581	185 0	84 72	0 091					
14	58 939	223 7	94 81	0 079					
15	66 946	231 9	57 37	0 086					
16	39 287	140 2	44 55	0 077					
17	54 8ɔ1	193 0	72 05	0 081					
18	90 15	299 8	147 6	0 15					
19	410 0	1230 0	850 0						

U^{238}

Group J =	σ_A	$3\sigma_{TR}$	$\nu\sigma_F$	σ_{IN} (J→k)					
				k=/J+1	J+2	J+3	J+4	J+5	J+6
1	2 625	14 22	1 45	0 532	0 75	0 437	0 137	0 119	0 09
2	1 277	14 67	0 104	0 432	0 35	0 22	0 11		
3	0 406	17 07		0 263					
4	0 482	20 67		0 354					
5	0 528	25 62		0 333	0 05				
6	0 614	30 9		0 414					
7	0 704	34 2		0 364	0 02				
8	0 595	37 2		0 135	0 02				
9	0 711	39 3		0 111					
10	0 873	60		0 073					
11	1 67	60		0 17					
12	1 091	50 6		0 111					
13	0 41	32 25		0 094					
14	0 669	29 52		0 072					
15	0 638	29 91		0 08					
16	0 59	28 02		0 067					
17	0 451	28 5		0 073					
18	0 734	28 5		0 134					
19	1 6	37 11							

Table XXI (Cont'd.)

Be

Group j =	σ_A	$3\sigma_{TR}$	σ_{IN} (j→k)					
			k=/j+1	j+2	j+3	j+4	j+5	j+6
1	0.43	4.5	0.32	0.17	0.01	0.01	0.01	0.01
2	1.09	7.38	1.09					
3	1.44	9.78	1.44					
4	1.51	10.26	1.51					
5	1.8	12.24	1.8					
6	2.14	14.46	2.14					
7	2.35	15.84	2.35					
8	1.22	16.41	1.22					
9	1.22	16.41	1.22					
10	0.57	16.67	0.57					
11	1.36	16.67	1.36					
12	1.05	16.67	1.05					
13	1.33	16.67	1.33					
14	1.16	16.67	1.16					
15	1.27	16.67	1.27					
16	1.13	16.67	1.13					
17	1.19	16.67	1.19					
18	0.147	16.67	0.147					
19	0.0059	19.5	0					

Fe

Group j =	σ_A	$3\sigma_{TR}$	σ_{IN} (j→k)					
			k=/j+1	j+2	j+3	j+4	j+5	j+6
1	0.739	6.41	0.417	0.283	0.016	0.011	0.006	0.004
2	0.51	5.73	0.111	0.156	0.094	0.057	0.035	0.054
3	0.155	6.47	0.152					
4	0.237	9.93	0.233					
5	0.215	8.88	0.209					
6	0.229	9.42	0.221					
7	0.281	11.58	0.272					
8	0.166	13.2	0.155					
9	0.135	10.38	0.122					
10	0.135	22.53	0.12					
11	9.384	28.5	0.367					
12	0.324	30.03	0.295					
13	0.426	30.24	0.378					
14	0.408	30.33	0.329					
15	0.494	30.48	0.361					
16	0.546	30.75	0.323					
17	0.726	31.26	0.338					
18	1.194	31.77	0.634					
19	1.78	39.24						

Table XXI (Cont'd.)

Na

Group j =	σ_A	$3\sigma_{TR}$	σ_{IN} (j→k)					
			k=/j+1	j+2	j+3	j+4	j+5	j+6
1	0.493	6	0.432	0.0259	0.0182	0.0118	0.005	7
2	0.671	8.3	0.607	0.064	0	0	0	0
3	0.865	12.4	0.716	0.0732	0.0441	0.0268	0.005	
4	0.541	9.6	0.54	0	0	0	0	
5	0.65	11.2	0.649					
6	0.552	9.8	0.551					
7	0.576	10.2	0.575					
8	0.382	13.5	0.379					
9	0.379	13.4	0.378					
10	0.682	6.0	0.68					
11	0.223	9.9	0.22					
12	0.196	9	0.19					
13	0.209	9	0.2					
14	0.216	9	0.2					
15	0.237	9	0.2					
16	0.244	9	0.2					
17	0.276	9	0.2					
18	0.571	9	0.46					
19	0.30	10.5						

Table XXII[a]

SET II. CROSS SECTIONS BARNS

Note: σ_A is total group removal cross section

Group	E, Mev	β (Fission Spectrum Distribution)
1	3-∞	0.204
2	1.4-3	0.344
3	0.9-1.4	0.168
4	0.4-0.9	0.180
5	0.1-0.4	0.090
6	0.017-0.1	0.014
7	0.003-0.017	0
8	550-3000 ev	0
9	100-550	0
10	30-100	0
11	10-30	0
12	3-10	0
13	1-3	0
14	0.4-1	0
15	0.1-0.4	0
16	thermal (0.025)	0

[a]Cross sections for elements other than Pu^{239} taken from Ref. (11,12) except for modifications as noted. The U^{235}, U^{238}, and Pu^{239} cross sections for the first six groups are identical with those of Hansen and Roach, Ref. (11,13) except for a variation in σ_A caused by a change in $\sigma(n,\gamma)$ of Pu^{239}. Thermal group cross sections were not adjusted to the operating temperature of the FFTR because of the negligible amount of thermal fissions in the reactor.

Table XXII (Cont'd.)

U^{235}(b)

Group j =	σ_A	$3\sigma_{TR}$	$\nu\sigma_F$	σ_{IN} (j→k)				
				k=/j+1	j+2	j+3	j+4	j+5
1	3.05	12.75	3.557	0.27	0.37	0.65	0.44	0.06
2	2.73	13.75	3.196	0.24	0.67	0.45	0.07	
3	2.35	13.95	3.087	0.55	0.40	0.07		
4	1.78	15.6	2.988	0.35	0.08			
5	1.74	23.7	3.518	0.08				
6	3.2	37.2	6.125	0.05				
7	5.55	45.3	10.29	0.05				
8	11.15	63.3	19.36	0.05				
9	25.55	106.5	42.87	0.05				
10	54.05	192.0	83.3	0.05				
11	43.05	159.0	66.2	0.05				
12	37.05	141.0	58.2	0.05				
13	38.05	144.0	75.95	0.05				
14	80.05	270.0	171.5	0.05				
15	224.04	702.0	463.05	0.04				
16	605.0	1845.0	1256.9					

(b) Read from homogeneous medium self-shielding curves given in Ref. (11,12) for σ_s per atom of 350 barns, corresponding to FFTR core.

Pu^{239}

Group j =	σ_A	$3\sigma_{TR}$	$\nu\sigma_F$	σ_{IN} (j→k)				
				k=/j+1	j+2	j+3	j+4	j+5
1	3.2	12.75	6.612	0.20	0.27	0.45	0.31	0.04
2	3.08	13.5	6.026	0.18	0.50	0.35	0.05	
3	2.71	14.4	5.472	0.45	0.30	0.06		
4	2.15	17.1	4.981	0.29	0.50			
5	2.05	25.2	4.810	0.05				
6	3.05	36.0	5.86					
7	3.57	40.71	7.15					
8	6.4	49.2	11.4					
9	22.1	96.3	37.2					
10	39.6	148.8	71.5					
11	33.86	114.3	67.6					
12	13.37	70.11	25.4					
13	30.3	120.9	58.1					
14	120.0	390.0	286.0					
15	530.0	1620.0	440.0					
16	1013.0	3069.0	2100.0					

Table XXII (Cont'd)

U^{238}

Group J =	σ_A	$3\sigma_{TR}$	σ_F	σ_{IN} (J→k)				
				k=J+1	J+2	J+3	J+4	J+5
1	2 746	12 00	1 725	0 33	0 46	0 79	0 53	0 07
2	2 575	13 2	1 213	0 35	0 96	0 64	0 09	
3	1 594	13 5	0 108	0 80	0 55	0 10		
4	0 72	15 75		0 50	0 08			
5	0 24	24 6		0 08				
6	0 55	36 0		0 10				
7	0 76	42 0		0 06				
	U^{238}-I(c) U^{238}-II(d)	U^{238}-I(c) U^{238}-II(d)						
8	2 06 0 80	45 0 41 22		0 06				
9	7 05 0 80	54 0 35 25		0 05				
10	21 06 5 0	90 0 41 82		0 06				
11	20 06 2 5	87 0 34 32		0 06				
12	41 06 5 0	150 0 41 82		0 06				
13	0 46	28 2		0 06				
14	0 61	28 65		0 06				
15	1 05	30 00		0 05				
16	2 44	34 32						

(c)Read from homogeneous medium self-shielding curves given in Ref 11, 12 for σ_s per atom of 4650 barns corresponding to FFTR core

(d)Read from homogeneous medium self-shielding curves given in Ref 11, 12 for σ_s per atom of 30 barns corresponding to dilute reactor core Used in "large" sample calculation

Beryllium

Group J -	σ_A	$3\sigma_{TR}$	σ_{IN} (J→k)	
			k=J+1	J+2
1	0 859	3 873	818	0 35
2	0 541	4 425	509	0 12
3	1 207	7 14	1 207	
4	0 913	9 93	913	
5	0 634	11 82	634	
6	0 655	15 54	655	
	Be-I(e) Be-II(f)		Be-I(e) Be-II(f)	
7	0 530 0 535	15 84	0 530 0 535	
8	0 426 0 464	16 11	0 426 0 464	
9	0 355 0 490	16 26	0 355 0 490	
10	0 465 0 658	16 38	0 465 0 658	
11	0 611 0 724	16 38	0 611 0 724	
12	0 535 0 693	16 38	0 535 0 693	
13	0 589 0 772	16 38	0 588 0 771	
14	1 332	16 38	1 332	
15	0 884	16 38	0 884	
16	0 009	16 707		

(e)Taken from Ref 11, 12 except that elastic removal cross sections in the intermediate region were adjusted to correspond to estimated core spectrum for a 15 1 Be/U^{235} atom ratio These cross sections were used for reactors with Be/U^{235} - 20

(f)Taken from Ref 11, 12 except that elastic removal cross sections in the intermediate region were adjusted to correspond to estimated core spectrum for a 33 Be/U^{235} atom ratio These cross sections were used for reactors with Be/U^{235} - 20

Table XXII (Cont'd.)

$Fe^{(g)}$

Group j =	σ_A	$3\sigma_{TR}$	σ_{IN} (j→k) k=/j+1
8	0.1016	21.342	0.0906
9	0.167	32.904	0.14
10	0.254	34.092	0.199
11	0.317	34.092	0.219
12	0.377	34.11	0.207
13	0.543	34.11	0.233
14	0.939	34.11	0.429
15	1.18	34.71	0.270
16	2.24	39.12	

$Na^{(g)}$

Group j =	σ_A	$3\sigma_{TR}$	σ_{IN} (j→k) k=/j+1
8	.141	13.635	0.140
9	.098	9.03	0.093
10	.141	9.03	0.130
11	.16	9.09	0.142
12	.17	9.207	0.138
13	.212	9.297	0.155
14	.394	9.630	0.294
15	.388	10.05	0.198
16	.447	11.241	

O^{16}

Group j =	σ_A	$3\sigma_{TR}$	σ_{IN} (j→k) k=/j+1
8	0.162	10.72	0.162
9	0.162	10.92	0.162
10	0.228	10.92	0.228
11	0.248	10.92	0.248
12	0.239	10.92	0.239
13	0.269	10.92	0.269
14	0.489	10.92	0.498
15	0.331	10.92	0.331
16	0.0002	10.924	

(g) Taken from Ref. 11, 12 except that elastic removal cross sections in the intermediate energy region were adjusted to correspond to estimated core spectrum for a 24 Be/U^{235} atom ratio. For values for Group 1 to 7 see these references.

APPENDIX B

DESIRED EXPERIMENTAL FUEL BURNUP RATES

It seems evident that in order to justify its construction, the FFTR should provide experimental Pu^{239} and U^{235} burnup rates significantly higher than those which can be attained in EBR-II or in the Fermi reactor.

Considering EBR-II, the maximum power density in the core volume is 1.37 Mw/liter; the fuel alloy is 31.8% of the core volume. The maximum fuel alloy power density is therefore

$$1.37 \text{ Mw/liter}/0.318 = 4.31 \text{ Mw/liter}.$$

The U^{235} specific power is

$$\frac{\text{Alloy Power Density}}{(\text{Alloy Density})\left(\frac{\text{wt \% U}}{100}\right)\left(\frac{\text{\% Enrichment}}{100}\right)} = \frac{4.31}{17.9\ (0.95)\ (0.484)} = 0.52 \text{ kw/g}.$$

Consider a fuel sample containing Pu^{239} placed in EBR-II. The equivalent Pu^{239} specific power, assuming that $(\sigma_f\ Pu^{239}) = 1.4\ (\sigma_f\ U^{235})$, is

$$1.4\ (0.52) = 0.73 \text{ kw/g}.$$

In the interest of accelerating rates of burnup, it seems reasonable to expect that the FFTR should provide experimentally available burnup rates at least 50% higher than those obtainable in EBR-II. In the case of plutonium samples, therefore, the FFTR should at least be able to produce a Pu^{239} specific power of 1.1 kw/g.

A more realistic estimate of desired burnup rates can be obtained by considering typical fuel sample irradiations that might be performed in the reactor. A few such examples which are believed to cover the extremes follow with the results summarized in Table XXIII.

It is recognized that the very high plutonium burnup rate specified for Example (2) probably could not be provided in the proposed reactor. However, specimens typified by Example (2) could be irradiated with larger diameters to increase center fuel temperatures. It would be highly desirable if about half of the test facilities in the core of the reactor provided Pu^{239} specific powers in the range of 1.25-1.50 kw/g. Experiments typified by Example (1), (3), and (4) could thereby be accommodated. The remainder of the test facilities, including those in the reflector, should provide Pu^{239} specific powers ranging downward to approximately 0.2 kw/g to accommodate experiments of the type shown for Example (5).

Table XXIII

MAXIMUM DESIRABLE BURNUP RATES FOR EXPERIMENTAL FUEL SPECIMENS IN FFTR

Example No.	Experimental Fuel	Desired Central Fuel Temp, °C	Fuel Power Density, kw/cm^3	Pu^{239} Specific Power, kw/g
(1)	EBR-II Fs Alloy	900	8.50	1.44
(2)	Th-20 wt % Pu	1000	10.3	3.87
(3)	PuC	1500	19.4	1.52
(4)	UO_2-20 vol % PuO_2	2530	4.15	2.06
(5)	Swaged PuO_2	1400	5.27	0.52

Example (1) - EBR-II Fuel Alloy

Assume EBR-II fuel elements, enriched as for EBR-II, to be irradiated with a central fuel temperature of 900°C. The total temperature difference in the fuel with 430°C coolant is 470°C. Since the total temperature difference in EBR-II fuel elements is 238°C with a fuel power density of 4.31 kw/cm^3, the required power density is

$$4.31\ (470/238) = 8.50\ \text{kw/cm}^3.$$

The U^{235} specific power is

$$\frac{\text{Alloy Power Density}}{(\text{Alloy Density})\left(\frac{\text{wt \% U}}{100}\right)\left(\frac{\text{\% Enrichment}}{100}\right)} = \frac{8.50}{17.9\ (0.95)\ (0.484)} = 1.03\ \text{kw/g}.$$

If Pu^{239} is substituted for U^{235}, assuming no change in flux, less plutonium than uranium will be needed because of the higher fission cross section of Pu^{239}. However, since the same total power would then be produced by a smaller amount of plutonium, the unit power requirements for the Pu^{239} will increase proportionately. Assuming that $\sigma_f\ Pu^{239} = 1.4\ (\sigma_f\ U^{235})$, the Pu^{239} specific power would thus be

$$1.4\ (1.03) = 1.44\ \text{kw/g}.$$

Example (2) - Th-20 wt % Pu Alloy

Assume EBR-II size fuel elements, with fuel thermal conductivity equal to U-Fs alloy. A maximum fuel temperature of 1000°C is desired. The total temperature difference, assuming 430°C coolant, is 570°C. Using the same procedure as in Example (1), the required alloy power density is

$$(4.31\ \text{kw/cm}^3)\ (570°\text{C}/238°\text{C}) = 10.3\ \text{kw/cm}^3.$$

The Pu^{239} specific power is

$$\frac{\text{Alloy Power Density}}{(\text{Alloy Density})\left(\frac{\text{wt \% } Pu^{239}}{100}\right)} = \frac{10.3}{13.3\ (0.2)} = 3.87\ \text{kw/g } Pu^{239}.$$

Example (3) - PuC

Assume EBR-II size elements, with fuel thermal conductivity equal to U-Fs alloy. A maximum fuel temperature of 1500°C is desired. The total temperature difference with 430°C coolant is 1070°C. Using the same procedure as in Example(1), the required PuC power density is

$$4.31\ (1070/238) = 19.4\ \text{kw/cm}^3.$$

The Pu^{239} specific power is

$$\frac{\text{PuC Power Density}}{(\text{PuC Density})\left(\frac{\text{At. wt. } Pu^{239}}{\text{Mol. wt. PuC}}\right)} = \frac{19.4}{13.4\ (239/251)} = 1.52\ \text{kw/g}.$$

Example (4) - UO_2-20 vol % PuO_2

The use of EBR-II size pins with a density of 11.4 g/cm^3 and with an effective fuel thermal conductivity of 0.021 watts/(cm)(°C) is assumed. A maximum fuel temperature near 2500°C is desired, with a 2000°C temperature difference in the fuel. As in Example (1), the oxide power density is

$$(\text{EBR-II Fuel Power Density})\ \frac{\text{Oxide } \Delta T}{\text{EBR-II Fuel } \Delta T}\ \frac{\text{Oxide Thermal Conductivity}}{\text{EBR-II Fuel Thermal Conductivity}}$$

$$= 4.31\left(\frac{2000}{135}\right)\left(\frac{0.021}{0.298}\right) = 4.15\ \text{kw/cm}^3.$$

The temperature difference through the balance of the fuel element assembly is

$$(\text{EBR-II } \Delta T)\left(\frac{\text{Oxide Power Density}}{\text{EBR-II Fuel Power Density}}\right) = 103\left(\frac{4.15}{4.31}\right) = 100°C.$$

With a coolant temperature of 430°C, the center fuel temperature is

$$2000 + 100 + 430 = 2530°C.$$

The corresponding Pu^{239} specific power is

$$\frac{\text{Oxide Power Density}}{\left(\frac{\text{vol \% } PuO_2}{100}\right)\left(\frac{\text{At. wt. } Pu^{239}}{\text{mol. wt. } PuO_2}\right)(\text{Density } PuO_2)} = \frac{4.15}{0.2\left(\frac{239}{271}\right)11.4}$$

$$= 2.06 \text{ kw/g } Pu^{239}.$$

Example (5) - Swaged PuO_2

Assume:

Fuel OD: a = 0.104 cm (0.090 in.)

Element OD: b = 0.127 cm (0.100 in.)

Thermal conductivity of fuel: k_f = 0.021 watts/(cm)(°C)

Thermal conductivity of clad: k_c = 0.236 watts/(cm)(°C) (stainless steel at 600°C)

Contact coefficient of fuel - clad: h_a = 1.13 watts/(cm^2)(°C) (Estimated from HAPO data)

Film coefficient of clad - coolant: h_b = 9.9 watt /(cm^2)(°C) (EBR-II Values)

Coolant Temp. = 430°C (800°F)

Desired Maximum Fuel Temp = 1400°C

Desired Element Temp Difference = 970°C.

Also assume that an oxide power density Q of 5 kw/cm^3 is required. Then the total temperature difference ΔT in the element will be

$$\Delta T = \frac{Qa^2}{4k_f} + \frac{Qa^2}{2}\left[\frac{1}{h_a a} + \frac{1}{k_c}\ln\left(\frac{b}{a}\right) + \frac{1}{h_b b}\right]$$

$$= \frac{5000 \times 0.104^2}{4 \times 0.021} + \frac{5000 \times 0.104^2}{2}\left(\frac{1}{1.13 \times 0.104} + \frac{1}{0.236}\ln\frac{0.127}{0.104} + \frac{1}{9.9 \times 0.127}\right)$$

$$= 645 + 230 + 24 + 21$$

$$= 920°C$$

Since 5 kw/cm^3 results in a ΔT of 920°C, the required oxide power density is 5 x 970/920 = 5.27 kw/cm^3 for the desired 970°C. The corresponding Pu^{239} specific power is

$$\frac{\text{Oxide Power Density}}{(\text{Oxide density})\left(\frac{\text{at. wt. } Pu^{239}}{\text{mol. wt. } PuO_2}\right)} = \frac{5.27}{11.4 \times (239/271)} = 0.524 \text{ kw/g } Pu^{239}.$$

ACKNOWLEDGEMENTS

The authors gratefully acknowledge cooperation and assistance by various groups and individuals of the Argonne National Laboratory.

In particular, appreciation is due to E. Hutter, H. Sandmeier, L. E. Link, P. Lottes, A. D. Rossin and B. I. Spinrad for their review of the manuscript and their valuable suggestions. Credit should be given to the Plant Engineering Division for preparation of the major portion of the cost estimate.

Valuable assistance with the physics computational work was given by K. E. Phillips, Sue Katilavas, Margaret McLean, and Lois Meyer. The authors are grateful to G. E. Hansen and W. H. Roach of Los Alamos Scientific Laboratory for permission to use unpublished cross-section data. The authors also thank R. E. Land and D. Okrent for use of their unpublished fast fuel test reactor studies which provided some orientation for the present work.